A MODEL FOR THE STUDY OF BRAIN METASTASIS CANCER STEM CELLS

THE DEVELOPMENT OF A MODEL SYSTEM FOR THE CHARACTERIZATION OF CANCER STEM CELL PROPERTIES IN BRAIN METASTASES FROM THE LUNG

By SARA M. NOLTE, B.H.Sc. (Hons.)

A Thesis Submitted to the School of Graduate Studies in Partial Fulfillment of the Requirements for the Degree Master of Science

McMaster University

MASTER OF SCIENCE, 2012: BIOCHEMISTRY AND BIOMEDICAL SCIENCE

McMASTER UNIVERSITY, Hamilton, Ontario

TITLE: The development of a model system for the characterization of cancer stem cell properties in brain metastases from the lung

AUTHOR: Sara M. Nolte, B.H.Sc. (Hons.)

SUPERVISOR: Dr. Sheila K. Singh

NUMBER OF PAGES: xvii, 154

ABSTRACT

Brain metastases are most common in adults suffering from lung cancer, predicting uniformly poor patient outcome and short survival time. Despite their frequency and severity, very little is known about the tumorigenesis of brain metastases. Previously developed primary brain tumour-initiating cell (BTIC) models were used to determine the presence of a stem-like population in brain metastases from the lung. Use of clinical samples and the NCI-H1915 cell line allowed for the development of useful strategies for study of brain metastasis.

The sphere formation capacity and expression of known BTIC markers in brain metastases was suggestive of a self-renewing population. Differentiation studies demonstrated that neither clinical samples nor NCI-H1915 cells had neural lineage potential. Intracranial xenotransplant of clinical samples and NCI-H1915 cells into NOD-SCID mice led to formation of multiple focal masses throughout the ventricles; the tumours were also serially transplantable, further implicating a TIC population. Of known BTIC markers, only CD15 expression levels and patterns were similar enough in clinical samples and NCI-H1915 cells to warrant prospective sorting experiments in the cell line. Use of CD15 failed to identify a CSC or TIC population in NCI-H1915 cells.

These findings suggest that a TIC population is present in brain metastases; however, this remains to be identified. It is recommended that due to the limitations of cell surface markers, the study of brain metastasis should use a selective gene expression approach, in order to target genes and pathways essential to metastasis. It was shown that NCI-H1915 cells could be useful for such an approach, studying the effects on proliferation, sphere formation, and tumour formation capacity of brain metastases from the lung. Further study using this model could ultimately lead to the disruption of pathways essential to the metastatic process, transforming a uniformly fatal disease into a more localized and treatable one.

ACKNOWLEDGEMENTS

First and foremost, I would like to extend my deepest thanks to my supervisor, **Dr. Sheila Singh**, without whom I would not have had this opportunity. Thank you for welcoming me into your lab, and for giving me a project that would challenge and develop my scientific ability. Most importantly, thank you for having more faith in my abilities and perseverance than I had in myself.

To my fellow Singh Lab members, past and present: thank you all for your continued help, encouragement, and kindness. **Dr. Chitra Venugopal**, **Nicole McFarlane**, and **Branavan Manoranjan** – thank you for your experimental contributions, technical expertise, and for listening to hours of presentations. Thanks to former Lab members **Kevin Wang** and **Monika Lenkiewicz** for initial training and integration into the Lab; to **Erin O'Farrell** for her support, both experimental and emotional, friendship, and mutual understanding of the joys and challenges of grad student life; and finally, **Fidelma DiFlorio**, for amazing administrative services. I consider you all as a second family, and will miss you dearly.

I also wish to express gratitude to my Committee Members **Drs. Mick Bhatia**, **Dino Trigatti**, and **Katrin Scheinemann** for taking time from their busy schedules for our meetings and discussions. Their scientific and clinical expertise and perspectives were invaluable to my success and the success of this project.

Thanks also go to all members of the SCCRI. Over the past two and a half years, you have all helped in some way; whether by providing experimental or career advice, encouragement, engaging conversation, empathy, or laughter. Special thanks to **Lillian Robson** for looking after our mice, and to **Jamie McNicol** for his imaging analysis expertise and assistance. Thanks also to **Andrew Allen** and **Ann Raback**, without whom, I am certain the SCCRI would no longer function effortlessly.

I would also like to thank our collaborators – **Dr. John Hassell** and **Robin Hallett**, **Drs. David Kaplan**, **Kelly Fathers** and **Loen Hansford**, and **Dr. Marco Marra** and **Olena Morozova** – for their contributions, excitement, and recognition of this project's potential and implications.

To my partner in life, **Calvin Yeh**: words cannot describe the depth of my gratitude for everything you have done for me these past few years. Your love, patience, understanding, and faith in me mean more than you will ever know. Without you, I doubt I could have made it.

Thank you to my parents, **Roy** and **Julie Nolte**, for instilling the qualities in me that have made me the student, scientist, and woman that I am today. To my friends and family: thank you for always asking how things were going, for being interested and understanding, even though none of us truly knew what I was doing.

Thank you to everyone, for although my name may be on the cover, it is wrong to think that I could have ever done this alone.

This project was completed with funding support from the Waterloo-McMaster Collaborative Research Grant, Ontario Institute for Cancer Research, and the Ontario Graduate Scholarship, as well as administrative and funding support from the Department of Biochemistry and Biomedical Science and McMaster University.

TABLE OF CONTENTS

LIST OF FIGURES

Figures 2 & 3 are reprinted with the kind permission of Springer Science and Business Media from the original Figures (Figures 11.1 & 11.3, respectively) in: Nolte, S.M., and S.K. Singh. (2012). Chapter 11: Origins of Metastasis-Initiating Cells in Srivastava, R., and S. Shankar (Eds.), *Stem Cells and Human Diseases* (p229-46). New York: Springer/Kluwer Academic Publishers.

LIST OF TABLES

Table 1 is reprinted with the kind permission of Springer Science and Business Media from the original Table (Table 11.1) in: Nolte, S.M., and S.K. Singh. (2012). Chapter 11: Origins of Metastasis-Initiating Cells in Srivastava, R., and S. Shankar (Eds.), *Stem Cells and Human Diseases* (p229-46). New York: Springer/Kluwer Academic Publishers.

LIST OF ABBREVIATIONS

7AAD	7-amino-actinomycin D
ABC (B5)	ATP-binding cassette (B5)
ALDH (1)	Aldehyde dehydrogenase (1)
APC	Allophycocyanin
AUC	Area under the curve
BAAA-DA	BODIPY-aminoacetylaldehyde diethyl acetal
BBB	Blood-brain-barrier
Bmi1	B-cell-specific Moloney murine leukemia virus insertion site-1
BMIC	Brain metastasis-initiating cell
BSA	Bovine serum albumin
BTIC	Brain tumour-initiating cell
BWA	Burrows-Wheeler Analysis
CAPN1	Calpain 1
CCSP	Clara cell specific protein
CD	Cluster of differentiation
CNTF	Ciliary neurotrophic factor
CSC	Cancer stem cell
COX2	Cyclooxygenase 2
CTSZ	Cathepsin
CXCR4	C-X-C chemokine receptor 4

DAPI	4’, 6-diamidino-2-phenylindole
DEAB	Diethylaminobenzaldehyde
DMSO	Dimethyl sulfoxide
DSG2	Desmoglien 2
DSP	Desmoplakin
EDTA	Ethylenediaminetetraacetic acid
EGF / hEGF	Epidermal growth factor / human epidermal growth factor
EIF4EBP1	Eukaryotic translation initiation factor 4E-binding protein 1
EMT	Epithelial-mesenchymal transition
EpCAM	Epithelial cell adhesion molecule (a.k.a ESA)
ESA	Epithelial-specific antigen (a.k.a. EpCAM)
FBS	Fetal bovine serum
FGF / bFGF	Fibroblast growth factor / basic fibroblast growth factor
FITC	Fluorescein
FoxM1	Forkhead box M1
GAPDH	Glyceraldehyde 3-phosphate dehydrogenase
gCIS	Gene-centric common insertion sites
GBM	Glioblastoma
GFAP	Glial fibrillary acidic protein
GFP	Green fluorescent protein
H&E	Hematoxylin and eosin
HIF1	Hypoxia-inducible factor-1

HNSCC	Head and neck squamous cell carcinoma
HOXB9	Homeobox B9
HSC	Hematopoietic stem cell
ID1	Inhibitor of DNA binding 1
IF	Immunofluorescence
IHC	Immunohistochemistry
IL11 / IL8	Interleukin-11 / Interleukin-8
KRT	Keratin
LAC	Lung adenocarcinoma
LAMC2	Laminin gamma 2
LEF1	Lymphoid enhancer binding factor 1
LIF	Leukemia inhibitory factor
LIMMA	Linear models for microarray data
LWS	Lung cancer WNT gene set
MAP2	Microtubule-associated protein 2
MIC	Metastasis-initiating cell
MMP	Matrix metalloproteinase
mTOR	Mammalian target of rapamycin
MYH14	Myosin
NOD-SCID	Non-obese diabetic severe combined immunodeficient
NSC	Neural stem cell
NSCLC	Non-small cell lung carcinoma

PBS	Phosphate buffered saline
PE	R-phycoerythrin
PI3K	Phosphatidylinostiol-3-OH kinase
PLEKHG6	Pleckstrin homology domain; family G, member 6
RA	Retinoic acid
RASAL1	RAS-protein activator-like 1
RBC	Red blood cell
RMA	Robust multi-array analysis
ROC	Receiver operator characteristic
RPKM	Reads per kilobase of exon model per million mapped reads
SCLC	Small cell lung carcinoma
SPC	Surfactant protein C
SSEA1	Stage-specific embryonic antigen 1
ST6GALNAC5	α2,6-sialytransferase
TGFβ	Transforming growth factor β
TIC	Tumour-initiating cell
TNFα	Tumour necrosis factor α
TTF1	Thyroid transcription factor 1
VEGF	Vascular endothelial growth factor

DECLARATION OF ACADEMIC ACHIEVEMENT

The completion of this Thesis was the result of my own work and several experimental contributions from Singh Lab members and collaborators. **Dr. Chitra Venugopal**, **Branavan Manoranjan**, and **Erin O'Farrell** (Laboratory of Dr. Sheila Singh, McMaster University) helped to collect and process clinical samples, and assisted with *in vivo* injections. **Nicole McFarlane** (Laboratory of Dr. Sheila Singh, McMaster University) performed all flow-associated staining, flow cytometry, flow-sorting, and assisted in the analysis of flow data. **Jamie McNicol** (SCCRI, McMaster University) assisted in the design of immunofluorescence experiments, scanned differentiation plates on the Operetta, and prepared several Acapella scripts for the analysis of immunofluorescence data. **Dr. John Provias** (Hamilton Health Sciences) provided H&E images of patient tumours. **Olena Morozova** (Laboratory of Dr. Marco Marra, BC Cancer Agency) was responsible for performing the initial transcriptome analysis, and subsequent generation of the candidate gene list. **Robin Hallett** (Laboratory of Dr. John Hassell, McMaster University) conducted analyses to determine the predictive value of the genes in the candidate gene list.

CHAPTER 1: INTRODUCTION

1.1 The cancer stem cell model

One of the current models of tumorigenesis is the cancer stem cell (CSC) model, where a subpopulation of CSCs, or tumour-initiating cells (TICs), is responsible for the initiation and maintenance of the entire tumour. As their name would suggest, CSCs possess several stem cell-like characteristics, such as self-renewal and hierarchical differentiation [1-3]. Like stem cells, CSCs are capable of dividing asymmetrically, where one of the daughter cells retains the parental cell's ability to self-replicate, thus renewing the stem population, and the other daughter cells is often a more lineage-restricted progenitor. This form of division is responsible for the development of a hierarchy of cell types, where cells farther down the hierarchy are committed to particular lineages, and the stem-like cell at the top of the hierarchy, is capable of producing all of the lineages below [1-3]. While capable of asymmetrical divisions, stem cells can also divide symmetrically to produce two stem daughter cells, increasing the stem cell pool, or to produce two more differentiated progeny, a process termed stem cell depletion [1-3]. Through the process of self-renewal and the associated differentiation, CSCs are hypothesized to form the entire bulk of a tumour (**Figure 1**).

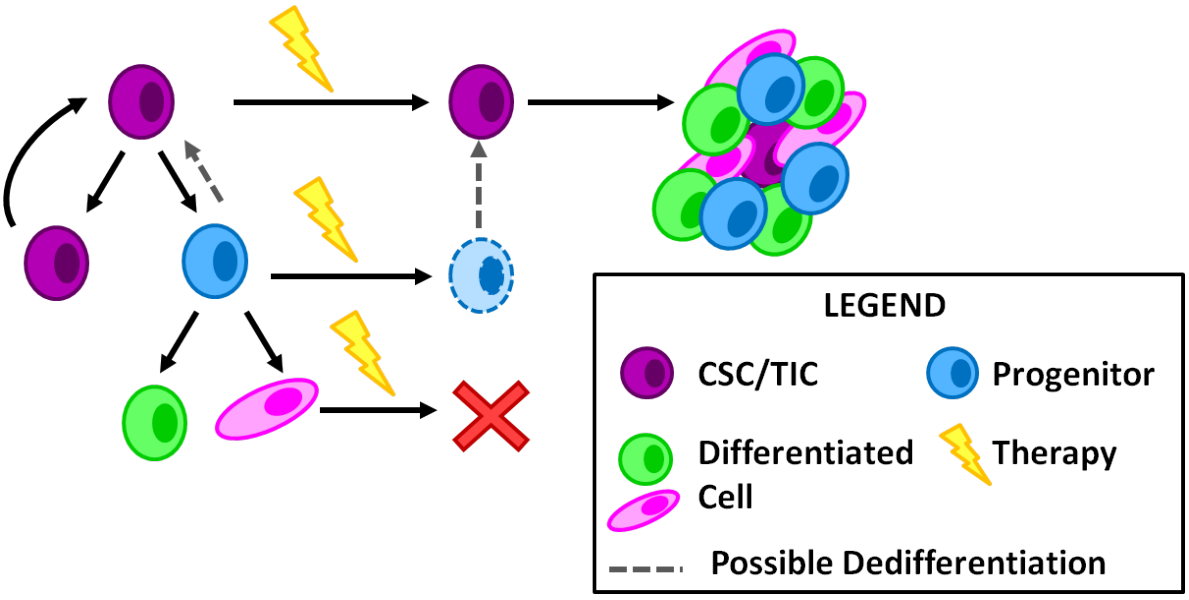

Figure 1: The cancer stem cell model. A cancer stem cell (CSC) or tumour-initiating cell (TIC) resides at the top of the hierarchy, and is capable of self-renewal and producing the more differentiated progeny comprising the tumour. Upon treatment with traditional therapies, the CSC population and possibly the progenitor population, remains viable, capable of re-forming the tumour, resulting in relapse.

It is important to note that the term “cancer stem cell” is not indicative of a stem cell as the cell of origin. It is quite plausible that CSCs are the product of mutations acquired by a stem cell; thus, allowing self-renewal and proliferation to go unchecked. However, it is also possible that a more mature cell or progenitor acquired these mutations and dedifferentiated, developing the ability to self-renew [1-3]. This distinction has led to much confusion and debate regarding the identification of CSCs, where in all likelihood, the cell of origin of the CSC population differs among cancers and cancer subtypes. For the purposes of this work and subsequent discussion, “cancer stem cell” is interpreted as a functional definition of a cancer cell with stem-like properties.

CSCs are often identified using cell-surface markers or functional assays, such as the Aldefluor (aldehyde dehydrogenase activity) and side-population or Hoechst exclusion (ABC transporter activity) assays. **Table 1** lists currently used CSC or TIC markers for a variety of solid tumours, including brain [4-6], breast [7-8], colon [9-10], and lung [11]. These TIC populations are most often a rare subset of cells [12], with some exceptions [13].

Tumour Type	TIC Population	Reference
Brain	$CD133^+$	[4],[5]
	$CD15^+$	[6]
Breast	$CD44^{+/hi}/CD24^{-/lo}$	[7]
	$Aldefluor^+$	[8]
Colon	$CD133^+$	[9],[10]
	$Aldefluor^+$	[14]
Lung	$CD133^+$	[11]
Melanoma	$ABCB5^+$	[15]
Head & Neck	$Aldefluor^+$	[16]
Pancreatic	$CD44^+/CD24^+/EpCAM^+$	[17]

Table 1: Markers used to identify and characterize tumour-initiating cell (TIC) populations in human primary tumours.

Such markers were shown to identify TIC populations by prospectively sorting bulk population tumour cells, and demonstrating their ability to be serially passaged in immunodeficient mice, while recapitulating the cell types of the original tumour. The ability to be serially passaged *in vivo* is indicative of self-renewal, as the TIC population is maintained and propagated throughout passaging, where non-TICs may be produced, but are unable to initiate tumour formation in a subsequent animal [1-3].

The CSC model also stipulates that TICs evade current therapeutic modalities, suggesting TICs are responsible for relapse and metastasis [1, 18-19]. This is evident in the correlation with poor patient survival and the presence of CSC markers in brain [20-21],

colon [22], breast [23], or lung [24-25] cancers. In addition to their tumour-initiating capabilities, CSCs are also desirable therapeutic targets due to their resistance to conventional chemotherapy and radiation. Current efforts to target TICs include induction of differentiation, resulting in a loss of self-renewal and increased susceptibility to bulk tumour therapy [26-29].

1.2 Identification of brain tumour-initiating cells

A stem-like population was first identified in primary brain tumours surgically resected from patients, such as glioblastoma (GBM) and medulloblastoma, using the cell surface marker CD133. CD133, or prominin-1, was first identified as a marker for human hematopoietic stem and progenitor cells [30], and later, for human neural stem cells [31]. It has since been used to find CSC populations in brain [4-5], colon [9], and lung [11] cancers. Cells prospectively sorted to enrich for CD133 expression demonstrated a higher index of self-renewal *in vitro*, as compared to $CD133^-$ populations [4]. $CD133^+$ cells were also capable of producing $CD133^-$ cells while maintaining the initial proportion of CD133 positivity; whereas, $CD133^-$ cells remained negative, indicating a hierarchical organization between CD133 positive and negative populations [4]. Further *in vivo* study of CD133 positive and negative populations demonstrated that as few as 100 $CD133^+$ cells could initiate tumour formation through intracranial injection in non-obese diabetic severe combined immunodeficient (NOD-SCID) mice; however, as many as 50,000 or 100,000 $CD133^-$ cells could not [5]. As seen *in vitro*, the $CD133^+$ tumours isolated from NOD-SCID mice were heterogenous for CD133, in addition to recapitulating the tumour

morphology and marker expression originally seen in the patient [5]. As such, $CD133^+$ cells were termed brain tumour-initiating cells (BTICs).

Following the initial identification of BTICs using CD133, several groups have used another marker, CD15, to identify similar stem-like populations both in normal neural tissue [32], and primary human brain tumours [6, 33-34]. CD15, also known as stage-specific embryonic antigen 1 (SSEA-1), is a cell surface carbohydrate expressed by pluripotent embryonic stem cells [35]. Mao *et al* reported that $CD15^+$ cells had a higher rate of sphere formation, an indication of self-renewing capabilities, than $CD15^-$ cells (41.6 vs. 1.1%, respectively) [6]. In addition, they also showed that after ten weeks post-injection, only mice injected with $CD15^+$ cells were observed to have tumour formation, where $CD15^-$ yielded no tumours [6]. Similarly, another group showed increased self-renewal *in vitro* of $CD15^+$ cells compared to $CD15^-$ cells, indicative of a higher stem cell frequency [34]. $CD15^+$ cells were also more capable of tumour formation with decreasing cell number injected, as compared to bulk unsorted and $CD15^-$ cells [34].

Aldehyde dehydrogenase (ALDH) is an enzyme found to be highly active in and selective for normal hematopoietic stem cell populations [36], and is increasingly useful for CSC identification in epithelial tumours [16, 24, 37-39]. ALDH activity has also been used to identify normal neural stem cells in mice [40], as has been associated with *in vitro* self-renewal [41] and tumour formation [42] in primary human brain tumours. Rasper *et al* observed a decrease in sphere and colony formation (indicative of self-

renewing populations) and sphere size in glioma cells highly positive for ALDH when treated with the ALDH inhibitor diethylaminobenzaldehyde (DEAB) [41]. Bar *et al* showed that treatment with cyclopamine of glioma cell lines resulted in a loss of ALDH activity as indicated by the Aldefluor flow cytometry assay, which corresponded with an inability to for secondary tumourspheres and a decrease in tumour formation [42]. While CD133, CD15, and ALDH have been shown to independently select for a CSC or TIC population in primary brain tumours, studies have yet to be shown using these markers in conjunction to identify a more elaborate hierarchy within brain tumours, as it is unlikely that all three markers can consistently select the same population.

1.3 The process of metastasis

Metastasis, the spread of a primary tumour to additional tissues in the body, is an extremely inefficient, multi-step process (**Figure 2**). In order to form a tumour in a secondary location, the metastatic cell must first escape the primary tumour, then intravasate into the circulation. Once in the circulation, the cell must survive host immunological defences and shearing forces. The cell then arrests in a secondary location, and extravasates into the tissue stroma. Most often this secondary site is the first capillary bed encountered [43-44], but occasionally homing mechanisms direct the cell to a specific secondary tissue [43]. Once in the secondary location, the cell must initiate growth of a micrometastasis. This in turn develops into a macrometastasis, with angiogensis occurring to supply the growing tumour with nutrients. Finally, the tumour becomes a well-vascularized and clinically-detectable tumour. Studies have shown that

while close to 90% of cells that have escaped the primary tumour are capable of completing all the steps up to and including extravasation, only 2 and 0.02% of these cells can develop micro- and macrometastases, respectively [45].

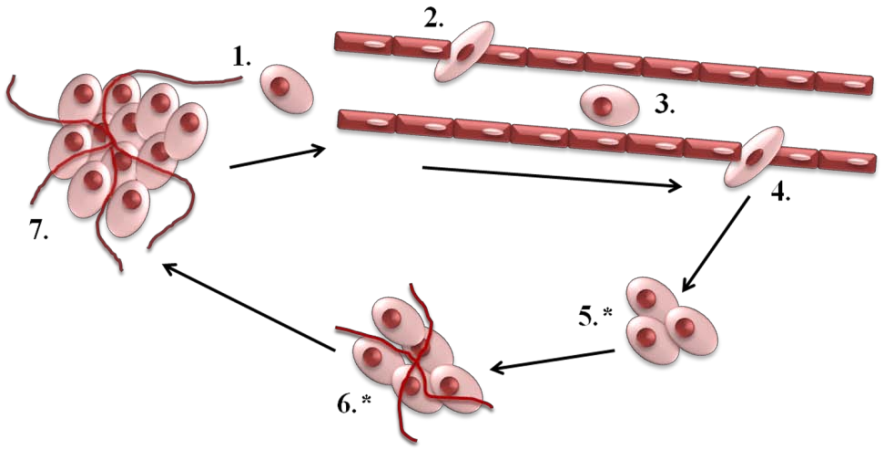

Figure 2: Metastasis is an extremely inefficient multi-step process. In order to form a tumour in a secondary location, the metastatic cell must complete several steps: **(1)** escape from the primary tumour, **(2)** intravasation into the circulation, **(3)** survival in the circulation, **(4)** arrest in a secondary location and extravasation into the tissue stroma, **(5)** initiation of a micrometastasis, **(6)** angiogenesis occurs to supply developing macrometastasis, and **(7)** development of a well-vascularized and clinically-detectable tumour. *****Denotes particularly inefficient stages in the metastatic process. © Springer Science and Business Media.

1.4 Inherent metastatic properties of primary tumours

1.4.1 Migration and invasion of primary tumour-initiating cells

The study of metastasis has been focused on breast cancer, and much of the research linking TICs to metastasis is modeled in breast cancer. Several studies have used $CD44^+/CD24^-$ with/without $Aldefluor^+$ populations to select breast TICs, and have found

these populations of cells to be intrinsically migratory and invasive *in vitro*, and metastatic *in vivo* [38, 46-49].

Croker *et al* used several breast TIC markers to select stem cell-like subpopulations from several human breast cancer cell lines. Populations that were $CD44^{+}/CD24^{-}/Aldefluor^{hi}$ or $CD44^{+}/CD133^{+}/Aldefluor^{hi}$ demonstrated enhanced abilities of adhesion, migration, and invasion *in vitro*, compared to $CD44^{-/lo}/Aldeflour^{lo}$ controls [38]. Immunodeficient mice injected with either $CD44^{+}/CD24^{-}/Aldefluor^{hi}$ or $CD44^{+}/CD133^{+}/Aldefluor^{hi}$ cells had significantly higher incidence of metastasis to the lung and developed larger metastases than mice injected with $CD44^{-/lo}/Aldeflour^{lo}$ cells [38]. Similarly, in a study of inflammatory breast cancer, MARY-X and SUM149 cell lines were sorted based on their Aldefluor activity. $Aldefluor^{+}$ and unsorted cells demonstrated tumour initiation capabilities *in vivo*, while $Aldefluor^{-}$ cells did not [46]. $Aldefluor^{+}$ TICs were more invasive *in vitro*; demonstrated an ability to initiate spontaneous, systemic metastases in NOD-SCID mice; and correlated with decreased overall survival and an increased probability of metastasis in inflammatory breast cancer patients, as compared to unsorted and $Aldefluor^{-}$ cells [46].

Furthermore, Sheridan *et al* showed that breast cancer cell lines with a $CD44^{+}/CD24^{-/lo}$ percentage of over 30% consistently expressed pro-invasive genes (i.e. *CXCR4, MMP1, osteopontin*) and had a higher capacity for invasion *in vitro* [48]. However, when intracardiac injection of $CD44^{+}/CD24^{-/lo}$ cells was performed in nude mice, a limited

number of metastases formed. Interestingly, these *in vivo* metastases were formed by $CD44^{+}/CD24^{-/lo}$ populations isolated from breast cancer cell lines derived from metastatic sites, rather than the primary breast tumour [48]. This suggests that while the primary TIC population may possess a higher level of invasiveness, it is not sufficient to form metastases *in vivo* [48].

Another group used an orthotopic xenograft model of human breast cancer in NOD-SCID mice, to show that use of an EGF (epidermal growth factor) gradient caused injected cells to be more invasive and migratory [49]. While not prospectively examining the formation of metastases by the $CD44^{+}$ population, analysis of the invasive portions compared to the tumour bulk by flow cytometry showed that the invasive portions were significantly enriched for the breast TIC marker CD44 [49]. In addition, this model allowed for the observation of spontaneous metastases to the lung where the lung metastases were found to possess a $CD44^{+}$ population similar to that of the primary tumour. When the $CD44^{+}$ cells from the metastases were injected into the mammary fat pad, they were able to recapitulate the primary tumour [49]. From these findings, it may be inferred that metastases do retain the TIC populations from the primary breast tumour (i.e. $CD44^{+}/CD24^{-/lo}$ cells) and that these populations are capable of recapitulating the primary tumour; however, it appears as though only a subset of the primary TICs are capable of forming a metastasis.

In a model of head and neck squamous cell carcinoma (HNSCC) it was also shown that $CD44^{high}$ TICs were more migratory *in vitro* and formed more lung metastases when injected via tail vein into NOD-SCID mice, compared to $CD44^{low}$ non-TICs [50]. However, $CD44^{low}$ cells demonstrated a trend towards being more invasive *in vitro* than $CD44^{high}$ cells, but this trend was not significant [50]. A study examining $CD44^{+}/CD24^{-}$ status in paraffin-embedded breast cancer patient samples also found a lack of correlation between the TIC population and event-free or overall patient survival; however, they did show that the majority of patients with metastasis had more than 10% of $CD44^{+}/CD24^{-}$ cells [51].

Together, these studies confirm that a link exists between stem cell-like populations and metastatic ability. What is not clear is whether this ability is truly inherent, or whether these cells acquire metastatic capability over time.

1.4.2 Organ-specific metastasis gene signatures in primary tumours

While not studying a TIC population, the Massague group has identified several gene signatures for organ-specific metastasis of breast cancer [52-54]. A list of 54 genes was identified as being upregulated in lung metastases from the breast, and a subset of these genes correlated with lung metastasis in clinical samples [52]. While the majority of the genes seemed to be important only for colonization of the lung, the transcription factor *ID1* (*inhibitor of DNA binding 1*) was found to be important for both growth of the primary tumour and metastasis to the lung [52]. Several genes were also identified as

being overexpressed in bone metastases from breast cancer. These genes have specific roles in homing (*CXCR4*), osteolysis (*interleukin 11*, *IL11; osteopontin*), and invasion (*matrix metalloproteinase 1*, *MMP1),* and when expressed in combination, significantly increased the ability of previously non-metastatic cells to successfully metastasize to bone [54]. This breast-to-bone signature was found to be independent of another signature predicting prognosis and tumorigenicity of breast cancer [54-55].

Another recent study by the Massague group has identified 17 genes that mediate breast cancer metastasis to the brain, and correlated with relapse of disease in the brain [56]. Several genes overlapped with the previously identified lung metastasis signature [57], including *COX2* (*cyclooxygenase 2*), *MMP1*, and other genes implicated in adhesion, migration, and invasion [56]. Another group identified a set of Wnt3a-regulated genes in lung adenocarcinoma that predicted for metastasis to the brain [58]; these genes were independent of those identified for brain metastasis by the Massague group [56]. Interestingly, some of these Wnt3a-regulated genes have also been shown to be involved in breast metastasis to the lung, suggesting there may be some genes and pathways universally involved in metastasis.

Through these gene signature studies, it is clear that primary tumours express genes that meditate metastasis and secondary site-specific colonization. It is possible that these gene signatures may contain putative metastasis-initiating cell (MIC) markers, yet separation of functionally distinct populations has yet to be shown. While important for metastasis,

these genes are not necessarily essential for primary tumour formation. No relationship of the metastasis gene signatures with a primary TIC population has been examined, nor how they are related temporally to primary tumour initiation and growth. Answering these questions may help further elucidate their role in secondary tumour development.

1.5 Acquisition of metastatic and stem cell-like properties

The epithelial-mesenchymal transition (EMT) is an important process in embryonic development, allowing for increased plasticity as epithelial cells lose their characteristics and acquire those of mesenchymal lineages [59-61]. It is becoming increasingly apparent that EMT is involved in metastasis: cells of the primary tumour may undergo EMT, becoming more motile, and invasive, allowing them to complete the initial steps of metastasis [61-65].

A variety of signalling cascades widely known to play roles in tumorigenesis are also implicated in the process of EMT: Wnt, Notch, and transforming growth factor β (TGFβ) signalling [59-60, 66-67]. Other regulators of EMT include hypoxia, epithelial-stromal cell interactions, and several microRNAs from the miR200 family [59-60, 67]. These signalling cascades ultimately result in the upregulation of the EMT promoters *Snail1, Snail2/Slug,* and *Twist1,* where Twist1 induces the expression of transcription factors Snail1 and Snail2/Slug, which in turn suppress *E-cadherin* expression, allowing cells to lose their epithelial phenotype (**Figure 3**) [68-69]. Genes upregulated by these EMT promoters are responsible for disruption of tight junctions, cytoskeleton remodelling, and

reorganization of the extra-cellular matrix. Of particular interest are the recent links between TICs and EMT, where TIC populations have been shown to express higher levels of EMT markers than the bulk population [70-74].

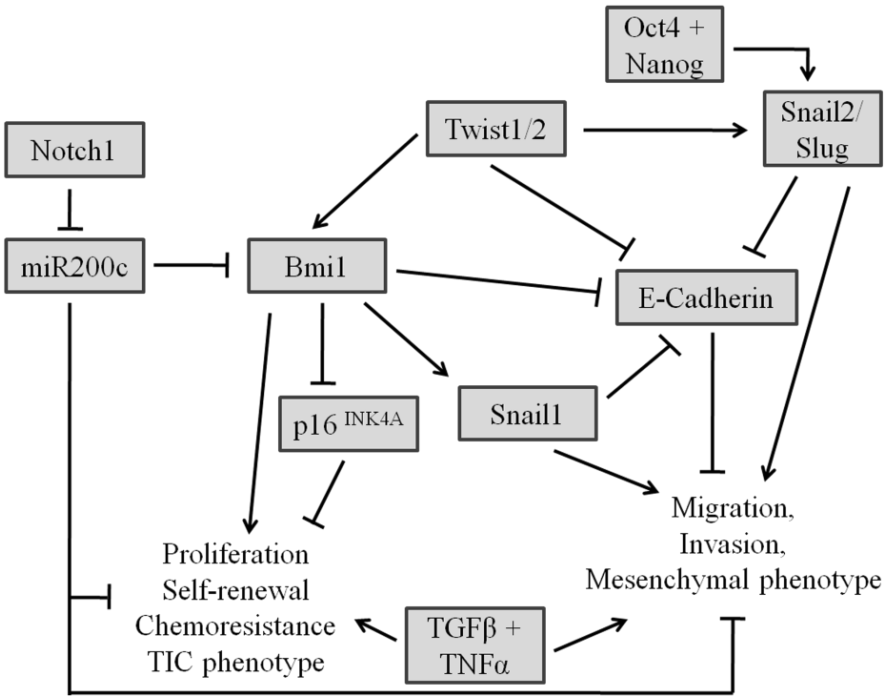

Figure 3: Regulators of tumour-initiating cell (TIC) populations are implicated to also have a role in the epithelial-mesenchymal transition (EMT). Bmi1 is a known oncogene, and has been found to regulate self-renewal, leading to an increase in TIC populations. Recently Bmi1 has been shown to be regulated by Twist1, and to also regulate genes downstream of Twist1 in the EMT pathway. Other stem cell-related genes and signalling pathways (Oct4, Nanog, and Notch) have also been implicated in this process. Thus, EMT allows for stem cell-like populations to possess mesenchymal cell properties. © Springer Science and Business Media.

In a study examining several HNSCC cell lines, Aldefluor$^+$/CD44$^+$/CD24$^-$ status was found to be indicative of invasion and expression of EMT markers (*Snail1, Twist1, Snail2/Slug*) [70]. Cell lines with higher proportions of Aldefluor$^+$/CD44$^+$/CD24$^-$ cells demonstrated higher expression levels of vimentin and α-smooth muscle actin, markers

of myofibroblasts, an important component of tumour stroma [70]. Similarly, naturally present $CD44^{+}/CD24^{low}$ cells in normal and tumorigenic breast tissue were found to have higher expression of EMT markers and genes than their non-stem cell counterparts [71].

In oral and cutaneous squamous cell carcinomas, epithelial-specific antigen (ESA) could further fractionate the $CD44^{hi}$ CSC population [75]. The $CD44^{hi}/ESA^{lo}$ cells also expressed significantly higher levels of EMT markers, which corresponded with an elongated fibroblast-like morphology [75]. Both $CD44^{hi}$ populations had similar orthotopic tumour formation and were capable of generating heterogenous tumours; however, only the $CD44^{hi}/ESA^{lo}$ cells showed any lymph node infiltration [75].

Mani *et al* showed that by overexpressing the EMT transcription factors *Snail* and *Twist1* in human mammary epithelial cells, the cells not only acquired a mesenchymal phenotype, but had also acquired the breast stem cell markers $CD44^{+}/CD24^{low}$, accompanied by increased self-renewal and the ability to differentiate into multiple breast lineages [71].

Several groups have made an effort to determine a genetic mechanism for the link between TICs and EMT-mediated metastasis. $Aldefluor^{+}$ HNSCC TICs were found to overexpress *Bmi1* (B-cell-specific Moloney murine virus insertion site), a potent oncogene and regulator of stemness in TICs [76-77], which subsequently led to higher levels of Snail1 [72]. Knockdown of Bmi1 in $Aldefluor^{+}$ cells led to a decrease in *Snail*

and *ALDH1* expression; whereas, overexpression of Bmi1 in Aldefluor$^-$ cells led to an increase in *Snail* and *ALDH1* expression, while enhancing tumorigenicity, metastasis, and radioresistance *in vivo* [72]. Similarly, Lo *et al* found Bmi1 to be highly expressed in Aldefluor$^+$/CD44$^+$ HNSCC cells, while miR200c, a suppressor of *Bmi1* [78] and EMT-mediated metastasis [79], was found to have lower expression levels [73]. Knockdown of *Bmi1* or overexpression of miR200c reduced properties of EMT, TIC ability, and the formation of lung metastases [73]. Overexpression of miR200c also lead to the sensitization of previously radioresistent Aldefluor$^+$/CD44$^+$ cells [73]. Overexpression of *Bmi1* in human nasopharyngeal epithelial cells induced a morphological change, causing the epithelial cells to resemble fibroblasts and acquire increased motility. Silencing of *Bmi1* reduced transformation and metastatic abilities [80]. High levels of Bmi1 were predictive of high grade melanoma with metastatic disease [81].

Twist1 overexpression consistently led to the upregulation of *Bmi1* in several human HNSCC cell lines; furthermore, both *Twist1* and *Bmi1* were found to be upregulated in Aldeflour$^+$/CD44$^+$ TICs [82]. Overexpression of *Twist1* or *Bmi1* was also correlated with increased radioresistence and tumour formation *in vivo* [82]. *Bmi1* and *Twist1* were found to be mutually essential in inducing EMT and tumour-initiation capabilities, and cooperatively bind and repress the *E-cadherin* and $p16^{INK4A}$ promoters [82]. These findings suggest that *Bmi1* plays a regulatory role in the initiation of EMT signalling while expanding the TIC compartment.

Other stemness genes, such as *Oct4* [83-84] and *Nanog* [84-85], have been linked to EMT. Multi-dimensional scaling analysis of $CD133^+$ and $CD133^-$ lung adenocarcinoma (LAC) cells, LAC metastases, and primary tumours showed that $CD133^+$ cells and metastases had similar gene signatures, and both had significantly higher levels of *Oct4* and *Nanog* than $CD133^-$ cells and the primary tumours [86]. When *Oct4* and *Nanog* were overexpressed in the A549 LAC cell line, $A549^{Oct4/Nanog}$ cells had higher levels of genes implicated in EMT, and a higher frequency of metastasis *in vivo* than control [86].

Bao *et al*. showed that overexpressing *Notch1*, where the Notch pathway has a role in cancer stem cell maintenance [87-88], in the AsPC-1 pancreatic cancer cell line resulted in an increase of CSC markers EpCAM (epithelial cell adhesion molecule) and CD44, while at the same time inducing a mesenchymal-like morphology, EMT genes, and increased migration [74]. This corresponded with a decrease of several microRNAs in the miR200 family [74], which have been shown to be negative regulators of EMT and cancer stem cell genes [78, 89-90].

In colonosphere cultures, $CD44^+$ populations were found to have much higher levels of *Snail1* than $CD44^-$ cells, and knockdown of *Snail1* resulted in a loss of CD44 expression, suggesting that *Snail1* has a regulatory role over this CSC marker [91]. Overexpression of *Snail1* also led to an increase in self-renewal, as demonstrated by sphere formation, as well as increased tumorigenecity *in vivo* and chemoresistance [91], further proving a role for an EMT regulator in acquiring stemness properties.

Twist has also been shown to regulate breast CSCs by increasing the percentage of $CD44^+/CD24^-$ cells through direct suppression of the CD24 promoter [92]. In addition to increases in the percentage of $CD44^+/CD24^-$ cells in MCF7 and MCF10A cell lines, these populations were also able to self-renew, produced both $CD44^+/CD24^-$ and $CD44^+/CD24^+$ cells, and were more tumorigenic *in vivo* [92]. They were also shown to have increased ALDH and ABC transporter activity through the Aldefluor and Hoechst-efflux assays, respectively [92]. Overexpression of *Twist2* in MCF7 and MCF10A cells resulted in increased migration, colony formation, and tumour formation *in vivo* [93]. Additionally, the $CD44^{high}/CD24^{low}$ population increased from 2.43 and 7.5% to 15.04 and 35.65% in MCF7 and MCF10A cells, respectively [93]. This was accompanied by increased self-renewal, and an increased expression of the stemness genes *Bmi1* and *Sox2* [93].

Taken together, these findings suggest that TIC capacity is inextricably linked to metastatic potential. TICs may very well be intrinsically primed to acquire metastatic ability through EMT. Conversely, the plastic state of cells undergoing EMT may prime them for acquisition of TIC capacity. It is clear that this relationship exists, and necessitates the need to identify the MIC population.

1.6 Brain metastasis

Brain metastases, the result of a primary cancer metastasizing to the brain, are the most common brain tumour in adults [94], developing in just under 10% of adult cancer patients [95]. Schouten and colleagues identified the most common primary tumours of brain metastasis origin as lung (67.2%), breast (18.1%), melanoma (5.2%), renal (5.2%), and colorectal cancers (4.3%) [95]. It is estimated that by 2010, the incidence of brain metastasis will have surpassed 200,000 cases per year in the United States [96], an incidence that could be anywhere from four to ten times that of primary brain tumours [94, 96]. The true incidence of brain metastasis is likely underestimated. This is likely due to a lack of reporting, either because the metastasis was asymptomatic, and therefore undetected; or because the primary tumour is often the only pathology recorded in autopsy reports, discharge papers, cancer databases, etc. [97].

It is not the incidence of brain metastasis that is alarming, but the poor patient prognosis. Once a tumour has metastasized to the brain, death is inevitable. Even with aggressive treatments, median patient survival time is still reduced to months [96-97]. When examined over a period of 25 years, this poor survival translates to 4.25 million deaths of cancer patients with brain metastases [96]. Surprisingly, despite the high rate of brain metastasis-associated mortality, there is very little research being conducted in this area. This lack of research and staggeringly low patient survival is indicative that a novel approach to brain metastasis and their treatment is needed.

1.6.1 Brain metastases from the lung

Due to the physiology of circulation patterns, one of the most common origins of brain metastases is from metastatic lung cancer. Lung cancer is classified as non-small cell lung carcinoma (NSCLC) and small cell lung carcinoma (SCLC). NSCLC, comprising close to 85% of all lung cancers [98], is further subclassified as either adenocarcinoma (includes bronchioalveolar carcinoma), squamous cell carcinoma, and large cell carcinoma. The different lung cancer subtypes are located in different regions of the lung, and are thought to arise from the normal lung stem cell compartment specific to that region. Squamous cell carcinomas occur in the trachea and proximal bronchi, and are thought to resemble tracheal basal progenitors that are $KRT5^{+}/KRT14^{+}/p63^{+}$ [99]. Adenocarcinomas are believe to originate from the bronchioalveolar stem cells (Clara cell specific protein and surfactant protein C positive, $CCSP^{+}/SPC^{+}$) [100] of the bronchioalveolar duct junctions and alveoli, and present with a glandular morphology [101]. However, $CCSP^{+}/SPC^{+}$ cells were later found to not identify the stem-like population in this region of the lung [102]. SCLC tends to be located in the distant bronchi and mid-level bronchioles, and is thought to arise from the neuroendocrine progenitors of that region [103]. Most recently, CD133 has been used to identify lung TICs in SCLC and several subtypes of NSCLC; however, this has not been correlated with any previously established normal lung stem cell population [11]. The variety of lung stem cell markers makes it difficult to assess the role of these putative populations in the development of brain metastases.

Lung cancer is the most common cancer-related death in men, and second most common in women [98]. This is due to the rapid progression of the disease, where patients often present with local lymph node or distant organ metastases during or shortly after the initial diagnosis [98]. Brain metastases can present within several months to a few years after diagnosis, and are fatal [95, 104]. Anywhere from 25% to 50% of patients with lung cancer develop brain metastases [104-107]. Brain metastases from the lung can arise from any of the primary lung tumour subtypes, and are diagnosed by morphology and immunohistochemistry (IHC) marker panels, indicating the primary tumour of origin. Brain metastases are most commonly from a primary lung adenocarcinoma [106], and exhibit the glandular morphology of the primary tumour, as well as expression of thyroid transcription factor 1 (TTF1) [108-109]. Development of brain metastases is extremely predictive of poor survival of lung cancer patients, with median survival often limited to 2-5 months [104, 110]. While patients with brain metastases can be treated with surgical removal of the tumour, this is most often only done for the rare number of patients presenting with few tumour masses of a small size; the remaining, non-surgical candidates may receive chemotherapy and/or radiation, but this is mainly palliative and largely ineffective [110].

1.7 Rationale

Given the invasive and deadly nature of brain metastases, it is evident that additional insight as to the mechanism of brain metastasis formation is necessary. The process of metastasis requires the capacity of a rare population of cells to establish the growth of a

heterogenous tumour, complete with supportive vasculature [44]; this resembles the CSC model, where a rare TIC population is capable of initiating growth of an entire tumour. Indeed, several groups have now shown associations of metastasis and migratory properties with markers and properties of a CSC population, particularly in breast cancer models [38, 46-49]. Additionally, several reports of organ-specific metastasis gene signatures are also suggestive of a population of cells in the primary tumour are primed for metastasis [52-54, 56-57]. However, clear evidence as to whether these associations are indicative of a MIC population has yet to be shown.

Due to these associations of CSC-properties and metastasis, this work employs previously established BTIC models to determine the presence of CSC- and TIC-like cells in brain metastases. Focus will be on brain metastases of primary lung cancer origin, as this is the site most commonly metastasizing to the brain. Additionally, any previous and current work on brain metastasis has been restricted to breast cancer models, suggesting that alternative sources of brain metastasis have yet to be explored. Furthermore, it is hoped that this work could be relevant and translatable to other origins of brain metastases, and perhaps to the metastatic process in general.

1.8 Hypothesis

It is hypothesized that a subpopulation of cells, termed brain metastasis-initiating cells (BMICs), are responsible for the initiation and maintenance of brain metastases from primary lung cancer. Using clinically obtained patient samples of brain metastases from

the lung, and a commercially available cell line (NCI-H1915) of the same origin, this Thesis work aims to:

1) Assess CSC-like characteristics of brain metastases from the lung *in vitro* through self-renewal and differentiation assays, including expression of known BTIC markers;
2) Demonstrate tumour formation capacity *in vivo* in a human-mouse xenograft model;
3) Determine whether known BTIC markers can be used to identify the putative BMIC population, and;
4) Develop a clinically relevant cell line-based model of brain metastasis for future studies of BMIC populations and/or lung-to-brain metastasis.

CHAPTER 2: METHODS

2.1 Clinical sample processing and cell culture

Clinical brain tumour samples were collected from consenting patients under Hamilton Health Sciences Research Ethics Board Approval Number 07-366. Upon collection, samples were mechanically dissociated and subjected to enzymatic digestion in artificial cerebral spinal fluid with 200µL Liberase BlendzymeTM (0.2 Wunisch units/mL, Roche) for 15min at 37°C on an incubator shaker (VWR). Undigested tissue was removed by filtering through a 70µm cell strainer (BD). Red blood cells were removed by using an ammonium chloride solution (RBC Lysis Buffer, Stem Cell Technologies) for 5min at room temperature. Cells were washed with PBS (Hyclone) and subsequently resuspended in complete neural stem cell (NSC) media, and plated in an ultra-low attachment plate (Corning). Complete NSC media is comprised of NSC basal media (1% N2 supplement (Gibco), 0.2% 60µg/mL N-acetylcystine, 2% neural survival factor-1 (Lonza), 1% HEPES, and 6mg/mL glucose in 1:1 DMEM:F12 media (Gibco)), supplemented with 1x antibiotic-antimycotic (Wisent), 20ng/mL hEGF (Sigma), 20ng/mL bFGF (Invitrogen), and 10ng/mL LIF (Chemicon). We also used two cell lines: NCI-H1915 (ATCC) cells were isolated from a brain metastasis of a 61 year-old female with a large cell, poorly differentiated lung carcinoma; BT241 is a lab-derived glioblastoma (GBM) cell line from a 68 year-old female. The NCI-H1915 and BT241 cell lines were also cultured in complete NSC media. Cultures were maintained at 37°C, 5% CO_2, and media was changed every other day, or as needed.

2.2 Sphere formation assay

Tumourspheres were dissociated using 5-10µL Liberase BlendzymeTM in 1mL PBS for 5min at 37°C. Cells were plated at limiting dilution (between 200 to 2 cells per well) in 100µL of complete NSC media in quadruplicate in a 96-well plate. Cultures were left undisturbed at 37°C, 5% CO_2. After seven days, the number of spheres per well were counted for each dilution, and was used to estimate the mean number of spheres per 2000 cells. For clinical samples, this assay estimated secondary sphere formation; whereas, cell lines were passage three or higher.

2.3 Differentiation assay

Single-cell suspensions were prepared as described above. For flow cytometry analysis, cells were plated at a minimum concentration of 100,000cells/well in 3mL of differentiation media (NSC basal media + 20% FBS) in a 6-well plate. For immunofluorescence analysis, cells were grown in 24-well plates at a density of 10,000-25,000 cells per well in 500µL of differentiation media. Cells were cultured at 37°C for 7 days; media was changed every other day. Cultures for flow cytometry analysis were harvested using 0.05% trypsin in 0.53mM EDTA (Hyclone).

2.4 Directed differentiation assay

Single-cell suspensions were prepared as described above. For flow cytometry or PCR analysis, cells were plated at a minimum concentration of 100,000cells/well in 2-3mL of differentiation media (NSC basal media + 10% FBS) in a 12-well or 6-well plate,

respectively. For immunofluorescence analysis, cells were grown in 96-well plates at a density of 2,500 – 5,000 cells per well in 200µL of differentiation media. To direct cells towards a neuronal lineage, retinoic acid (RA; Sigma), diluted in DMSO (Sigma) was added to the cultures to total concentrations of DMSO only, 10µM, 100µM, or 1mM. The astrocytic lineage was directed by adding ciliary neurotrophic factor (CNTF; Chemicon), diluted in PBS, to the media to final concentrations of 10ng/mL or 20ng/mL. Cells were cultured at 37°C for 7 days; media was changed every other day, with fresh RA or CNTF factors added to the culture. Differentiation media (NSC basal media + 10% FBS) only cultures were grown concomitantly to serve as controls. Cultures for flow cytometry or PCR analysis were harvested using 0.05% trypsin in 0.53mM EDTA (Hyclone).

2.5 Immunofluorescence (IF) staining and analysis

Cells were differentiated as described above, and on day 7, were fixed using 2% PFA for 20min. Cells were blocked using 10% goat serum in PBS (Santa Cruz) for 1 hour, and then incubated with primary antibodies to cell surface antigens (diluted in PBS + 1% BSA) overnight at 4°C, followed by washing with PBST (0.01% Tween-20 in PBS). Cells were permeabilized with 0.01% Triton-X (in PBS) for 5min, and blocked a second time. Primary antibodies to internal antigens (diluted in PBST + 1% BSA) were incubated overnight at 4°C, and washed 3x for 5min with PBST. Secondary antibodies were added for 1 hour, and then washed 3x for 5min with PBST. Nuclei were stained with Hoechst (1:20,000 in PBS) for 10min, and washed 1x with PBST and 1x with PBS for 5min each. All steps were performed at room temperature, unless otherwise indicated;

antibody dilutions can be found in **Supplemental Table 1**. 24-well plates were visualized using an Olympus IX81 fluorescence light microscope and Metamorph software at 4x magnification under the "Multi-Dimensional Acquisition" settings of DAPI (50ms), GFP (400ms), and Cy5 (400ms); sufficient fields of view per well were imaged to capture a minimum of 1,000 nuclei. 96-well plates were visualized by the Operetta high-content imaging system (Perkin Elmer) at 10x magnification for DAPI, GFP/Alexa-488, and Cy5/Alexa-647 channel fluorescence; 15 fields of view per well were imaged. Images were analyzed by custom Acapella (Perkin Elmer) scripts, where nuclei were assessed for positivity in the GFP/Alexa-488 and Cy5/Alexa-647 channels. The percentage of positive cells for each marker of interest was calculated as a fraction of the total number of nuclei in each well. Representative images of IF, taken at 10-20x magnification using an Olympus IX81 fluorescence light microscope were processed in ImageJ 1.43 to subtract background, merge, and colourize individual channel images.

2.6 Flow cytometry analysis and cell sorting

The Aldefluor assay (Stem Cell Technologies) was used as a non-immunological method to analyze the ALDH activity of samples, where high enzyme activity is an indication of stem cell populations. The Aldefluor assay was performed according to the manufacturer's instructions. Briefly, 5µL of reconstituted BODIPY-aminoacetaldehyde diethyl acetal (BAAA-DA) is added to $1x10^6$ cells in 1mL of Aldefluor buffer (1:200 dilution); 500µL of this cell-substrate solution is immediately removed and transferred to a tube containing 5µL diethylaminobenzaldehyde (DEAB) which inhibits ALDH and

serves as a negative control. Samples were incubated at 37°C for 45min. Samples were then washed once to remove excess substrate. For extracellular antibody staining, single cells were suspended in 100µL of PBS or Aldefluor buffer (when using Aldefluor assay), and stained with conjugated antibody (see **Supplemental Table 1** for staining information), and incubated for 30min on ice. For intracellular staining, cells were fixed and permeabilized using the CytoFix/CytoPerm kit (BD Sciences), resuspended in 100µL of Perm-Wash Buffer, and incubated with conjugated antibodies for 30min on ice. Isotype controls were similarly prepared. Samples were sorted using a MoFlo XDP Cell Sorter (Beckman Coulter) and analyzed using Kaluza 1.1 software (Beckman Coulter). Gates were determined by isotype and/or DEAB negative (Aldefluor assay) controls. Dead cells were excluded using 7-AAD viability dye. Compensation was performed using mouse IgG CompBeads (BD). Cells were sorted (purify settings) into tubes of NSC basal media, and allowed to equilibrate at 37°C for 1-2hrs post-sort, prior to their use in experiments. Aliquots of sorted populations were taken for purity assessment immediately after sorting. For clonal analysis of single-cells, $CD15^+$ or $CD15^-$ cells were sorted one cell per well of a 96-well plate into 100µL of 25% NCI-H1915 conditioned complete NSC media. Cultures were left undisturbed for 7 days post-sort, and received an additional 50µL of complete NSC media after 7 days.

2.7 Cell survival assay

Single cells were plated at a density of 5,000cells/well in complete NSC or differentiation media in triplicate, in a 96-well plate (100µL/well) for each time point. Alamar Blue

(Invitrogen), a Resazurin-based fluorescent indicator of cell metabolism, was added (20µL) to each well approximately 18hrs prior to the readout time point. Fluorescence was measured using a FLUOstar Omega Fluorescence 556 Microplate reader (BMG LABTECH) at excitation and emission wavelengths of 535nm and 600nm, respectively, according to recommendations given by the manufacturer. Readings were analyzed using Omega analysis software, and were taken at Day 1 and Day 7, with Day 7 results normalized to those on Day 1.

2.8 Quantitative reverse-transcription PCR (qRT-PCR)

RNA was extracted using a Total RNA Purification Kit (Norgen Biotek), as per manufacturer's instructions. RNA was quantified using the NanoDrop Spectrophotometer ND-1000. Complementary DNA (cDNA) was synthesized from 0.5-1µg RNA and qScript cDNA Super Mix (Quanta) by a BIORAD C1000 Thermo Cycler^{TM} (Bio-Rad) using the following protocol: 4min at 25°C, 30min at 42°C, 5min at 85°C, hold at 4°C. qRT-PCR was performed using Perfecta Sybr Green (Quanta) and a BIORAD Chromo4^{TM} quantitative PCR machine (Bio-Rad). Primers and annealing temperatures are listed in **Supplemental Table 2**. Gene expression analysis was done using the $2^{\Delta Ct}$ method, all samples were run in duplicate, and expression levels were normalized to *GAPDH* expression.

2.9 Intracranial injections

Four to eight week old non-obese diabetic severe combined immunodeficient (NOD-SCID) mice were used for *in vivo* experiments, in accordance with our Animal Utilization Protocol. Single cell suspensions of NCI-H1915 cells were prepared as described above; the appropriate number of live cells (determined through Trypan Blue exclusion) were suspended in 10µL of PBS. Animals were anaesthetized using isofluorane gas (5% induction, 2.5% maintenance), and the incision site was prepared. An incision was made in the scalp of the animal to expose the skull, allowing a small hole to be drilled in the skull above the right frontal lobe. A 10µL Hamilton syringe was used to inject the 10µL cell solution. Post-operative suturing and analgesics were given, and animals were observed during recovery for acute complications. Animals were monitored for endpoints suggestive of tumour formation, such as decreased body condition and neurological symptoms, or 6 months post-injection if no such indications developed. Upon reaching endpoint, animals were sacrificed through perfusion or Avertin overdose. The brains of perfused animals were harvested and embedded in paraffin for hematoxylin and eosin (H&E) staining; images were taken using an Aperio Slide Scanner and analyzed using ImageScope v11.1.2.760 software (Aperio). The brains of non-perfused animals were processed for tissue culture, as described for the processing of clinical samples. Complete NSC media selected for the human NCI-H1915 cells after a week of culture; this was confirmed with flow cytometry analysis of anti-human EpCAM staining. Tumour-derived NCI-H1915 cells were then subjected either *in vitro* assays, or re-injected into new animals to assess serial transplantation capacity.

2.10 Intrathoracic injections

Four to eight week old NOD-SCID mice were used for *in vivo* experiments, in accordance with our Animal Utilization Protocol. Single cell suspensions of NCI-H1915 cells were prepared as described in above. The appropriate number of live cells (determined through Trypan Blue exclusion) were suspended in 75µL of Matrigel solution (1:2 Matrigel in PBS, i.e. 25µL Matrigel + 50µL PBS). Intrathoracic injections were performed as described by Onn *et al* [111]. Animals were anaesthetized using isofluorane gas (5% induction, 2.5% maintenance), placed on their right side, and left flanks were shaved. A 30G insulin syringe (0.5mL volume) was used to inject cells into the left lateral thorax, by inserting the needle just below the inferior border of the scapula, in the middle of the flank [111]. The needle was advanced 5-7mm straight into the thorax, and cell suspension quickly injected [111]. After injection, the mouse was turned onto its left side, and observed closely for at least 45min post-injection, in case of acute complications. Animals were then monitored for endpoints suggestive of tumour formation, such as decreased body condition, difficulty breathing, and/or neurological symptoms. Upon reaching endpoint, animals were sacrificed through perfusion. The brains of perfused animals were harvested and embedded in paraffin for H&E staining.

2.11 Transcriptome analysis

RNA was extracted using the Qiagen RNeasy Micro Kit (Qiagen), as per manufacturer's instructions. Total RNA was quantified using UV spectroscopy (NanoDrop). Approximately 5-10µg of total RNA at a concentration greater than 100ng/µL were

required for RNA-sequencing. Isolated total RNA was shipped to the Michael Smith Genome Sciences Centre (BC Cancer Agency, British Columbia) for RNA-sequencing (RNA-Seq) using the Illumina sequencing platform. The RNA-Seq expression data were generated on the Illumina Genome Analyzer according to manufacturer's instructions and raw reads were processed as previously described [112]. Briefly, the reads were aligned to the reference human genome (HG18) and a database of known exon-exon junctions using Burrows-Wheeler analysis (BWA) [113]. The differential expression analysis was conducted using the LIMMA Bioconductor package [114] based on square root-transformed RPKM (reads per kilobase mapped) values computed for each gene [115]. Genes found to be overexpressed in brain metastases were ranked according to their ability to predict patient survival in a dataset of 226 primary lung tumour samples (GSE31210) [116] using receiver operator characteristic (ROC) curve analysis [117]. Raw Affymetrix .CEL files (Affymetrix Human Genome U133A Array) were downloaded from the Gene Expression Omnibus (http://www.ncbi.nlm.nih.gov/geo/, GSE31210), and normalized using robust multi-array analysis (RMA) [118]. Associated clinical data were also downloaded from the same location. Genes with an AUC (area under the curve) value > 0.5 and $p \leq 0.05$ were considered significantly associated with outcome. Survival analysis was completed using Kaplan-Meier survival curves, where the median value of the probe set was used as a cut-point to discriminate patients into either good or poor outcome groups. To evaluate candidate genes as a gene set, the expression values for each probe set were transformed such that the mean and standard

deviation were set to 0 and 1 in each dataset, respectively. A target index was calculated for each patient as follows:

$$\frac{\sum_{i \in P} x_i}{n_P}$$

Where x is the transformed expression, n is the number of probe sets, and P is the set of probe sets under analysis [119-120]. Finally, Log-Rank tests were used to measure differences between survival to predict good and poor outcome groups.

2.12 Statistical analyses

Statistical analyses were performed using GraphPad Prism 5. Two-tailed *t*-tests were used for comparisons of sphere formation. Multi-variant ANOVA with Bonferroni post-hoc tests were used for comparisons of flow cytometry results between cell lines and different culture conditions, as well as for sphere formation of sorted populations at different passages, and cell survival analysis. Survival curve analysis was performed using the Log-Rank (Mantle-Cox) test. Statistical significance was set at $p<0.05$.

CHAPTER 3: RESULTS PART I

Assessment of cancer stem cell properties in the NCI-H1915 cell line compared to clinically obtained patient samples

3.1 Clinical samples and NCI-H1915 cells grow as tumourspheres when cultured in neural stem cell conditions, but show variable sphere formation capabilities

It has previously been shown that primary brain tumours, such as glioblastoma (GBM) possess a cancer stem cell (CSC) [4, 6, 42] and brain tumour-initiating cell (BTIC) [5, 34] population. Other primary solid tumour types, such as breast [7-8], colon [9-10, 14], and lung [11] cancer have also been shown to have CSC subpopulations. Based on these observations, and the fact that brain metastases derive from a limited number of primary tumour cells [45, 121], it was hypothesized that brain metastases may also possess a stem-like population, capable of self-renewal and multi-lineage differentiation.

Clinical samples of high-grade primary brain tumours (i.e. GBM) and brain metastases originating from the lung were cultured in NSC media conditions (sample information in **Supplemental Table 3).** When in culture, it was observed that the primary brain tumours and brain metastases had a similar capacity to form secondary tumourspheres, where secondary sphere formation is a hallmark of the stem cell property of self-renewal [1]. GBMs demonstrated an average sphere formation capacity of 19 spheres/2000 cells ± 12.55, which was not significantly different from that of brain metastases: 33 spheres/2000 cells ± 33.40 (*p=0.5306*) (**Figure 4A**).

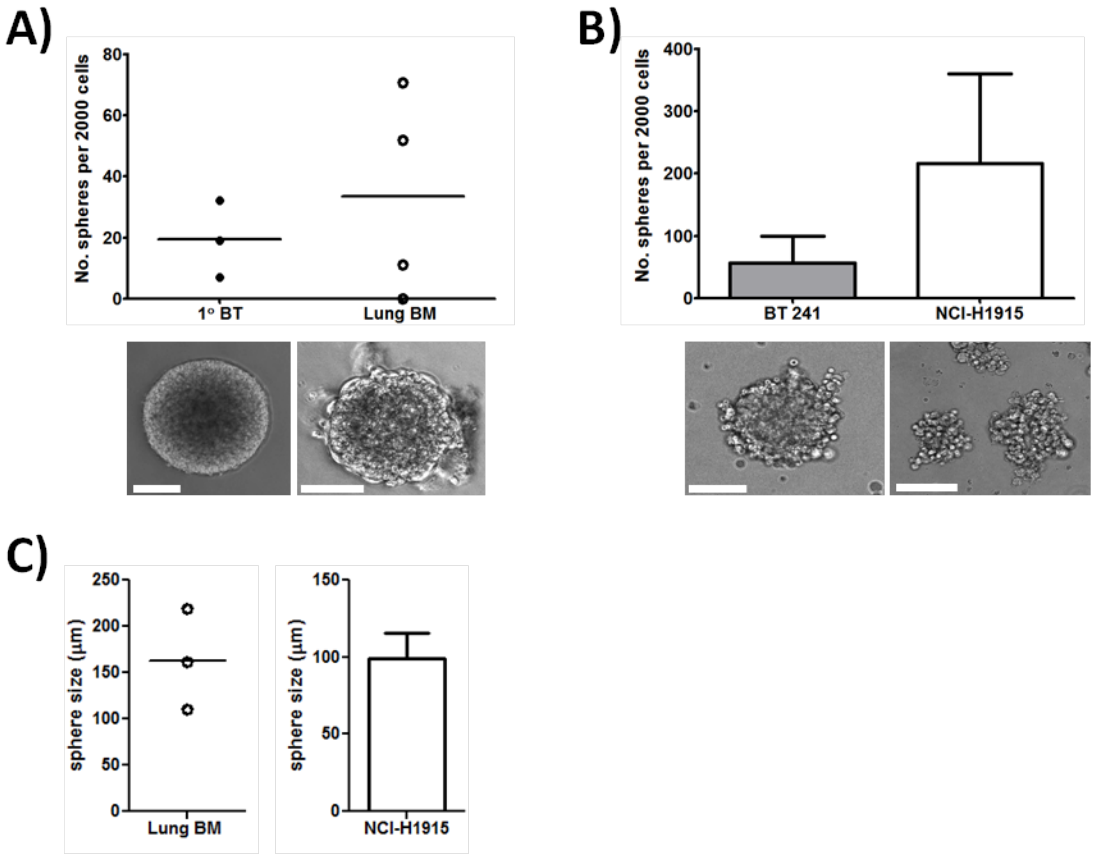

Figure 4: Clinical samples and cell lines of primary brain tumours and brain metastases have similar sphere-forming capacities. Cells were plated at limiting dilution to estimate sphere-forming capacity per 2000 cells. Corresponding bright field images of representative spheres are shown below each graph. Scale bar is 100µm. **(A)** Sphere formation of clinical primary brain tumours (GBM; *n=3*: BT41, BT47, BT82), and clinical brain metastasis (from lung; *n=4*: BT199, BT219, BT222, BT256) samples obtained from brain tumour patients. Each dot is representative of one clinical sample; bar represents biological mean. **(B)** Sphere formation of cell lines BT241 (GBM cell line) and NCI-H1915 (lung-to-brain metastasis cell line). Results of three independent experiments are shown, and presented as mean ± SD. **(C)** Sphere size was measured 7 days post-sample collection (clinical samples) or passage (NCI-H1915 cell line) for six spheres per sample (left panel) or experiment (right panel). Left panel: each dot represents the mean sphere size for a single patient sample; bar represents biological mean (*n=3*: BT390, BT391, BT397). Right panel: results of three independent experiments are shown, and presented as mean ± SD (*n=3*). BT, primary brain tumour; BM, brain metastasis.

Due to the limitations surrounding the use of clinical samples (e.g. low cell number, low viability, unpredictable acquisition), this work was supplemented with representative cell lines. This also served to test the validity of future cell line use as a model system for the study of brain metastasis. The NCI-H1915 cell line is derived from a brain metastasis originating from a lung tumour, while BT241 is a lab-derived GBM cell line. NCI-H1915 cells were originally grown adherently in RPMI (with 10% FBS) conditions, and were characterized prior to and after growing them in NSC conditions (**Supplemental Figure 1**). Like their clinical counterparts, when in NSC conditions both cell lines formed spheres. However, the capacity for secondary sphere formation was much higher than the minimally-cultured clinical samples: BT241, 57 spheres/2000 cells ± 42.30; NCI-H1915, 217 spheres/2000 ± 143.50 (*p=0.1384*) (**Figure 4B**). The increased ability to form secondary or higher spheres is likely due to their ability to be propagated as a cell line, and is not entirely unexpected as several groups have documented increased stem cell frequency and proliferation with prolonged culture [122-123]. Despite this increase in sphere formation capacity, NCI-H1915 cells had a similar sphere size as the clinical brain metastases: 99.07µm ± 16.80 and 164.4µm ± 76.91 respectively (**Figure 4C**). Together, these data suggest that while there may be an enhanced stem cell-like compartment in the cell line, NCI-H1915 cells may be an appropriate system for studying self-renewal among brain metastases originating from the lung, when corroborated by data from clinical samples.

3.2 Known brain tumour-initiating cell markers are variably expressed by clinical samples and NCI-H1915 cells

Primary brain tumour CSC and BTIC populations have previously been identified using CD133, CD15, and Aldefluor (ALDH activity), where positive populations possess increased self-renewal, hierarchical differentiation, and tumour-initiating capacities [4-6, 34, 42]. Presence of these BTIC markers in brain metastases would be further suggestive of the presence of a stem-like population.

Clinical brain metastases were analyzed for their expression of known BTIC markers using flow cytometry. All three markers selected for subpopulations within the samples, but to varying degrees. $CD133^+$ and $Aldefluor^+$ cells were relatively small populations, 9.7% ± 11.8 (*n*=5) and 10.8% ± 15.8 (*n=5*), respectively (**Figure 5A&C**). CD15 on the other hand, selected for an average of 39.2% ± 33.3 (*n*=7) of cells, but with much more variability (**Figure 5A&C**). When looking at the same populations within the NCI-H1915 cell line, only 0.05% ± 0.08 of cells were positive for CD133 (**Figure 5B&D**). Aldefluor and CD15 demonstrated much more positivity (36.6 ± 20.2, and 14.8 ± 8.1, respectively; **Figure 5B&D**). However, only CD15 appeared to select for a semi-distinct population (**Figure 5D**, left panel; **Supplemental Figure 2**, left panels), compared to the whole population shift seen when using Aldefluor (**Figure 5D**, right panel). On average, CD15 was expressed in a comparable population of cells in both the NCI-H1915 cell line and clinical samples (**Figure 5A&B**; **Supplemental Figure 2**, left panels); any discrepancies are likely attributed to the variability among individual patient tumours.

Interestingly, unlike CD133 [9-11] and Aldefluor [14, 16, 24, 37-38], CD15 has yet to be shown to select for epithelial TICs, which may be suggestive of a population within the primary tumour primed for growth in the neural microenvironment. Further prospective-sorting experiments would need to be done in order to confirm whether CD15 does indeed select for a TIC-like population in brain metastases (see **Chapter 4: Results Part II**).

It is recognized that there are substantial differences in BTIC marker-positive populations between the NCI-H1915 cells and the clinical samples. However, the proportions of CD133, CD15, and Aldefluor positive cells in the cell line and clinical brain metastases are all within or close to the range of the respective established BTIC populations [4-6, 34, 42]. It should be emphasized that a single cell line is not necessarily representative of all the variation seen among patient tumours. However, the similar behaviour of NCI-H1915 cells to clinical brain metastases suggests that it could be used appropriately in models where use of clinical samples would be impractical, particularly for the functional examination of the $CD15^+$ population in brain metastases.

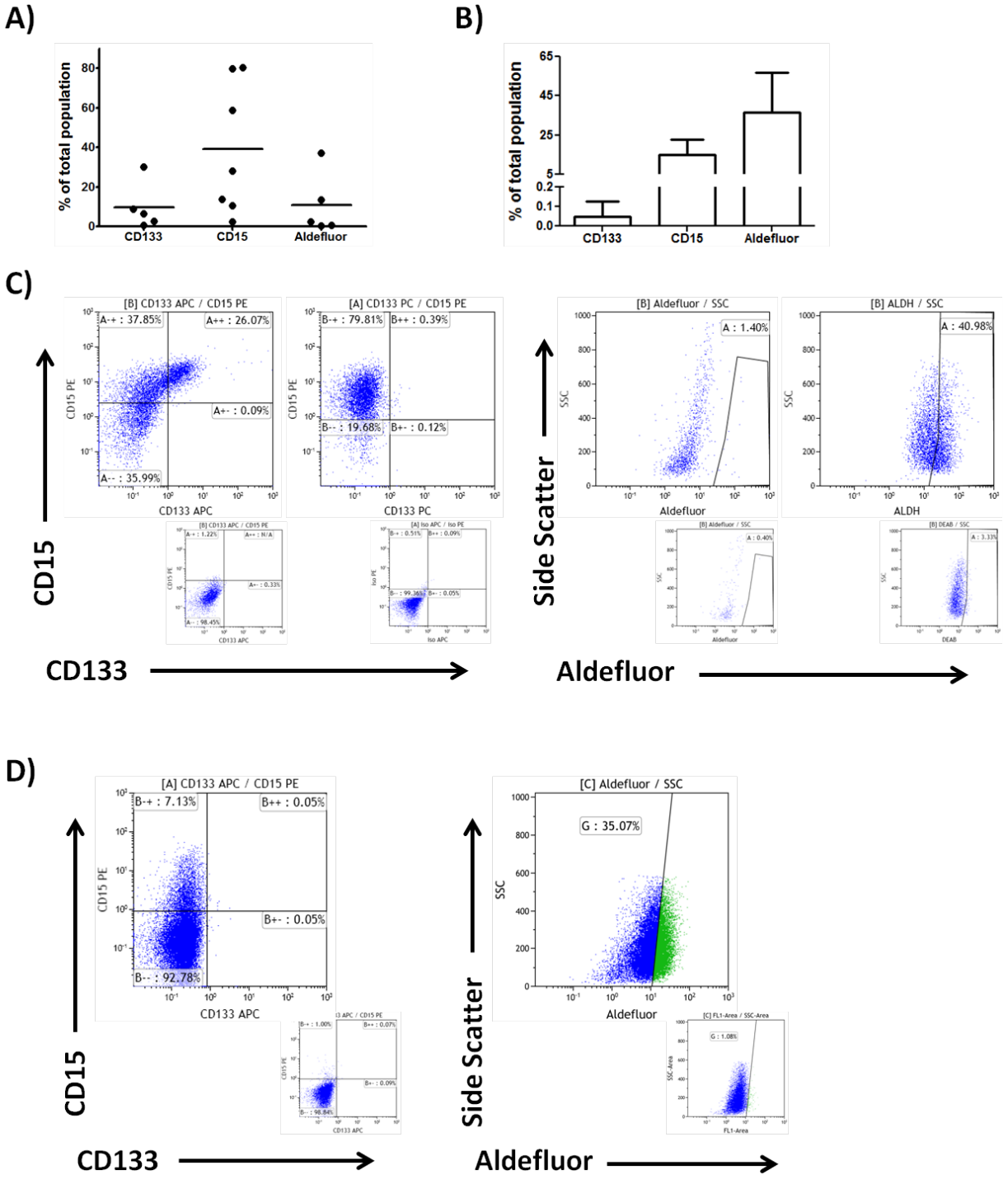
A)
% of total population
CD133
CD15
Aldefluor
B)
% of total population
CD133
CD15
Aldefluor
C)
[B] CD133 APC / CD15 PE
A-+ : 37.85%
A++ : 26.07%
A+- : 0.09%
A-- : 35.99%
[A] CD133 PC / CD15 PE
B-+ : 79.81%
B++ : 0.39%
B-- : 19.68%
B+- : 0.12%
[B] Aldefluor / SSC
A : 1.40%
[B] ALDH / SSC
A : 40.98%
CD15
CD133
Side Scatter
Aldefluor
D)
[A] CD133 APC / CD15 PE
B-+ : 7.13%
B++ : 0.05%
B+- : 0.05%
B-- : 92.78%
[C] Aldefluor / SSC
G : 35.07%
CD15
CD133
Side Scatter
Aldefluor

Figure 5: BTIC markers CD133 and ALDH are differentially expressed in clinical brain metastases and the NCI-H1915 cell line. Samples were stained with CD133-APC, CD15-PE, and/or Aldefluor, and assessed by flow cytometry. **(A)** Clinical brain metastases (from lung) cultured in NSC media conditions. Each dot represents the percent positive for a single clinical sample; bar represents biological mean: CD133, *n=5* (BT219, BT222, BT291, BT296, BT381); CD15, *n=7* (BT219, BT222, BT291, BT296, BT381, BT382, BT390); Aldefluor, *n=5* (BT296, BT298, BT382, BT390, BT397). **(B)** The NCI-H1915 brain metastasis (from lung) cell line was cultured in NSC media conditions. The results of three independent experiments are shown as mean ± SD. Representative flow plots of **(C)** clinical samples (left to right) BT219 and BT381 (CD15 & CD133), and BT296 and BT390 (Aldefluor), and the **(D)** NCI-H1915 cell line are shown. Plots from left to right are CD15-PE/CD133-APC, and side-scatter/Aldefluor, respective isotype and DEAB controls are show below the corresponding flow plot.

3.3 Clinical samples and NCI-H1915 cells minimally co-express neural lineage and lung/epithelial markers when exposed to differentiation conditions

Previous studies of primary BTICs demonstrated their ability to respond to neural differentiation cues *in vitro*, producing astrocytes, neurons, and/or oligodendrocytes [4, 34]. To assess the differentiation capacity of brain metastases, clinical brain metastasis samples were subjected to differentiation conditions, then stained with antibodies against microtubule-associated protein 2 (MAP2, neuronal marker), glial fibrillary acidic protein (GFAP, astrocyte marker), epithelial cell adhesion molecule (EpCAM), and thyroid transcription factor 1 (TTF1), followed by labeling with fluorescent secondary antibodies. Positive cells were counted and percentage of total nuclei was calculated. Positivity was based on fluorescence thresholds established through staining of positive and negative controls (**Supplemental Figure 3**). The majority of clinical brain metastases

(*n=4*) were strongly positive for EpCAM, with a mean expression level of 33.13% ± 26.44, and had variable, weak nuclear TTF1 staining (1.41% ± 1.30) (**Figure 6A**; **Supplemental Table 4)**. All samples had little to no expression of MAP2 (0.11% ± 0.16) or GFAP (0.013% ± 0.016), where only a few individual cells per field of view were positive for either marker (**Figure 6A**; **Supplemental Table 4**). Any cells expressing MAP2 or GFAP were independent of EpCAM or TTF1 expression (**Figure 6D**; **Supplemental Table 4**), suggesting that any MAP2 or GFAP positivity may be due to infiltrating host cells, as brain metastases have been observed to recruit and interact with cells of the host niche [124-125]. Due to limited cell numbers and poor viability, assessment of marker expression by flow cytometry for clinical samples was not possible.

Differentiation experiments were also performed on NCI-H1915 cells, with expression levels of EpCAM, TTF1, GFAP, and MAP2 assessed by flow cytometry. NCI-H1915 cells were almost completely positive for EpCAM and TTF1, and had minimal, weak expression of GFAP and MAP2, 7.4% ± 3.5 and 2.7% ± 0.91, respectively (**Figure 6B**). It was also observed that NCI-H1915 cells expressed similar levels of mature lineage markers and CSC markers whether grown in differentiation or NSC conditions (**Supplemental Figure 4**), suggesting they may be refractory to passive differentiation, and may require directed differentiation to assess their full neural lineage potential. The co-expression of GFAP and MAP2 with TTF1 and EpCAM by flow cytometry in NCI-H1915 cells was confirmed with IF analysis (**Figure 6C**; **Supplemental Table 5**). This may suggest expanded differentiation potential in brain metastases, as expression of

markers of the primary tumour with mature neural lineage markers is not a property of primary epithelial or brain tumours.

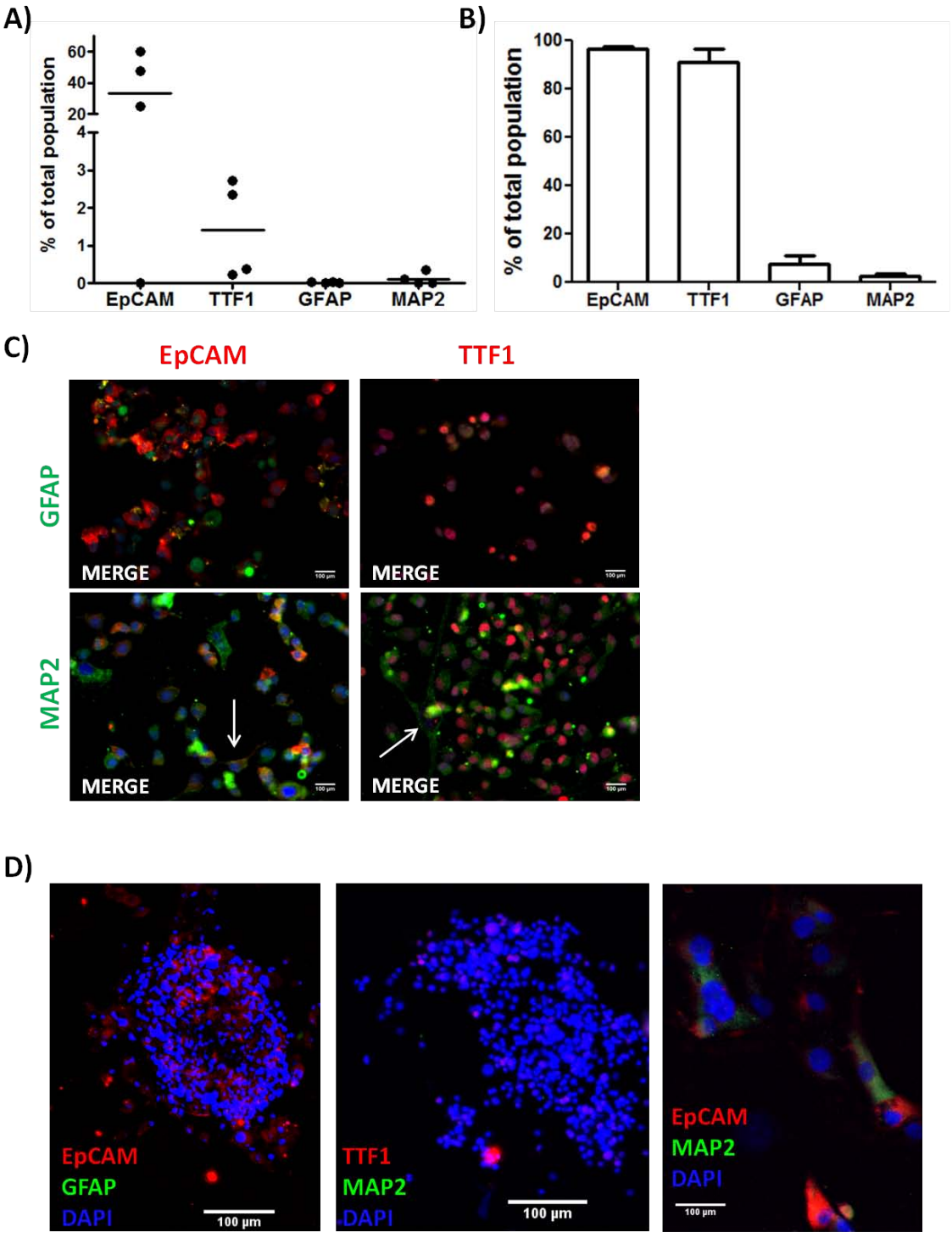

Figure 6: NCI-H1915 cells and clinical brain metastases variably express epithelial (EpCAM) and lung cancer diagnostic (TTF1) markers, and have little to no expression of neural markers when cultured in differentiation conditions. Clinical samples and NCI-H1915 cells were cultured in differentiation conditions for seven days prior to analysis by flow cytometry or IF staining. **(A)** Clinical samples were stained with primary antibodies to EpCAM, TTF1, GFAP, and MAP2, followed by appropriate fluorescently-labeled secondary antibodies. Fluorescence was quantified using Acapella software. Each dot represents the percent positive for an single clinical sample; bar represents the biological mean (*n=4*: BT222, BT312, BT324, BT364). **(B)** NCI-H1915 cells were assessed by flow cytometry for EpCAM, TTF1, GFAP, and MAP2 expression. Results are presented as the mean ± SD of three independent experiments. **(C)** Representative images of IF staining of NCI-H1915, demonstrating the co-expression of epithelial (EpCAM) and primary lung tumour (TTF1) markers with neural lineage makers (MAP2, GFAP). White arrows indicate cells with a neuronal morphology, co-expressing EpCAM or TTF1 with MAP2. **(D)** Representative images of IF staining of clinical samples are shown, demonstrating strong expression of EpCAM, and weak expression of other markers (left & middle, BT222; right, BT324). Blue, DAPI; red, EpCAM or TTF1; green, GFAP or MAP2; EpCAM, epithelial cell adhesion molecule; TTF1, thyroid transcription factor 1; GFAP, glial fibrillary acidic protein; MAP2, microtubule-associated protein 2. Scale bars are 100μm.

Primary brain tumours have been shown to produce various mature cell types of their tissue of origin [4, 34], and more recently primary brain tumour CSCs and BTICs have been shown to produce endothelium as part of the tumour vascularisation process [126-127]. From these studies, it could be inferred that brain metastases may also contain a stem-like population capable of expanded differentiation, originating in the primary lung tumour, suggestive of a bipotent or multipotent nature. Alternatively, as found by Morshead *et al*, apparent expanded differentiation potential may be due to cell fusion or contaminating cell types [128], although the latter is much less likely in the case of NCI-H1915 cells, as co-expression of different lineage markers is observed.

To assess the full neural lineage differentiation capacity of the NCI-H1915 cell line *in vitro*, directed differentiation was performed to select for neuronal (using retinoic acid, RA) or astrocytic (using ciliary neurotrophic factor, CNTF) lineages. Using flow cytometry, NCI-H1915 cells were assessed for changes in MAP2 expression after exposure to increasing concentrations of RA; little or no increase in MAP2 expression was seen when compared to 10% FBS only (2.35%) and DMSO (5.11%) controls: 3.36% (10µM), 3.48% (100µM), and 5.45% (1mM) (**Figure 7**). Similarly, no increase in GFAP expression was seen using CNTF: 0% (10% FBS only), 0.15% (10ng/mL), and 0% (20ng/mL) (**Figure 7**). These results were confirmed by qRT-PCR **(Supplemental Figure 5A**). Treatment with RA or CNTF did not show a decrease in the expression of other lineage markers, including EpCAM, TTF1, and those of type II pneumocytes (surfactant protein C, SPC) in NCI-H1915 cells (**Supplemental Figure 5**). These findings indicate that brain metastases are unresponsive to *in vitro* neuronal or astrocytic differentiation cues, as the H9-derived NSC cell line responded as expected upon treatment with RA and CNTF (**Supplemental Figure 6**). Clinical samples were not assessed by directed differentiation as none of the rare neural lineage-expressing cells showed co-expression with lung tumour markers EpCAM and TTF1, suggesting that any perceived expanded differentiation potential may have been an observation restricted to the cell line.

Based on these experiments, it is highly unlikely that the NCI-H1915 cell line possesses a stem cell population with expanded neural lineage differentiation potential. It is quite possible that cell fusion events have occurred in terminally differentiated cells, and that this population is propagated through culture at fixed proportions. What is unclear; however, is whether such fusion events occurred in the primary lung tumour, as there is a small population of neurons within the lungs, or whether EpCAM or TTF1 positive tumour cells have fused with normal neural cells in the brain. Substantial experimental evidence using fluorescent-reporter based lineage tracing throughout the metastatic process, combined with chromosomal analysis is required to determine the source of these cells; however, this is beyond the scope of the current work.

Neither clinical samples nor NCI-H1915 cells demonstrated a significant ability to differentiate into the neural lineages *in vitro*. Furthermore, the evidence suggests that the NCI-H1915 cell line is refractory to both passive and directed differentiation cues, as measured by the expression of neural markers GFAP and MAP2. Aside from the fact that brain metastases do not appear to have *in vitro* neural lineage capacity, the NCI-H1915 cell line is likely not an appropriate model with which to study this stem cell property. It is also possible that brain metastases (NCI-H1915 cells included) do have differentiation potential for other lineages *in vitro*, or that assessment of differentiation *in vivo* may lead to alternate neural lineage observations, as the microenvironment may be more conducive to neural differentiation. Such studies are beyond the scope of the current work; however any examination of these possibilities would require careful observation to ensure that

any mature neural cells detected are of tumour origin, and not simply an artefact of host cell recruitment.

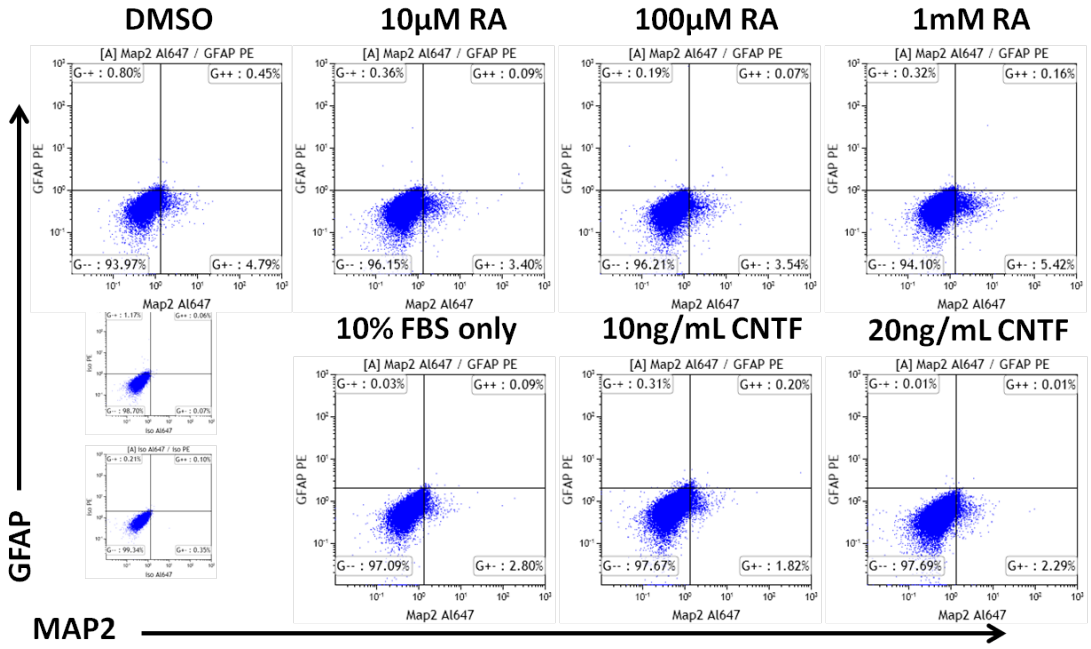

Figure 7: NCI-H1915 cells are unresponsive to directed-differentiation cues for neuronal or astrocytic lineages. NCI-H1915 cells were subjected to directed differentiation using increasing concentrations of retinoic acid (RA; diluted in DMSO), or ciliary neurotrophic factor (CNTF; diluted in PBS) added to basal NSC media +10% FBS. DMSO, and 10% FBS only conditions served as controls. After 7 days, cells were analyzed for their expression of GFAP and MAP2 by flow cytometry. No change was observed in expression of either MAP2 or GFAP in treatment conditions as compared to controls. Plots are GFAP-PE/MAP2-Alexa647; inset, isotype controls for DMSO and RA-treated cells (top), and 10% FBS and CTNF-treated cells (bottom). GFAP, glial fibrillary acidic protein; MAP2, microtubule-associated protein 2.

3.4 Clinical samples and NCI-H1915 cells form multiple focal tumours in NOD-SCID mouse brains after intracranial injection

The gold-standard for identification of a CSC population is serial passage and tumour formation in immunocompromised mice [1]. As such, tumour formation of clinical brain metastases and NCI-H1915 cells was assessed with intracranial injections into NOD-SCID mice. The cell line and clinical samples behaved similarly *in vivo*, forming multiple focal masses seeded throughout the ventricles (**Figure 8A,** i & ii; **Table 2**), despite being injected into the right frontal lobe. This behaviour is consistent with the clinical presentation of brain metastases in patients with metastatic disease, and is reflected in the similarities between patient tumour and clinical xenograft tumour cell morphology and organization (**Figure 8B,** i-iv).

Sample	Cell #	Tumour formation
BT16	100,000	1 / 2
	50,000	2 / 2
BT69	34,000	2 / 4
BT250	100,000	1 / 1
	50,000	0 / 1
BT296	100,000	1 / 2*
BT367	180,000	1 / 1
BT370	21,000	1 / 1*
BT381	200,000	1 / 1†
BT382	275,000	1 / 1†

Table 2: Tumour formation from clinical samples. NOD-SCID mice were subjected to intracranial injection of the indicated numbers of tumour cells. Tumour formation was based on H&E staining of mouse brains upon reaching endpoint or 6 months post-injection. *BT296 & BT370 were observed to have tumour cell infiltration into the cerebellum with no tumour mass formation; †BT381 & BT282 cells were injected into 4 week old NOD-SCID gamma mice.

3.5 NCI-H1915 tumour cells are serially transplantable in NOD-SCID mice with an associated decrease in survival

Serial intracranial injections were then performed using NCI-H1915 cells to assess their ability to be serially passaged *in vivo.* Two of the initial (P1) tumours, designated as H1915-A or H1915-B derivatives, were processed and cultured in NSC conditions for one week to select for the human stem-like tumour cells. Selection was confirmed by flow cytometry analysis of anti-human EpCAM staining, as EpCAM is not expressed in normal mouse brain tissue (data not shown). Three mice each were used for injection of 100,000 cells of H1915-A or H1915-B derivatives. One of each derivative from the subsequent (F1) tumours was similarly cultured and injected to give rise to F2 tumours. Serial passage *in vivo* resulted in similar tumour morphology and behavior (**Figure 8A**, iii & iv; **Figure 8B**, v & vi). With each passage, percent survival was significantly decreased (*p=0.0198*, **Figure 8C**), indicating that tumours were forming more quickly through *in vivo* passaging. This may be a result of selection of a TIC population, or an artefact of *in vivo* selection, where cells more adaptable to survival in a mouse neural microenvironment may be selected.

To address the question of *in vivo* selection, sphere formation and expression of known BTIC markers on P1, F1, and F2 tumours for both H1915-A and H1915-B derivatives was examined. If the decrease in survival is due to selection of a TIC population, this should be accompanied by increased self-renewal (sphere formation), maintenance of

expanded differentiation profiles, and possibly an increase in expression of known BTIC markers.

While sphere formation did not consistently increase with each subsequent injection, it was noted that F1 and F2 tumours of both derivatives had higher sphere-forming capacity than the initial (P1) generation (*p=0.2238,* **Figure 8D**). As for BTIC marker expression, CD133 remained less than 1% of the population for all tumours (data not shown); whereas, CD15 positivity decreased with each passage (**Figure 8E**; **Supplemental Figure 7**). This suggests that $CD15^+$ cells are not selected for during serial *in vivo* passaging, and may not be a TIC marker of brain metastases. Alternatively, perhaps the accelerated growth of the serial tumours is due to an increase in the production of bulk ($CD15^-$) tumour cells, as a result of $CD15^+$ cells may be undergoing stem cell depletion, where the stem-like cells divide symmetrically to produce two daughter cells that are more differentiated, and may lose their expression of CD15. This is not in conflict with sphere formation capabilities, as progenitors are also thought to be capable of minimal sphere formation [129].

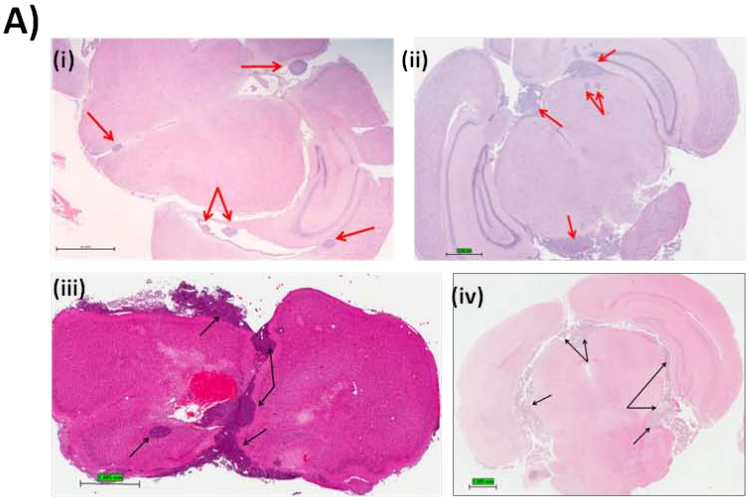
A)
(i)
(ii)
(iii)
(iv)

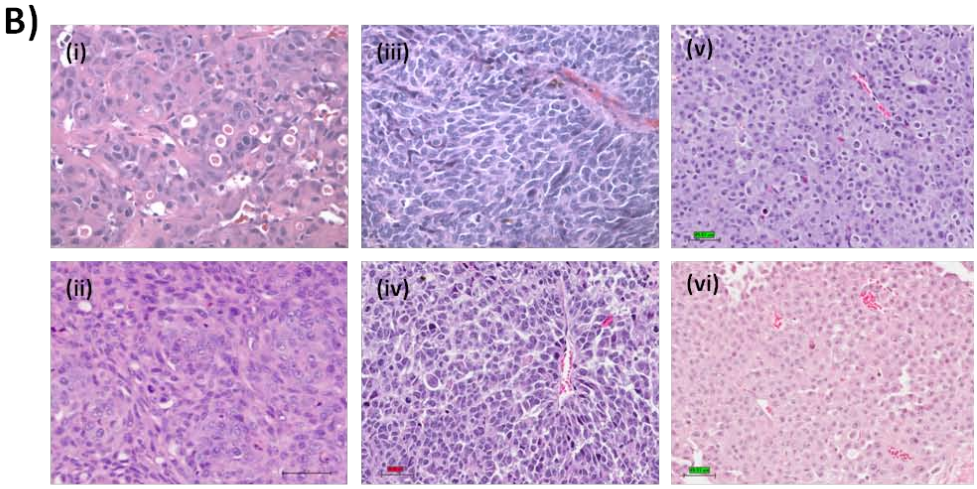
B)
(i)
(iii)
(v)
(ii)
(iv)
(vi)

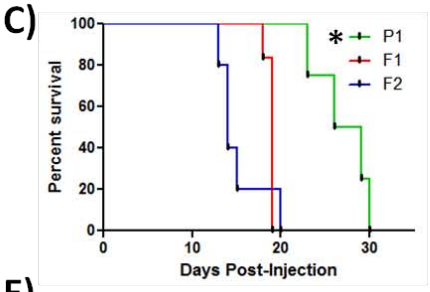
C)
Percent survival
Days Post-Injection
P1
F1
F2
*

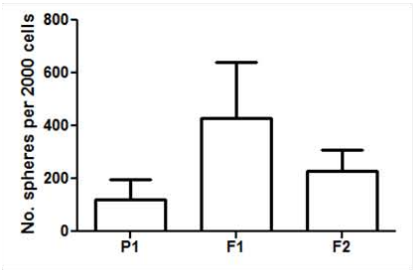
D)
No. spheres per 2000 cells
P1
F1
F2

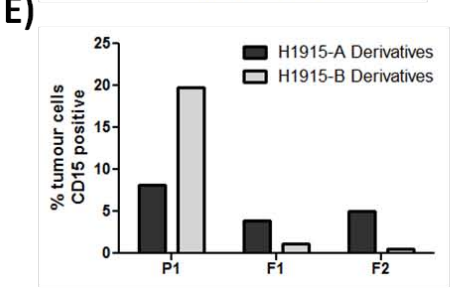
E)
% tumour cells CD15 positive
H1915-A Derivatives
H1915-B Derivatives
P1
F1
F2

Figure 8: Cells from brain metastases are capable of forming serially transplantable tumours when injected orthotopically into the frontal lobes of NOD-SCID mice. (A) Intracranial injection of clinical brain metastases **(i)** and the NCI-H1915 cell line **(ii)** allows for the growth of multiple focal masses seeded throughout the ventricles (red arrows), recapitulating the clinical presentation of patients with brain metastases. Serial injection of the NCI-H1915 cell line demonstrated similar growth patterns to the original tumour; F1 **(iii)** and F2 **(iv)**. Representative H&E stained sections are shown. **(B)** High magnification (40x) of patient tumours BT16 **(i)** and BT367 **(iii)** with their respective xenograft tumours **(ii & iv)** below. P1 **(v)** and F2 **(vi)** NCI-H1915 tumours are also shown, demonstrating cellular organization similar to both patient tumours and clinical xenografts. Scale bars, 50µm. **(C)** Serially injected NCI-H1915 cells resulted in a significant ($p=0.0198$) decrease in overall survival with subsequent injections (F1 & F2, $n=6$), compared to the initial injection (P1, $n=4$). $*p<0.05$. **(D)** Sphere formation of each tumour generation (P1, F1, F2) per 2000 cells. There was no significant difference in sphere-formation ($p=0.2238$). **(E)** After 7 days in complete NSC media, tumour cells were assessed by flow cytometry for expression of the CD15 antigen. Percent $CD15^+$ is shown.

3.6 Summary and interpretation of results

Based on sphere formation and the expression of known BTIC markers, an indication of functional stem-like populations, brain metastases may contain a self-renewing population *in vitro*. Both clinical brain metastasis samples and the NCI-H1915 cell line behaved similarly in NSC conditions in terms of sphere formation and CD15 expression. Differences were noted in the increased self-renewal capacity of the cell line compared to the clinical samples; however, this is likely a product of long-term propagation in culture, allowing for NCI-H1915 cells to still be representative of self-renewal in brain metastases. While CD15 was variably expressed among clinical brain metastasis samples, the mean expression level was similar to that of NCI-H1915 cells, suggesting further

characterization of this marker may be done in this cell line, with minimal corroborating data from clinical samples.

Differentiation studies showed that neural lineage markers MAP2 and/or GFAP were occasionally co-expressed with epithelial and lung tumour markers in NCI-H1915 cells. At first this seemed to be suggestive of a stem-like population with expanded differentiation potential; however, upon exposure to directed differentiation conditions (RA and CNTF), the NCI-H1915 cells showed expansion of either neuronal or astrocytic lineages. This may be explained by the possible occurrence of fusion events in terminally differentiated cells, but the location of such events was not determined. Further confirmation of cell fusion through spectral karyotyping, or similar technique, would also be required; however, this is beyond the scope of the current work.

Intracranial injections into NOD-SCID mice demonstrated tumour formation of brain metastases. Both clinical samples and NCI-H1915 cells behaved similarly in terms of their growth patterns, forming multiple masses throughout the ventricles, cerebellum, and other areas of the brain. NCI-H1915 cells were used to assess the ability of brain metastases to be serially transplanted. The subsequent results are suggestive of a TIC population, as serial tumours demonstrate increased tumour growth, and potentially associated with higher levels of self-renewal. While an increase in TIC markers was expected with each passage, none was seen with the known BTIC markers. The decrease in CD15 expression could be a result of CD15 not being a marker of TICs in brain

metastases (where the unidentified TIC population is actually being enriched), or $CD15^+$ cells undergo stem cell depletion to increase tumour growth. Further sorted experiments using CD15 are needed to determine its role in brain metastases. In summary, brain metastases do not appear capable of *in vitro* neural lineage differentiation, and possess a sphere-forming and tumour-initiating population; however, this population remains to be identified. Use of the NCI-H1915 cell line would be appropriate for identifying such a population based on markers with levels of expression similar to the mean of several clinically-derived samples.

3.7 Caveats and limitations

While the data suggest that the NCI-H1915 cell line is representative of patient-derived brain metastases from the lung, there are several limitations to the use of this model. First, due to the nature of cell lines, NCI-H1915 cells are much more proliferative than those of clinical samples, and due to their long-term propagation in culture, NCI-H1915 cells may also have acquired a larger stem-like population culture [122-123], as evidenced by their enhanced sphere-forming capacity. Similarly, the long-term culture of NCI-H1915 cells may have allowed them to become refractory to differentiation, suggesting they may not be appropriate for differentiation studies, particularly without further marker and assay validation in clinical samples. Their increased proliferative ability makes NCI-H1915 cells attractive for use in prospective flow-sorting experiments, where cell survival is often reduced; thus, making it difficult to use clinical samples, which may have low viability and poor growth prior to sorting.

Secondly, it is important to aware of the fact that like all cell lines, the NCI-H1915 cell line is derived from a single patient, implying that discoveries made with the sole use of the cell line cannot be attributed to the entire population of brain metastases from the lung. This is particularly relevant when assessing the expression of potential population markers. The data regarding BTIC marker expression indicate that only the $CD15^+$ population is suitable for further study using NCI-H1915 cells, as the expression levels and patterns of CD133 and Aldefluor are not representative of the clinical samples studied. Use of alternative markers should be validated in clinical samples and the NCI-H1915 cell line, prior to additional study in the cell line. Proof of functional similarity of the same subpopulations in both clinical samples and the NCI-H1915 cell line would further validate the use of the cell line.

The cell line seems most appropriate for use in examining tumour formation *in vivo*; NCI-H1915 cells form tumours more efficiently and consistently than clinical samples. However, when assessed for their ability to be serially transplanted, it was uncertain as to whether the increased tumour formation rate was due to *in vivo* selection for a subpopulation of cells adapted for survival in the mouse neural microenvironment, or with enhanced tumorigenic potential. This suggests that the third limitation of the model is the use of *in vivo* serial injection as a representation of tumour-initiating capacity. Future use of the the NCI-H1915 cell line *in vivo* may be best suited to the study of various therapies in their ability to inhibit and/or reduce tumour growth of brain

metastases in the brain microenvironment. This approach takes advantage of unlimited supply and proliferative capacity of NCI-H1915 cells, as numerous treatment and control groups would be necessary, and clinical samples are both low in cell number, and refractory to tumour formation *in vivo*.

Use of NCI-H1915 cells is a suitable model for study of brain metastases for assessing sphere formation, examining BTIC marker profiles, and initial tumour formation and treatment. However, limitations of the model include discrepancies in the nature of long-term cell lines and minimally-cultured clinical samples, lack of total patient population representation, and an unspecified propensity for passaging *in vivo*. To compensate for these limitations, the NCI-H1915 cell line should not be used exclusive of clinical samples for the study of brain metastases. Rather, NCI-H1915 cells should be used as a consistent population of cells in all experiments, in effort to supplement the limitations of using minimally-cultured clinical samples.

CHAPTER 4: RESULTS PART II

Use of the NCI-H1915 cell line to examine CD15 as a potential marker of a cancer stem cell population in brain metastases from the lung

4.1 CD15 does not select for sphere-forming populations

It was of interest to test whether any of the known BTIC markers were also capable of selecting for a stem-like population in brain metastases. As CD133 and Aldefluor were extremely differentially expressed between the clinical samples and the NCI-H1915 cell line (CD133: 9.7% ± 11.8 vs. 0.05% ± 0.08 Aldefluor: 10.8% ± 15.8 vs. 36.6% ± 20.2; **Figure 5A&B**), and as they did not identify any distinct populations (CD133: **Figure 5C&D**, left panels; **Supplemental Figure 2**, right panels; Aldefluor: **Figure 5C&D**, right panels), these markers were not explored further. CD15 had comparable expression between the clinical samples and NCI-H1915 cells (39.2% ± 33.3 vs. 14.8% ± 8.1; **Figure 5A&B**), and had a definable positive population in the NCI-H1915 cell line (**Figure 5D**, left panel; **Supplemental Figure 2**, left panel). Furthermore, the $CD15^+$ population increased when NCI-H1915 cells were grown in NSC conditions, as compared to their original RPMI media conditions (**Supplemental Figure 1**), suggesting that CD15 may represent the stem-like population in NCI-H1915 cells. Based on these observations, the brain metastasis model cell line, NCI-H1915, was prospectively flow-sorted into $CD15^+$ and $CD15^-$ populations (**Figure 9A**; **Supplemental Table 6**).

Sorted cells were allowed to equilibrate for one to two hours post-sort at 37°C, prior to the plating of experiments. Sorted cells were plated at limiting dilution in NSC conditions to assess secondary sphere formation. Cultures of $5.0x10^4$cells/mL were simultaneously plated. After seven days post-sort, spheres from cells plated at limiting dilution were counted, and CD15 expression was reanalyzed from dissociated spheres of the larger

cultures. Cells from dissociated spheres were re-plated for tertiary sphere formation at limiting dilution, with the remaining cells re-plated at $5.0x10^4$cells/mL. After an additional seven days (total of 14 days post-sort), tertiary spheres were counted, and CD15 expression was also reanalyzed.

No significant difference in sorted $CD15^+$ or $CD15^-$ cells in terms of secondary or tertiary sphere formation was observed (*p=0.4597*, **Figure 9B**). Secondary (2°) and tertiary (3°) sphere formation capacity was 225.8 spheres/2000cells ± 157.0 and 170.0 spheres/2000 cells ± 59.39 for $CD15^+$ cells, and 436.5 spheres/2000 cells ± 308.0 and 249.4 spheres/2000 cells ± 135.3 for $CD15^-$ cells. While $CD15^-$ cells gave rise to significantly more $CD15^-$ than $CD15^+$ cells in both secondary (84.7% ± 15.3 vs. 12.0% ± 15.4; *p<0.001*) and tertiary spheres (82.4% ± 4.4 vs. 10.6 ± 9.2; *p<0.001*), the percentage of CD15 positivity was similar to that pre-sort (10.9% ± 4.0), (**Figure 9C, Supplemental Figure 8A**). Similarly, $CD15^+$ cells produced both populations, which were almost equally distributed (*p>0.05*) in secondary and tertiary spheres: $CD15^-$ 56.7% ± 29.5 and 58.4% ± 22.4 vs. $CD15^+$ 39.6% ± 28.0 and 31.7% ± 9.2, respectively (**Figure 9C, Supplemental Figure 8A**). These data indicate that both $CD15^+$ and $CD15^-$ cells are capable of producing both populations, where previously it was reported that only $CD15^+$ cells could give rise to both populations [6, 34]. These results suggest that CD15 does not select for the sphere-forming (self-renewal) capabilities observed in brain metastases, nor does CD15 represent hierarchical organization in brain metastases.

It was noted that for the above sorting experiments, the purities of the $CD15^-$ population were on average 97.87% ± 1.66 (**Supplemental Table 6**, Sort No. 1-6), meaning that there could be a 3.79% contaminating $CD15^+$ population that may have been responsible for the stem-like properties observed in the $CD15^-$ population. Single cell clonal analysis was performed to ensure that the small percentage of $CD15^+$ cells in the sorted $CD15^-$ population were not responsible for reconstituting the $CD15^+$ cells 14 days post-sort.

There was no difference in sphere formation of single $CD15^+$ or $CD15^-$ cells at 7 days post-sort (42.0 spheres/2000 cells ± 6.6 vs. 55.9 spheres/2000 cells ± 6.4; $p>0.05$) or 14 days post-sort (38.2 spheres/2000 cells ± 13.6 vs. 51.7 spheres/2000 cells ± 11.5; $p>0.05$) (**Figure 9E**). When CD15 positivity was analyzed by flow cytometry 14 days post-sort, $CD15^+$ and $CD15^-$ single cells were capable of generating both populations, in approximately equal percentages; $CD15^+$ clones produced 33.1% ± 19.7 $CD15^+$ cells and 63.2% ± 24.2 $CD15^-$ cells ($p>0.05$), similar to the $CD15^-$ clones that produced 30.4% ± 18.2 $CD15^+$ cells and 65.5% ± 19.5 $CD15^-$ cells ($p>0.05$), (**Figure 9F**, **Supplemental Figure 8B**). Furthermore, analysis of the growth kinetics of the sorted populations using Alamar Blue showed that $CD15^-$ cells were more viable and proliferative than $CD15^+$ cells 7 days post-sort: 5.97 a.u. ± 1.45 and 3.07 a.u. ± 0.79 vs. 2.62 a.u. ± 0.66 and 1.80 a.u. ± 0.52 (**Figure 9G**), suggesting any contaminating $CD15^+$ population would not be able to increase substantially in the given time period. Together, these results further support that while somewhat heterogeneously expressed, the primary BTIC marker CD15, does not select for a CSC population in brain metastases *in vitro.*

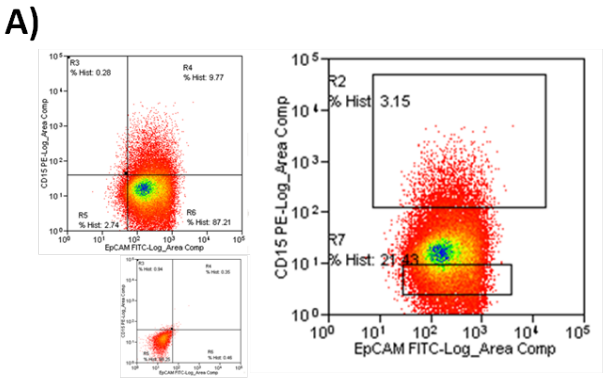
A)
R2
% Hist: 3.15
R7
% Hist: 21.43
CD15 PE-Log_Area Comp
EpCAM FITC-Log_Area Comp

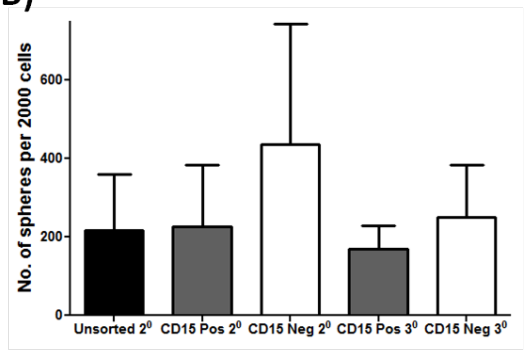
B)
No. of spheres per 2000 cells
Unsorted 2^0
CD15 Pos 2^0
CD15 Neg 2^0
CD15 Pos 3^0
CD15 Neg 3^0

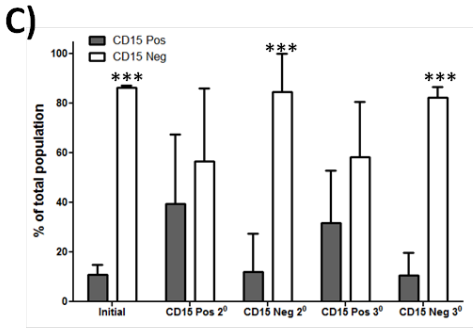
C)
CD15 Pos
CD15 Neg
% of total population
Initial
CD15 Pos 2^0
CD15 Neg 2^0
CD15 Pos 3^0
CD15 Neg 3^0

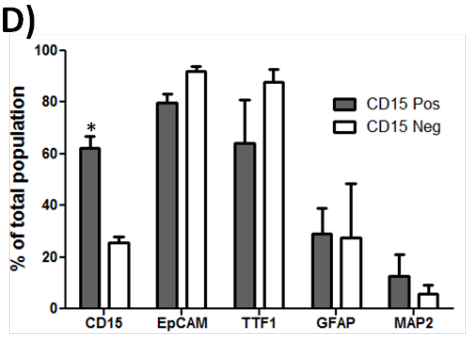
D)
CD15 Pos
CD15 Neg
% of total population
CD15
EpCAM
TTF1
GFAP
MAP2

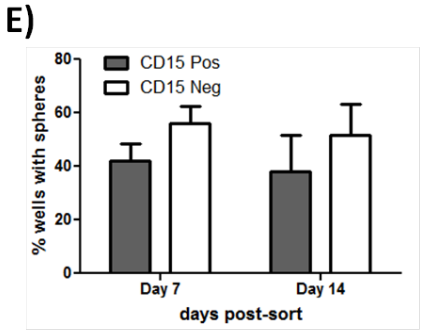
E)
CD15 Pos
CD15 Neg
% wells with spheres
Day 7
Day 14
days post-sort

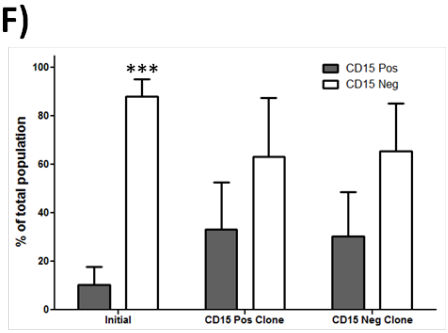
F)
CD15 Pos
CD15 Neg
% of total population
Initial
CD15 Pos Clone
CD15 Neg Clone

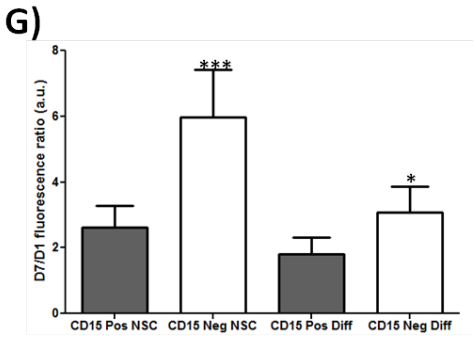
G)
D7/D1 fluorescence ratio (a.u.)
CD15 Pos NSC
CD15 Neg NSC
CD15 Pos Diff
CD15 Neg Diff

Figure 9: CD15 does not select for a sphere-forming population or establish a hierarchy in NCI-H1915 cells. NCI-H1915 cells were cultured in complete NSC conditions, and were flow sorted into $CD15^+$ and $CD15^-$ populations; representative sort gates are shown in **(A)**. All data are presented as mean ± SD of three independent sort experiments. *, $p<0.05$; ***, $p<0.001$ **(B)** Analysis of sphere formation per 2000 cells showed no significant difference in the formation of secondary (2°) or tertiary (3°) spheres between $CD15^+$ and $CD15^-$ cells. **(C)** Both sorted populations were capable of producing $CD15^+$ and $CD15^-$ cells in similar proportions, as assessed by flow cytometry upon formation of secondary or tertiary spheres. $CD15^-$ cells did produce significantly more $CD15^-$ than $CD15^+$ progeny ($p<0.001$), but neither of these progeny populations were significantly different than those produced by $CD15^+$ cells. **(D)** Sorted cells were plated in differentiation conditions, and assessed for their expression of CD15, EpCAM, TTF1, GFAP, and MAP2 seven days later by flow cytometry. The only significant difference in marker expression between $CD15^+$ and $CD15^-$ cells was that of CD15 ($p<0.05$). **(E&F)** Single $CD15^+$ or $CD15^-$ NCI-H1915 cells were sorted into 96 well plates for assessment of clonal properties. **(E)** There was no significant difference in sphere formation between the populations at 7 or 14 days post-sort. **(F)** At 14 days post-sort, clonal spheres were pooled, and reassessed for CD15 expression by flow cytometry. There was no difference in the proportion of CD15 between $CD15^+$ and $CD15^-$ clones. **(G)** Sorted cells were plated in NSC or differentiation conditions for viability and proliferation by Alamar Blue analysis. $CD15^-$ cells grown in NSC conditions were significantly more viable and proliferative than all other populations and conditions ($p<0.001$); whereas, $CD15^-$ cells grown in differentiation conditions were significantly more viable and proliferative than their $CD15^+$ counterparts ($p<0.05$).

4.2 CD15 does not select for cells capable of differentiating into neural lineage marker-expressing cells

While previous data indicated that NCI-H1915 cells were refractory to neural lineage differentiation, suggesting that cell fusion events may have occurred, it was thought that perhaps these cells may be restricted to a single subpopulation, particularly one marked

by an NSC marker. It is possible that the cells co-expressing neural and lung tumour markers may be maintained by a stem-like or progenitor population, as terminally differentiated cells are not propagated in NSC conditions [130]. It was thought that perhaps separation using CD15 would in fact reveal a differentiation potential previously masked by analysis of the bulk population. If this were the case, it could be that only the $CD15^+$ cells would be able to produce the cells expressing MAP2 and GFAP, as CD15 has only been shown to be a stem cell marker in neural [6, 32-34], but not epithelial tissues.

Sorted NCI-H1915 cells were subjected to differentiation conditions. Neural lineage markers MAP2 and GFAP were similarly expressed in $CD15^+$ (12.6% ± 8.5 and 29.1% ± 9.9, respectively) and $CD15^-$ (5.9% ± 3.3 and 27.4% ± 21.2, respectively) differentiated populations (*$p>0.05$*; **Figure 9D**). As expected, expression levels of EpCAM and TTF1 were comparable in differentiated $CD15^+$ (79.9% ± 3.4 and 64.1% ± 16.9, respectively) and $CD15^-$ (91.9% ± 2.1 and 87.6% ± 5.0, respectively), (*$p>0.05$*; **Figure 9D**). Contrary to the hypothesis, both $CD15^+$ and $CD15^-$ cells were able to produce cells co-expressing the neural lineage markers with EpCAM and TTF1 (**Figure 9D**; **Supplemental Figure 8C**). Only CD15 was significantly differentially expressed between differentiated $CD15^+$ (62.2% ± 4.7) and $CD15^-$ (25.5% ±2.3) populations (*$p<0.05$*; **Figure 9D**; **Supplemental Figure 8C**); however, both sorted populations were capable of producing both positive and negative progeny.

This suggests that CD15 does not select for a stem-like population with an expanded differentiation potential, and further supports the conclusion that NCI-H1915 cells lack a population with expanded neural differentiation capacity (see **Results 3.3**). The observations of cells co-expressing markers of different lineages could be the products of fusion of terminally differentiated cells. Due to the proliferative nature of the cell line, it is possible that terminally differentiated cells could be propagated, regardless of culture conditions; alternatively, these cells may still be maintained by a stem-like population, which has yet to be identified.

4.3 CD15 does not select for a tumour-initiating population when sorted cells are injected into NOD-SCID mice

Some recent studies have shown that *in vitro* measures of stem cell-like capacity are not necessarily reflective of tumour-initiating ability *in vivo* [131]. Additionally, some cells may not recognize their full tumorigenic potential until they are in an appropriate niche, surrounded by supporting structures and secreted factors that are difficult to simulate in the *in vitro* culture environment [124, 132-133]. To this end, serial intracranial injections into NOD-SCID mice were performed with CD15-sorted cells to see whether CD15 would fractionate NCI-H1915 cells into functionally distinct populations *in vivo*.

NCI-H1915 cells grown in NSC conditions were flow-sorted for CD15 (**Supplemental Table 6**), and $1x10^4$ $CD15^+$ or $CD15^-$ cells were injected into the frontal lobes of NOD-SCID mice (*n=6* each). Of the initial (P1) tumours, two from each group were collected

for H&E staining, and four were harvested for culture. After one week of selection for NCI-H1915 cells, of one each $CD15^+$ and $CD15^-$ -derived tumours were re-sorted for $EpCAM^+/CD15^+$ and $EpCAM^+/CD15^-$ cells, respectively, and re-injected ($1x10^4$ cells) into new NOD-SCID mice (n=3 each). Upon endpoint, the tumours (F1) were harvested for H&E staining (*n=1*) and culture (*n=2*). This procedure of culturing, sorting, injecting, and harvesting was repeated for an additional generation of mice (F2). Insufficient cells were obtained from the processing of one of the $CD15^+$ -derived F1 tumours; thus, this sample was unable to be used for several of the subsequent experiments.

Both $CD15^+$ and $CD15^-$ cells were able to generate P1 tumours, as well as subsequent F1 and F2 tumours (**Figure 10A**). $CD15^-$ -derived tumours appeared to develop similarly to the typical clinical presentation of brain metastases in patients and the unsorted NCI-H1915 tumours; while a large tumour mass is observed, several smaller focal masses can be seen throughout the ventricles, and tumour cell infiltration is observed near the cerebellar region of the brain (**Figure 10A**, lower panels). $CD15^+$ -derived P1 and F1 tumours also presented with large central masses and several smaller focal masses; however, there appears to be an increase in the amount of tumour cell infiltration near the cerebellum, expanding into the ventricles (**Figure 10A**, upper left & middle panels). The F2 generation of $CD15^+$ tumours did not seem to grow as a large tumour mass, but rather as infiltrating tumour cells in the cerebellum and ventricles (**Figure 10A**, upper right panel), despite the mice presenting with domed craniums as a result of raised intracranial pressure, indicative of tumour growth. It is possible that the F2 tumours harvested for

culture resembled the P1 and F1 tumours, or that the cell infiltration in the ventricles was sufficient to increase intracranial pressure, causing the mice to reach endpoint.

In addition to similar tumour presentation, mice of both $CD15^+$ and $CD15^-$ -derived tumours reach endpoint at approximately the same time in each generation. There was a significant difference in the survival of mice ($p<0.001$); however, this was restricted to between generations, rather than the cells injected (**Figure 10B**). In fact, both $CD15^+$ and $CD15^-$ -derived F2 tumours had the exact same survival proportions over time. The survival data suggest that there is no difference in tumorigenicty of $CD15^+$ or $CD15^-$ cells, and that a similar selection process is occurring with passage *in vivo* in both cell populations as was observed in the unsorted NCI-H1915 injections.

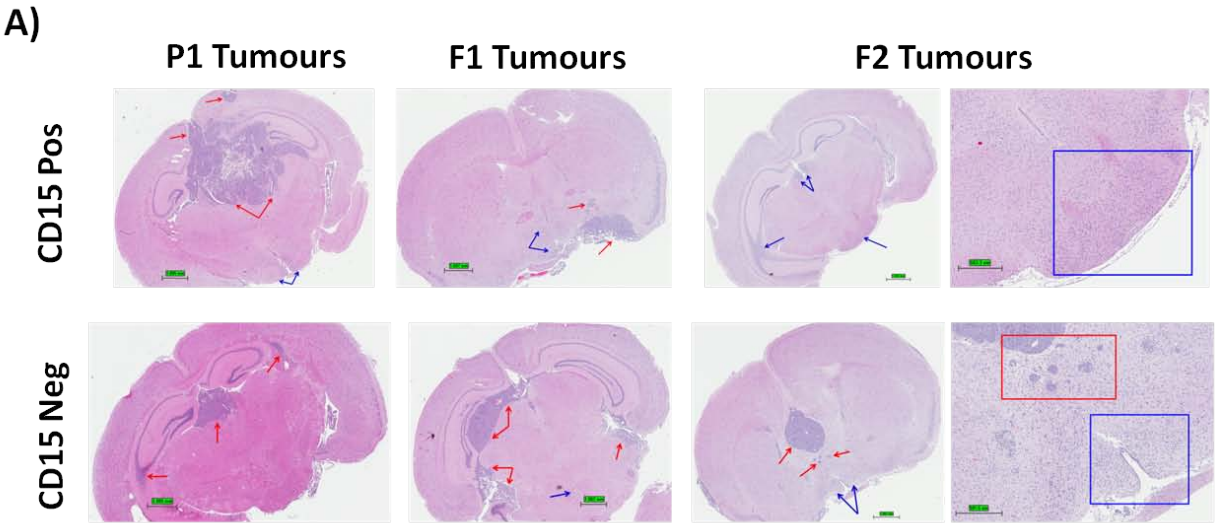
A)
P1 Tumours
F1 Tumours
F2 Tumours
CD15 Pos
CD15 Neg

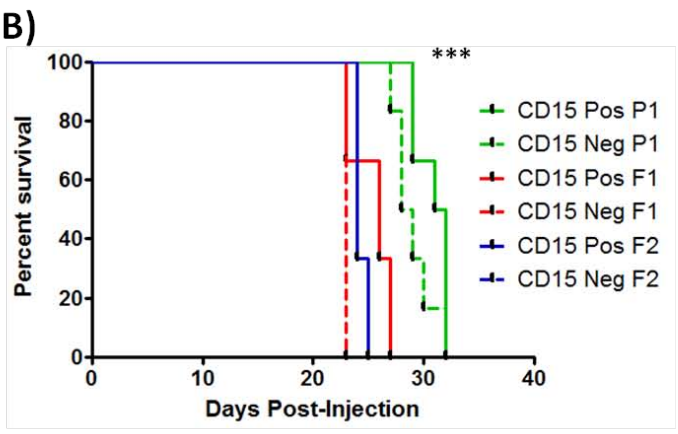
B)
***
Percent survival
Days Post-Injection
CD15 Pos P1
CD15 Neg P1
CD15 Pos F1
CD15 Neg F1
CD15 Pos F2
CD15 Neg F2

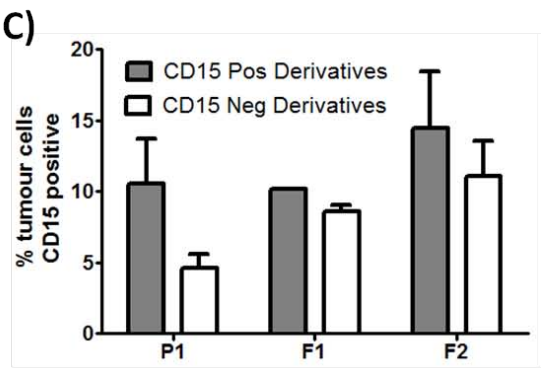
C)
% tumour cells CD15 positive
CD15 Pos Derivatives
CD15 Neg Derivatives
P1
F1
F2

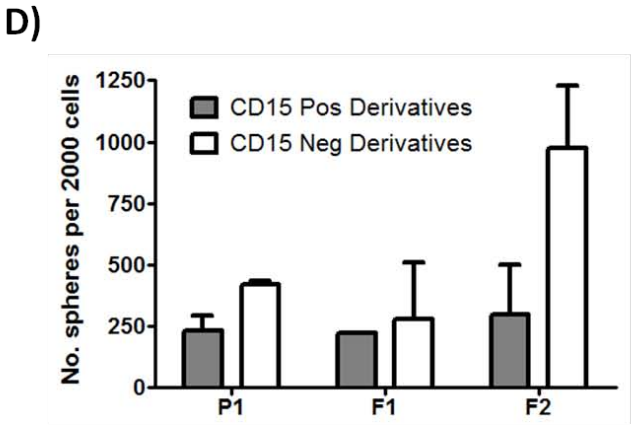
D)
No. spheres per 2000 cells
CD15 Pos Derivatives
CD15 Neg Derivatives
P1
F1
F2

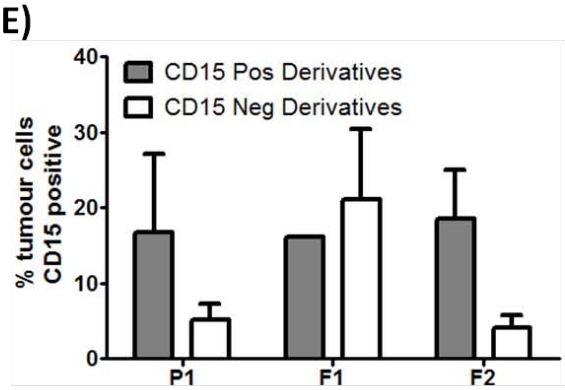
E)
% tumour cells CD15 positive
CD15 Pos Derivatives
CD15 Neg Derivatives
P1
F1
F2

Figure 10: CD15 does not select for tumorigenic potential of NCI-H1915 cells *in vivo*. NCI-H1915 cells cultured in NSC conditions were flow-sorted for CD15, and $CD15^+$ or $CD15^-$ cells were injected ($1x10^4$ cells) into the frontal lobes of NOD-SCID mice. For serial propagate *in vivo*, tumours were collected and cultured in NSC conditions for 7 days, re-sorted, and injected into new mice. **(A)** Some tumours from each generation were collected and stained for H&E. Red arrows indicate tumour growth; blue arrows indicate tumour cell infiltration; scale bar, 1mm. Far right, increased magnification of F2 tumours (ventricular & cerebellar region): blue box, infiltrating tumour cells; red box, small, focal masses; scale bar, 0.5mm. **(B)** Survival curves of $CD15^+$ and $CD15^-$ -derived tumours over generations; for F2, $CD15^+$ and $CD15^-$ -derived tumours had the same survival proportions (*n=6, n=3, n=3*). ****p<0.001*; significance was between generation, not cell type injected. **(C)** There was no difference in the percentage of CD15 in the different tumours over passaging at the time of collection, as determined by flow cytometry (*n=2*; *p>0.05*). **(D)** Sphere formation assays were performed on various tumours (*n=2*) to assess for selection of a stem-like population. There was no significant difference in sphere formation between cell type injected over tumour generation (*p>0.05*). **(E)** After 7 days in NSC culture conditions, neither $CD15^+$ or $CD15^-$ -derived tumours demonstrated any predisposition to propagate either population, as assessed by flow cytometry (*n*=2; p>*0.05*).

The CD15 status of each tumour collected for culture was assessed using flow cytometry immediately after collection. To determine the percentage of CD15 specific to the tumour, cells were co-stained with EpCAM-FITC, and gated based on side-scatter/forward-scatter profile, live cells (7AAD viability dye), and EpCAM positivity, as contaminating mouse neural cells have higher side-scatter, lower forward-scatter, and are negative for EpCAM (**Supplemental Figure 9A)**. $CD15^+$ -derived tumours showed approximately equal levels of CD15 expression for P1 (10.6% ± 6.3), F1 (10.2%), and F2 (14.4% ± 5.7) generations (**Figure 10C**; **Supplemental Figure 10A**). $CD15^-$ -derived tumours showed a slight increase in the percentage of CD15 with each generation: P1,

4.6% ± 1.9; F1, 8.6% ± 0.62; and F2, 11.1% ± 3.5 (**Figure 10C**; **Supplemental Figure 10B**). Despite these observed trends, there was no significant difference in CD15 expression in either $CD15^+$ or $CD15^-$ -derived tumours (*p>0.05*). This indicates that both pure populations were able to generate a heterogenous tumour, resembling the initial percentages observed in cells prior to injection (**Supplemental Table 6**, sort No. 11-14). These findings are suggestive of a potential underlying stem-like population in NCI-H1915 cells; however, it is becoming more evident that CD15 does not identify this population.

Again, to assess whether the observed increase in tumorigenicity over generations was due to selection of a stem-like population or for cells more suited to growth in the mouse neural microenvironment, sphere formation (self-renewal) was measured for each cultured tumour. Cells were plated at limiting dilution after 7 days exposure to NSC conditions in order to select for the human NCI-H1915 cells. There was no observed significant difference in sphere formation of either $CD15^+$ or $CD15^-$ -derived tumours over P1 (232.1 spheres/2000 cells ± 62.3 vs. 420.5 spheres/2000 cells ± 12.9), F1 (222.9 spheres/2000 cells vs. 278.1 spheres/2000 cells ± 229.6), or F2 (297.7 spheres/2000 cells ± 201.4 vs. 972.0 spheres/2000 cells ± 257.3) generations (*p>0.05*). It is of interest to note that the F2 $CD15^-$ -derived tumours did have a much higher level of sphere formation than the previous P1 and F1 tumours, which may be a factor of using the F1 tumour with greater sphere formation for the serial injection. The higher levels of sphere formation in $CD15^-$ -derived tumours may also be a factor of an observed enhanced

proliferation capacity (data not shown), as seen with *in vitro* analysis of proliferation of the sorted populations (**Figure 9G**). Perhaps $CD15^-$ cells are primed for increased proliferation, as seen in the sustained large tumour growth with passaging (**Figure 10A**, lower panels).

After seven days in NSC culture conditions, the tumours were re-assessed for their CD15 expression using flow cytometry in order to examine any differences in predisposition to propagate the CD15+ population. This also served to determine the proportion of mouse cells remaining in the culture, where cells could be gated on side-scatter/forward-scatter and viability alone, as all cells were now $EpCAM^+$ (**Supplemental Figure 9B**). There was no significant difference ($p>0.05$) in the expression of CD15 in $CD15^+$ and $CD15^-$ -derived tumours at either P1 (16.8% ± 10.4 vs. 5.2% ± 2.1), F1 (16.1% vs. 21.2% ± 9.3), or F2 (18.6% ± 6.5 vs. 4.0% ± 1.7) generations (**Figure 10E**; **Supplemental Figure 11**). These results indicate that the CD15+ populations in $CD15^+$ and $CD15^-$ -derived tumours have an almost equal ability to be propagated *in vitro*, re-establishing initial proportions of CD15 prior to passaging *in vivo*. This further supports the idea that an underlying stem like-population exists in NCI-H1915 cells, capable of producing both $CD15^+$ and $CD15^-$ progeny.

4.4. Results summary and interpretation

Prospective sorting of NCI-H1915 cells into $CD15^+$ and $CD15^-$ populations does not fractionate the cell line into functionally distinct populations. Contrary to the hypothesis,

$CD15^+$ cells did not exhibit increased sphere formation (self-renewal), or differentiation potential for neural lineage markers, as compared to $CD15^-$ cells. Both cell populations were able to reconstitute the absent population over secondary and tertiary passages post-sort, and demonstrated a similar clonal analysis profile. $CD15^-$ cells were found to be significantly more proliferative in both NSC and differentiation conditions than $CD15^+$ cells, indicating an enhanced proliferative capacity; however, this did not appear to have any bearing on stem-like capabilities *in vitro*. When examined for differences in tumorigenic potential *in vivo*, both $CD15^+$ and $CD15^-$ cells demonstrated similar survival profiles and tumour growth patterns. $CD15^+$ -derived tumours did seem to present more often as smaller tumours and with more tumour cell infiltration, than the more proliferative $CD15^-$ -derived tumours. All tumours had a similar percentage of $CD15^+$ cells, regardless of the cell type injected, and were not predisposed to the enrichment of either $CD15^+$ or $CD15^-$ cells when cultured in NSC conditions. Again, contrary to the hypothesis and current literature, $CD15^+$ cells were not more tumorigenic *in vivo*. Taken together, these data indicate that CD15 does not fractionate NCI-H1915 cells into functionally distinct populations, nor does it identify a stem-like or TIC population.

There are several potential explanations for these findings regarding CD15. The first of which could be that no CSC or TIC population exists in NCI-H1915 cells. However, this most likely not the case, as there is evidence of self-renewal (sphere formation) at limiting dilution and the clonal level. Furthermore, as evidenced by sorting with CD15, a

single cell type (i.e. $CD15^+$ or $CD15^-$) is capable of producing multiple cell types ($CD15^+$ and $CD15^-$). This is very suggestive of an underlying CSC or TIC population.

Second, contaminating $CD15^+$ cells in the $CD15^-$ population may have been responsible for the apparent CSC-like behavior *in vitro*. This was shown to not be the case, as clonal experiments demonstrated that both single $CD15^+$ and $CD15^-$ cells could form a similar proportion of spheres, and that these spheres were a mixture of both phenotypes. Additionally, $CD15^-$ cells were found to be much more proliferative than the $CD15^+$ cells, suggesting any contaminating positive fraction would be unable to proliferate to the point where they could significantly contribute to the experimental readout.

Alternatively, CD15 may in fact select for a CSC or TIC population in minimally-cultured clinical samples, but the effects of prolonged propagation in culture may have altered the NCI-H1915 cells to the point where the majority of cells have stem-like capabilities. This is possible, but not as likely given the similarities between NCI-H1915 cells and cells from clinical samples in terms of BTIC marker expression (specifically CD15) and behavior in unsorted experiments, such as sphere formation, sphere size, lack of expanded differentiation potential, and *in vivo* tumour formation. Previous use of minimally-cultured clinical samples and a cell line (Daoy) to study CSC properties in medulloblastoma demonstrated correlation with BTIC marker expression and function in both clinical samples and the Daoy cell line [134]. BTIC markers, CD15 and CD133, were similarly expressed in clinical samples and the cell line, and both sources of cells

demonstrated similar sphere formation and proliferation capacity [134]. This suggests that equivocal BTIC marker expression in cell lines and clinical samples is reflective of similar stem-like function. Therefore, if applied to the current work, the similar expression of CD15 across clinical samples and NCI-H1915 cells would suggest that the functional characterization of CD15 populations in the NCI-H1915 cell line is reflective of clinical sample behavior; however, this would require additional experimental confirmation.

A very plausible explanation for the similarities between $CD15^+$ and $CD15^-$ populations is that CD15 does not select for a CSC or TIC population in NCI-H1915 cells. The data are very suggestive of a CSC-like population in brain metastases (clinical samples and cell line), where CD15 may mark the phenotypes of more differentiated cells below the true underlying CSC population in the brain metastasis hierarchy. Support of this possibility could be garnered by prospectively sorting alternative markers, followed by a series of *in vitro* CSC and *in vivo* TIC assays; alternate markers would also have to be validated in both the cell line and clinical samples.

Finally, an equally plausible explanation for these observations is the possibility of a dynamic equilibrium between $CD15^+$ and $CD15^-$ cells. An increasing amount of evidence in the literature is suggesting that stem and non-stem cell populations propagate in an effort to maintain specific proportions of each cell type. These studies demonstrate that isolated cell populations will repopulate the absent population in efforts to re-establish

pre-sort proportions [135-137]. Therefore, it is possible to suggest that sorted $CD15^-$ NCI-H1915 cells may repopulate the $CD15^+$ fraction, and vice versa. If this is occurring, it is possible that the $CD15^+$ cells produced by $CD15^-$ cells are responsible for the observed sphere and tumour formation, as well as the reconstitution of the $CD15^+$ population seen by flow cytometry. The mechanism of these dynamic relationships is currently unknown [135-137], but is likely linked to feedback signaling between cell types. Perhaps, in the case of NCI-H1915 cells, enhanced proliferative capacity is required for $CD15^-$ cells to convert or produce $CD15^+$ cells; whereas, production of $CD15^-$ progeny from the stem-like $CD15^+$ cells is a more passive process and the cells more quiescent, explaining the differences in proliferation between the two phenotypes. Regardless of the whether CD15 is a CSC or TIC marker or not in brain metastases, it is apparent that the different populations in a tumour are not mutually exclusive, and have a very dynamic relationship.

4.5 Caveats and limitations

The most likely explanations for the lack of a functional difference in $CD15^+$ and $CD15^-$ populations are that CD15 does not mark a CSC population, or that a dynamic equilibrium exists between the populations within the NCI-H1915 cell line. While these observations and explanations regarding CD15 can be applied to NCI-H1915 cells, they cannot be extrapolated to brain metastases from the lung as a whole. In order for this to be possible, this work would need to be supplemented with sorting experiments done with clinical samples, in order to demonstrate similar functional readouts, suggesting the

observations made with NCI-H1915 cells could be applicable to the majority of brain metastases from the lung.

Such prospective-sorting experiments with clinical samples were attempted to confirm sphere formation of $CD15^+$ and $CD15^-$ populations. Unfortunately, none of the clinical samples used were able to survive flow-sorting of either clonal or sphere-forming assays at a minimum of 200 cells per well (data not shown), even with the use of conditioned media or an extended assay period of 14 days post-sort. Additional flow-sorts could be attempted with the goal of increasing the number of cells per well (i.e. several thousand); however, this would limit the number of replicates, as the number of viable cells pre-sort is often very low. Alternatively, magnetic bead sorting could be performed, as previously done with patient samples [4-6, 34], allowing for the enrichment of $CD15^+$ and $CD15^-$ populations. This method also requires a larger number of cells, as a subset of the sorted cells is needed to check population purities via flow cytometry, in addition to the cell numbers necessary for experiments. Furthermore, purity checks often reveal modest enrichment of the minority population, as previously seen with CD133 (46.9% to 79.8%) [4]. Unless there is an extremely potent functional difference between populations, modest enrichment presents the potential problem of being unable to detect significant functional differences between populations.

In addition to the difficulty in using clinical samples to functionally validate findings made with the NCI-H1915 cell line, there are several other potential issues surrounding

the use of surface markers to identify CSC or TIC populations. As seen with the assessment of BTIC marker expression, clinical brain metastasis samples are extremely variable in their expression among patients. This could lead to difficulty in confirming the functional similarities of any of the subpopulations, as the markers themselves are variably expressed, to the point where detection of function may not be possible. In addition, surface markers, in particular, do not necessarily confer function. As shown by Kemper *et al*, the expression of the glycosylated epitope of the CD133 glycoprotein, recognized by the majority of anti-CD133 antibodies, was lost during differentiation of colon carcinoma CSCs, and correlated with a loss in clonogenicity [138]. However, these otherwise $CD133^-$ differentiated cells continued to have CD133 promoter activity, CD133 mRNA expression, and even surface CD133 protein expression (via biotinylation experiments), suggesting that CD133 expression does not have a functional role, and that glycosylation status may be culture dependent [138]. Similar findings regarding glycosylation of CD133 in GBM have been reported [139]. These results suggest that the detectable status of CD133 expression is a result of functional changes in cell populations due to external differentiation cues.

For these reasons, and based on the findings in this work, it is suggested that a more functional approach be used in the study of brain metastases. This could involve the identification of subpopulations using functional flow cytometric assays (e.g. Aldefluor, Hoechst-exclusion), or a reporter-based system for relevant internally-expressed markers, that have functional roles in tumorigenesis and/or metastasis (e.g. Bmi1). These alternate

methods also have limitations, as they require a great deal of optimization, and are still limited by the variability among patients and model cell lines. Therefore, it is strongly suggested that future study of brain metastasis move away from identifying and targeting subpopulations, and move towards an approach that targets genes and/or pathways important to the metastatic process. If genes essential to metastasis and/or tumorigenesis of the bulk population can be identified and used as therapeutic targets, it may be possible to halt the process of metastasis entirely, providing a greater therapeutic benefit than attempting to treat established brain metastases. This proactive approach has a great chance of increasing lung cancer patient survival, as the prevention of metastasis would keep the disease in a more localized, and treatable state.

CHAPTER 5: DISCUSSION

Primary brain tumours such as GBM and medulloblastoma have been shown to follow a cancer stem cell model of tumorigenesis, where a BTIC population is responsible for the generation and maintenance of the tumour. *In vitro*, these populations would demonstrate increase self-renewal (sphere formation) and differentiate into the multiple cell types present in the tumour [4, 6, 34, 41]. *In vivo*, these populations have the ability to serially recapitulate the original tumour [5-6, 34, 42].

This work demonstrates that brain metastases also possess such stem-like populations. Both clinical samples and the model cell line had comparable sphere-forming capacity to their primary brain tumour counterparts (**Figure 4**), indicating self-renewal capacity. Brain metastases also expressed known primary BTIC markers (**Figure 5**), which is correlated with the presence of CSC or TIC populations in primary brain tumours. While the NCI-H1915 cell line was found to co-express neural lineage markers with that of epithelial and lung cancer cells, expansion of the neural compartment was not possible through passive or directed differentiation (**Figure 6**, **Figure 7**). Clinical samples of brain metastases had little to no expression of neural lineage markers (**Figure 6**). Taken together, these results suggest that brain metastases do not possess neural lineage differentiation capabilities in response to *in vitro* differentiation cues; this is likely a factor of their epithelial origin. Expression of neural markers within the tumour could be the result of host cell recruitment, as suggested by a lack of neural and lung tumour marker co-expression; or cell fusion events, potentially the cause of neural and lung tumour marker co-expression in NCI-H1915 cells; rather than derivation from a CSC

population with expanded neural lineage potential. Both clinical samples and NCI-H1915 cells were able to initiate tumour growth in NOD-SCID mice, and the cell line was able to be serially passaged *in vivo* (**Figure 8**; **Table 2**); however, it is uncertain as to whether the ability to be passaged *in vivo* is due to a selection process, or the presence of a TIC population.

While the use of a cell line eliminates many of the disadvantages of relying on clinical samples – low viability and cell number, lack of consistency across experiments, and collection of samples – it is important to be aware of the caveats surrounding use of cell lines. As seen with the comparison of sphere formation between clinical brain metastases and the NCI-H1915 cell line, while both are capable of forming spheres, the cell line had a much higher sphere-forming frequency, which could potentially be a result of long term culture, as previous reports indicate that stem-like or tumorigenic properties can be acquired over time in culture [122-123]. Such culture effects may make identifying a CSC population in a cell line difficult, as the majority of the cells may possess such capabilities.

In addition, the NCI-H1915 cell line, like all cell lines, is only representative of a single patient. This means that results regarding marker expression may only be a reflection of that patient's tumour. The differentiation studies performed using NCI-H1915 cells first seemed to indicate the potential presence of a population with expanded-lineage potential; however, such cells were unresponsive to neuronal and astrocytic

differentiation cues, suggesting the cells expressing neural lineage markers were terminally differentiated. This may have been the result of cell fusion events between tumour and neural cells, allowing for the co-expression of lung tumour and neural markers. Conversely, such expression patterns were not observed in the clinical samples, which would suggest that cell fusion events may not occur in all tumours, or if they do, the fused cells may not proliferate. While neural lineage differentiation does not seem relevant to brain metastases, with the *in vitro* conditions used, it seems likely that NCI-H1915 cells are not representative of clinical samples, indicating that findings regarding the NCI-H1915 cell line in these differentiation systems cannot be applied to brain metastases as a whole. As such, it is necessary to validate results obtained through use of cell lines in clinical samples for each method of differentiation or marker panel proposed for study.

Therefore, the NCI-H1915 cell line does seem to be an appropriate model for the study of brain metastases, when used in sphere formation, proliferation, and tumour formation assays. This cell line may be a suitable supply of cells when assessing the efficacy, optimal concentration, or function of new therapeutics for their effects on cell or tumour growth. It is encouraged that the findings of any work performed using NCI-H1915 cells be confirmed through testing in a subset of clinical samples, or at the very least, additional cell lines.

To truly assess whether brain metastases possess a CSC or TIC population, it is imperative to identify and functionally characterize such a population. Primary BTIC populations have been identified using cell surface markers CD133 and CD15, as well as the Aldefluor assay for ALDH activity. The clinical brain metastasis samples and NCI-H1915 brain metastasis cell line used in this Thesis expressed these BTIC markers within established ranges: CD15, 39.2% ± 33.3 and 14.8% ± 8.1 (vs. $CD15^+$ 2.4-70.5% [6, 34]); CD133, 9.7% ± 11.8 and 0.05% ± 0.08 (vs. $CD133^+$ 19-29% [5]); and Aldefluor, 10.8% ± 15.8 and 36.6% ± 20.2 (vs. $Aldefluor^+$ 4.8-12.3% [42]) (**Figure 5**). However, only CD15 was similarly expressed and identified a more distinct population in both clinical samples and NCI-H1915 cells (**Supplemental Figure 2**). Prospective flow-sorting experiments using CD15 as a marker were performed with NCI-H1915 cells (**Figure 5A**). Attempts to flow-sort clinical samples with CD15 were unsuccessful in producing a sufficient number of viable cells post-sort (data not shown).

While validation of CD15-based sorting in clinical samples was not performed, there is evidence to suggest that the findings made using NCI-H1915 cells could be applied to clinical brain metastases as well. Clinical samples and NCI-H1915 both grew as neurospheres in NSC conditions, with similar neurosphere size and morphology, and also formed tumours with similar presentation *in vivo*. Their similarities in lack of neural differentiation, and expression of BTIC markers, particularly CD15, also suggest compatibility across the different cell sources. Furthermore, studies of medulloblastoma have validated the use of a cell line (Daoy) for additional experiments in patient samples

based on common marker expression and function. Both Daoy cells and primary medulloblastoma cells possessed similar levels of the BTIC markers CD133 (both 0 – 25%), and CD15 (26 – 50% and 0 – 25%, respectively), and had similar functional readouts of sphere formation (mean of 21-26 spheres/2000 cells, and 30 spheres/2000 cells, respectively) and proliferation when cultured in NSC conditions [134]. This validation indicates that similar unsorted function and BTIC marker expression is indication that a cell line is likely an accurate representation of clinical samples.

Unlike in their primary brain tumour counterparts, CD15 did not segregate the bulk NCI-H1915 cell population into self-renewing, neural lineage-producing, or tumour-initiating populations (**Figures 9**; **Figure 10**). Similarly, both $CD15^+$ and $CD15^-$ cells could produce both populations, where the proportion of positivity began to resemble that of pre-sort proportions (**Figure 9C**) While it is possible that brain metastases may not contain a CSC or TIC population, and hence it cannot be identified, the data regarding sphere formation (bulk and clonal), and the production of two cell types from a single isolated cell type indicate that this is not the case; a CSC population is indeed present. Potential contamination of the $CD15^-$ population with $CD15^+$ cells was not the reason for the observed CSC capabilities of $CD15^-$ cells. This was shown through clonal analysis, where both single $CD15^+$ and $CD15^-$ cells were able to generate spheres, and that these spheres contained similar proportions of both populations, regardless of the initial cell phenotype (**Figure 9E&F**). It is clear that both cell phenotypes are capable of possessing the observed CSC characteristics. In addition, $CD15^+$ were less proliferative than $CD15^-$

in differentiation and NSC culture conditions (**Figure 9G**), suggesting any contaminating $CD15^+$ cells would be unable to repopulate the $CD15^+$ fraction in sorted $CD15^-$ cells.

Several more likely explanations for the lack of functional distinction between $CD15^+$ and $CD15^-$ populations exist. First, CD15 may not identify the CSC population within brain metastases, as the results suggest. This is not surprising, as CD15 has not been shown to identify a CSC population in primary lung or other epithelial tumours, the origins of brain metastases. Similarly, other BTIC markers have show discrepancies in their ability to be the sole identifier of CSC or TIC populations. Using CD133 as an example, Chen *et al* have indicated that a subgroup of $CD133^-$ glioma cells possess a similar clonogenicty to $CD133^+$ cells, can also give rise to both populations, differentiate into multiple neural lineages, and can generate serially-transplantable tumours [140]. This suggests that there may be multiple CSC populations in primary brain tumours. In fact, when assessed for CD133 expression, Son *et al* found no expression of the antigen in xenograft tumours generated by $CD15^+$ cells [34]. Another group also showed that $CD15^+/CD133^-$ cells were capable of sphere formation, and generating heterogeneous populations that were no different than those produced by $CD15^+$ only cells [6]. Taken together, it can be inferred that not all markers identify the same CSC or BTIC population, whether this is suggestive of a hierarchy among BTIC markers, or that markers may be tumour or subtype-dependent, remains to be seen.

In addition, several of these groups observed changes in the expression of CD133 over long periods in culture requiring passaging of neurospheres [6, 140]. All cultures either maintained or developed enhanced clonogenicty and/or tumour formation, irrespective of gain or loss of CD133 expression [6, 140]. These results seem to be congruent with the idea that long term culture can lead to an increase in stem-like properties [122-123], as seen in this report's comparison of minimally-cultured clinical samples and the NCI-H1915 cell line. While some surface markers may be more reliable for the identification of CSC or TIC populations, in the case of CD133 for primary brain tumours, this functional distinction may reside only in freshly obtained patient samples [4-5, 140]. It is possible that while in primary brain tumours use of CD15 does seem to consistently segregate CSC and non-CSC population, perhaps a similar conundrum to that surrounding CD133 in primary brain tumours, surrounds the use of CD15 in brain metastases. Without comparison to functional analysis of populations in clinical samples, it is difficult to determine if this is the case with brain metastases, specifically NCI-H1915 cells. This potential discrepancy aside, it is becoming clearer that use of surface markers, particularly a singular marker, is no longer as dependable as previously thought, and alternative methods of identifying CSC or TIC populations needs to be developed.

An alternative explanation to the observations made in this report surrounding CD15, is that the apparent non-selection of stem-like populations may be due to a dynamic equilibrium between stem and non-stem populations. As suggested by Gupta *et al*, isolated populations will repopulate the absent population in effort to re-establish pre-sort

population proportions [135]. Using breast cancer cell lines (SUM159 and SUM149), bulk cultures were flow-sorted into stem-like, basal, and luminal populations, with at least 96% purity. After six days in culture, the sorted populations were reassessed by flow cytomerty, revealing that each population had reproduced all three of the cell types, in almost equal proportions, approaching those of the pre-sort culture [135]. As with the findings in this Thesis, it was considered that a contaminating stem-like population could be responsible for the observations; however, growth dynamics confirmed this was not the case [135]. Further *in vivo* experiments demonstrated that when basal or luminal (non-stem-like) cells were injected into mice with irradiated carrier cells (no tumorigenic potential) as a method of prolonging their survival *in vivo*, both populations developed tumours with a population heterogeneity profile almost identical to that of the stem-like cell-generated tumours [135]. These results are indicative of conversion, possibly through dedifferentiation, of non-stem-like cell populations into stem-like cells with tumour-initiating abilities, suggesting that in the absence of TICs, non-TICs are able to compensate when in an appropriate niche to preserve survival and promote the conversion process.

Further evidence to support the theory of non-stem populations converting to stem-like cells has been shown in other models. While using a transformed fibroblast model to assess CSC properties, Scaffidi *et al* demonstrated that $CD15^-$ cells could spontaneously convert to $CD15^+$ cells. This was proven to not be due to contaminating $CD15^+$ cells, as this phenomenon was observed in clonal populations arising from a single $CD15^-$ cell

[136]. Another group has also shown that in breast tissue models, normal basal and tumour non-stem cell populations ($CD44^{lo}$) can spontaneously convert to a stem-like state ($CD44^{hi}$), with increased self-renewal and stem cell marker expression (CD44) [137]. Due to transduction with the SV40 early region and H-RAS oncogenes, all tumour cell types were able to generate tumours *in vivo*; however, what was surprising was the generation of heterogenous tumours, with increased levels of $CD44^{hi}$ cells, from flow-sorted non-stem, $CD44^{lo}$ cells [137].

The observations in the current work regarding CD15 may in fact be due to such a stochastic equilibrium, where $CD15^-$ cells convert to and repopulate $CD15^+$ cells. This would give $CD15^-$ cells their apparent self-renewal and differentiation capacities. Given the timeframe described in the other studies (5 to 6 days) for this conversion process to occur [135-136], assessment of the CD15-sorted populations at 7 and 14 days provide a sufficient amount of time for such conversion events to take place. The increased proliferative capacity of $CD15^-$ cells (**Figure 9G**) may be a reflection of increased metabolic demand as the conversion process takes place; whereas, differentiation of $CD15^+$ cells may be a more metabolically-passive process. To truly determine whether such equilibrium exists between $CD15^-$ and $CD15^+$ NCI-H1915 cells, a reporter-based system could be used to monitor the CD15 status of single $CD15^+$ or $CD15^-$ cells and their resulting clones. Time-lapsed video of the single cells over the initial 7 day period post-sort, combined with sphere formation data, would indicate whether $CD15^-$ cells convert to $CD15^+$ cells prior to forming spheres, or if they possess intrinsic sphere-

forming capabilities. This would clarify if the phenomena observed in NCI-H1915 cells are due to a stochastic equilibrium between $CD15^+$ stem-like and $CD15^-$ non-stem-like cells, or an inability of CD15 to identify the CSC population.

While the theory of dynamic population equilibrium is intriguing, it enforces the difficulty surrounding selection for and targeting of CSC populations. In the case of brain metastasis, perhaps the best way to approach study and treatment of the disease is to explore genes and signaling pathways important for metastasis of lung and other cancers to the brain. Several reports suggest that CSC populations of primary breast tumours may be intrinsically migratory and invasive *in vitro*, and metastatic *in vivo* [38, 46-49], while other reports suggest migratory cells in breast and other carcinomas can acquire self-renewal and tumorigenic capabilities through an epithelial-mesenchymal transition [71, 82, 91-93]. Again, such seemingly dynamic relationships between populations of cells indicate that targeting cell populations in metastases may not be ideal. In addition, cell population-based studies using cell lines may not always be reflective of cell populations in clinical samples, as is the case for CD133 [4-5, 140], and validation in such minimally-cultured cells is often technically difficult and limiting. For these reasons, it is suggested that focus be placed on genes overexpressed in brain metastases as potential therapeutic targets, rather than targeting a specific subpopulation (see **Chapter 6: Future Directions**).

A recent study of metastatic medulloblastoma now suggests that there is in fact a distinct subpopulation of primary tumour cells responsible for dissemination of disease throughout the spinal column [141]. Using a murine sleeping beauty transposon model of spontaneously metastatic medulloblastoma, the Taylor group demonstrated that there was only a 9.3% overlap in gene-centric common insertion sites (gCISs) between the primary cerebellar tumour and the matched spinal metastases, suggesting that the matched tumours arose from a common transformed progenitor cell, and were then subjected to clonal divergence during dissemination [141]. The genes affected in metastases were found to be involved in the cytoskeleton and PI3K pathway; whereas *Notch2* and *Tert* were found to be highly affected in the primary tumour [141]. Study of matched patient tissues confirmed these findings, showing that while there is a distinct similarity between an individual's primary tumour and metastases, the metastases are more closely related, suggesting that the metastases arise from a subclone of the primary tumour through clonal selection [141]. This study is indicative of a metastasis-initiating population derived from the primary tumour, but becomes distinct from the initial primary TIC population. It is important to note that this study differs from the current work in that the metastases remain in the same organ system (CNS), rather than spanning several organ systems (i.e. lung to brain). In the metastasis of lung cancer to the brain, it is quite possible that there would be an even greater distinction between the primary tumour and metastasis, making relation to a common "ancestral" population more difficult. This further suggests that primary TIC markers may not be useful markers of such a

population in metastases, and that a genetic approach may be required to target the initiating events of metastasis.

Several research groups, predominantly the Massague group, have determined organ-specific metastasis gene signatures in breast cancer [53-54, 56, 142], including those to the lung [142], bone [54], and brain [56]. Of particular interest was their study of breast cancer metastasis to the brain. By using genomic expression analysis to compare *in vivo*-selected brain metastasis cell lines (MDA231-BrM2; CN34-BrM2) to the corresponding parental lines (MDA231; CN34), 17 genes were identified as correlating with brain relapse of breast cancer patients [56]. Several genes overlapped with the previously identified lung metastasis signature [57], including *COX2* (*cyclooxygenase 2*), *MMP1*, and other genes implicated in adhesion, migration, and invasion [56]. Knockdown of these genes reduced the migration and invasiveness of MDA231-BrM2 cells. Of the genes identified as being overexpressed in breast-to-brain metastases, compared to non-metastazing cells genes, *ST6GALNAC5* (α2,6-sialyltransferase), a gene normally restricted to the brain [143], was found to be functionally important brain infiltration. Knockdown of *ST6GALNAC5* prevented the formation of brain metastases, by arresting the crossing of metastatic cells through an artificial blood-brain-barrier (BBB), suggesting the role of *ST6GALNAC5* is to aid in the infiltration of the BBB [56].

Another group also used *in vivo* selection to obtain metastatic derivatives of the PC9 and H2030 lung adenocarcinoma cell lines that consistently metastasized to the brain.[58] A

set of Wnt3a-regulated genes (lung cancer WNT gene set; LWS) were found to predict for metastasis to the brain. The LWS signature did not correspond with the signature previously determined for brain metastasis by the Massague group [56]. Among these LWS genes were *LEF1* (*lymphoid enhancer binding factor 1*) and *HOXB9* (*homeobox B9*), which in addition to being required for brain colonization [58], they have also been shown to promote the metastasis of breast cancer to the lung through acquisition of mesenchymal characteristics [144].

From these studies, it is clear that primary tumours express genes that aid tumour cells in migrating, invading, and adapting to a secondary niche. Some genes (e.g. *COX2, HOXB9,* and *MMP1*) appear to have a common role in the metastasis of primary cancers to several secondary locations, suggesting a universal role in the metastatic process. Further characterization of these genes and the identification of genes and pathways essential for the metastasis of lung cancer to the brain, may prove more useful and effective for the use of therapeutic targets, rather than targeting a dynamic CSC population of brain metastasis, as selected by a non-functional surface marker. By blocking the metastatic process, formation of brain and other metastases would be prevented, transforming a systemic and fatal disease into a locally-controlled and much more treatable one.

CHAPTER 6: FUTURE DIRECTIONS

Given the limitations of using single, or even multiple surface markers, to identify cell populations that may be in a state of dynamic equilibrium, an alternative method for the identification of the brain metastasis-initiating cell (BMIC) is necessary. Rather than investigate potentially non-functional surface markers for BMIC identification, future studies should focus on identifying genes important for BMIC function, providing insight into the metastatic pathway from the lung (or other primary tumour) to the brain. While some studies have identified organ-specific metastasis gene signatures from breast tumours, they neglect to study the candidate genes in the context of the cancer stem cell model, and depend on the process of *in vivo* selection which is potentially fraught with bias [52-54, 56-57]. Similarly, previous work regarding gene signatures for lung metastasis to the brain was also dependent on *in vivo* selection, and did not test the identified genes as therapeutic targets [58].

The future directions of the current work would not only allow for the study of lung-to-brain metastasis gene signatures and/or pathways in the context of invasion and metastasis, but also in that of the cancer stem cell model. Not only would such genes and pathways be useful therapeutic targets, but it is also possible they may only be expressed in the rare subset of cells that successfully form brain metastases from the bulk primary tumour. Identification of a putative BMIC population would not only provide an alternative therapeutic target to genes or pathways, but would also help elucidate the relationship between CSC/TIC and metastatic potential, as it has been suggested that these are divergent characteristics [141].

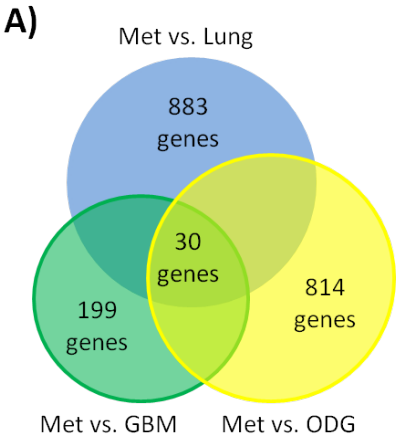

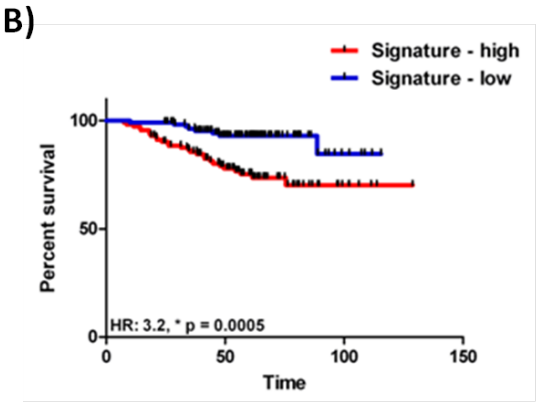

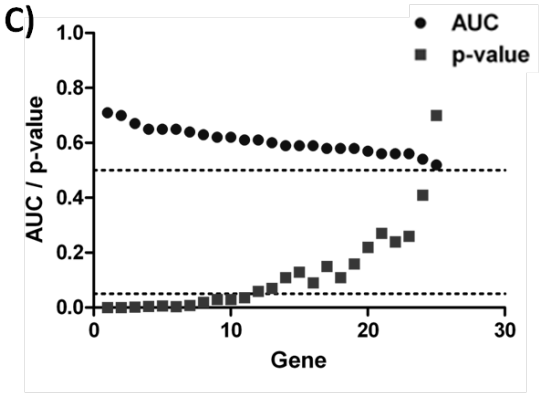

Gene	AUC	p-value	Gene	AUC	p-value
EIF4EBP1	*0.71*	*0.0001*	BAT3	0.59	0.09
DSP	*0.70*	*0.0002*	TCP1	0.59	0.11
MRPL3	*0.67*	*0.002*	CYC1	0.58	0.11
PLEKHG6	*0.65*	*0.005*	NARS	0.59	0.13
DSG2	*0.65*	*0.006*	CAPN1	0.58	0.15
LAMC2	*0.65*	*0.004*	SRC	0.58	0.16
NOC4L	*0.64*	*0.008*	LPGAT1	0.57	0.22
KRT7	*0.63*	*0.02*	SLC9A3R2	0.56	0.24
MYH14	*0.62*	*0.03*	IRF6	0.56	0.26
RPS7	*0.62*	*0.03*	PROM1	0.56	0.27
CTSZ	*0.61*	*0.036*	RASAL1	0.54	0.41
ZNF768	0.61	0.06	CTNND1	0.52	0.7
MCRS1	0.60	0.07			

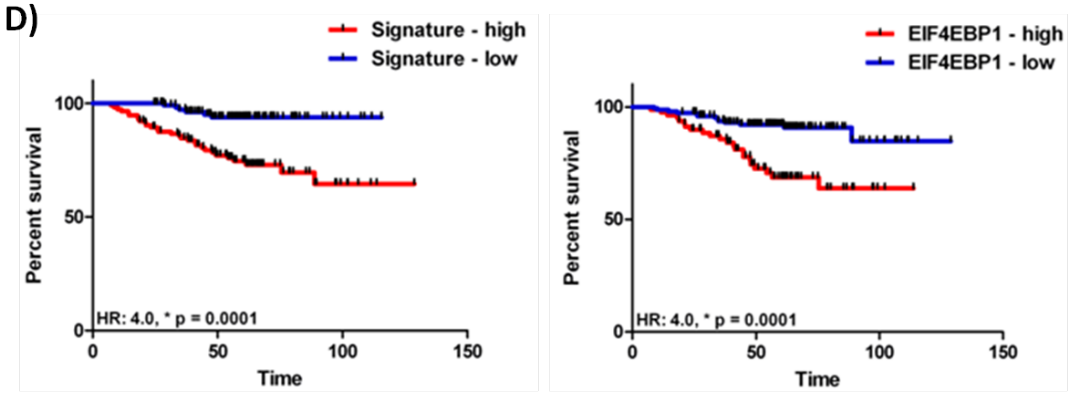

Figure 11: Identification of candidate genes overexpressed in brain metastases from lung, as compared to primary brain and lung tumours. RNA from two clinical brain metastases from the lung (BT219 & BT291; "Met") and an early culture of BT241 (GBM cell line, "GBM") were sent to the Michael Smith Genome Sciences Centre (MSGSC) for transcriptome analysis using the Illumina platform. Normalized transcriptome profiles were compared between the Met and GBM samples, along with primary lung ("Lung;" *n=2*) and oligodendroglioma ("ODG;" *n=2*) samples in the MSGSC database. **(A)** Individual analyses between Met samples and GBM, ODG, or Lung samples were done to indentify significantly overexpressed genes in brain metastases ($p<0.05$). **(B)** 25 of the 30 candidate genes were assessed in a dataset of 226 primary lung tumours (GSE31210) for their predictive value of overall patient survival (high signature expression, red; low signature expression, blue). **(C)** ROC curve analysis showed that 11 genes had a significant predictive role in lung cancer survival (AUC > 0.5, $p < 0.05$); significant genes are highlighted in the black box, right panel. **(D)** The survival curves for the 11 significant genes (left panel) and the most predictive gene, *EIF4EBP1*, are shown (right panel).

As suggested after unsuccessful attempts to identify the TIC population in brain metastases using primary BTIC markers, it was decided that identification of novel genes and/or pathways involved in brain metastasis from lung cancer would prove more useful as potential alternative therapeutic targets. Two clinical samples of brain metastases from the lung (BT219 and BT291) grown in the stem cell-enriching NSC conditions, along with an early culture of BT241 (GBM cell line), were used for RNA-Sequencing (RNA-Seq) and subsequent transcriptome analysis. Additional RNA-Seq data for oligodendrogliomas (grade III primary brain tumours) and primary lung tumours previously obtained by the Michael Smith Genome Sciences Centre were also used in the analysis. Comparisons between brain metastases, primary lung and brain tumours were done to determine genes overexpressed exclusively in brain metastasis, as shown in **Figure 11A**. Thirty candidate genes were identified as being overexpressed in brain

metastases from the lung (**Supplemental Table 7**), and included genes involved in cell adhesion (LAMC2, laminin gamma 2), cytoskeleton rearrangements (MYH14, myosin; PLEKHG6, pleckstrin homology domain containing family G member 6), proliferation/tumorigenesis (CAPN1, calpain 1; CD133, promini-1; CTSZ, cathepsin; RASAL1, RAS protein activator-like 1), and formation/disruption of cell-cell junctions (DSP, desmoplakin; DSG2, desmoglein 2).

In order to further determine their relevance to brain metastasis, it was desired to test the predictive power of the candidate genes for metastasis to the brain in additional primary lung tumour samples; however, this data was unavailable. Instead, the genes were examined for their ability to predict overall patient survival in a dataset of 226 primary lung tumours (GSE31210) [116], as survival of lung cancer patients is dependent upon metastasis [104-107, 110]. Twenty-five of the 30 candidate genes encoded transcripts that were recognized by the probe sets comprising the microarrays used to acquire the gene expression data of the primary lung tumours. As a gene set, these 25 genes were successful in identifying patients with poor survival (hazard ratio = 3.2, *p=0.0005*; **Figure 11B**). Individual genes were ranked according to their area-under-the-curve (AUC) values, where AUC values >0.5 with *p* values <0.05 are considered significant predictors of survival (**Figure 11C**). Based on this AUC analysis, eleven genes were further identified as significant predictors of lung cancer patient survival: hazard ratio = 4.0, *p=0.0001* (**Figure 11C,** right panel; **Figure 11D**, left panel); the most predictive gene was *EIF4EBP1* (hazard ratio, 4.0; *p=0.0001*; **Figure 11D**, right panel), a repressor

of mammalian target of rapamycin (mTOR)-mediated proliferation, where its repressive effects are relieved by phosphorylation by mTOR complex 1 [145]. High levels of phosphorylated EIF4EBP1 (eukaryotic translation initiation factor 4E-binding protein 1) are associated with poor clinical prognosis and increase proliferation in breast [146-147] and ovarian [148] cancers. While at first it may seem counter-intuitive to have increased transcript levels of a suppressor protein, it is quite likely that once translated, EIF4EBP1 becomes phosphorylated, allowing for mTOR-medidated cell growth. This preliminary analysis provides a ranking of candidate genes identified as being upregulated in brain metastases and correlated to poor lung cancer patient survival.

Future work to functionally characterize the roles of the top-ranking genes in stem-like and migratory properties, as well as *in vivo* tumour formation and metastasis would be integral in determining the ability of these genes to regulate the metastatic process, potentially identifying a BMIC population. Candidate genes, most likely in order of rank, would first be assessed using small-interfering RNA mediated knockdown for their *in vitro* effects on sphere formation (surrogate for self-renewal) and invasion through a collagen matrix with astrocytes and/or endothelial cells (simulating the BBB) [56, 149]. These *in vitro* studies would be performed with clinical samples and the NCI-H1915 cell line cultured in the stem cell-enriching NSC conditions, making the study outcomes more applicable to CSC populations. Some genes may prove important for regulation of invasion or self-renewal alone, or both. Genes with significant effects as compared to

controls, in either readout, would then be further assessed for their ability to regulate tumour formation and/or metastasis from the lung *in vivo*.

A)

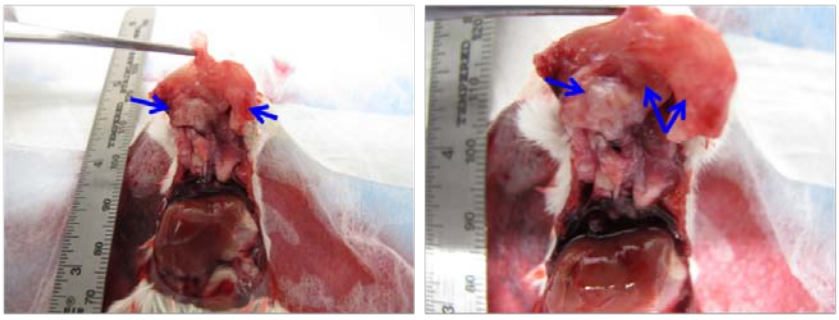

B)

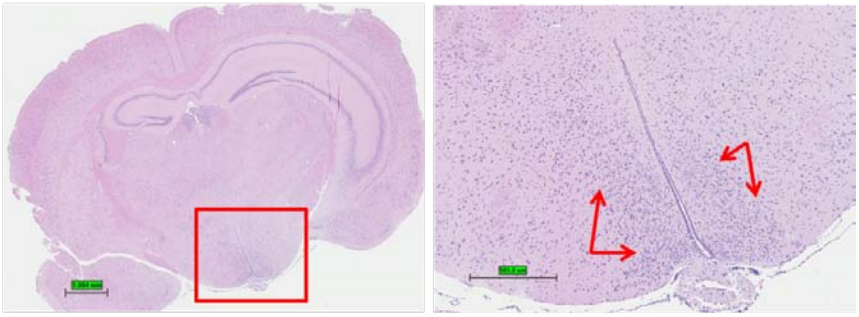

C)

Cell #	Primary Tumour Formation	Neural Infiltration
1,000,000	2/2	2/2
100,000	2/2	1/2

Figure 12: NCI-H1915 cells form lung tumours when injected intrathoracially into NOD-SCID mice. Either $1x10^6$ or $1x10^5$ NCI-H1915 cells were injected into the left thoracic cavity of NOD-SCID mice. Mice were sacrificed via perfusion, once endpoint was reached. **(A)** Nodules were visible throughout the thoracic cavity and on the lungs, irrespective of left-side injection (blue arrows); right panel is a closer view of the left picture. The brains of mice with thoracic tumours were also harvested, sectioned, and stained for H&E. **(B)** H&E staining revealed the presence of infiltrating NCI-H1915 cells near the cerebellar region of the brain (red box, left panel; red arrows, right panel). Scale bars are 1mm and 0.5mm for left and right panels, respectively. **(C)** Table documenting mice injected, formation of primary (lung) tumour formation, and presence of neural infiltration.

Knockdown using a lentiviral short harpin RNA, with an associated fluorescent protein, would allow for sustained inhibition of gene expression, and also for the prospective flow-sorting of knockdown populations. Sorted knockdown and control cells would be injected into NOD-SCID mice in order to demonstrate the effects these genes have on tumour formation (intracranial injections), or primary tumour and metastasis recapitulation (intrathoracic injections); any functional outcomes could have roles specific to a TIC or MIC population, respectively. Intrathoracic injection models with lung carcinoma cells have previously been shown to accurately represent the progression of human lung cancer [111, 150], and preliminary testing of this route of injection shows that NCI-H1915 cells, cultured in NSC conditions, are capable of forming primary lung tumours similar to those seen in lung cancer patients (**Figure 12A&C**). Collection of brains from mice with intrathoracic-injected NCI-H1915 cells demonstrated a large degree of tumour cell infiltration in the cerebellar region (**Figure 12B&C**). This suggests NCI-H1915 cells may be capable of re-forming the primary tumour, as well as metastasizing to the brain, making them an ideal model for the future study of the metastatic process and associated pathways.

CHAPTER 7: CONCLUSIONS

Based on *in vitro* and *in vivo* CSC assays performed on clinical samples and a cell line, these data strongly suggest that brain metastases do possess a CSC and TIC population. However, this population is distinct from that of primary brain tumours, as it lacks any neural lineage differentiation capacity. Similarly, the CSC/TIC population of brain metastases is not identifiable by the BTIC marker CD15, further suggesting a distinction from primary brain tumours. In addition, from this work, the NCI-H1915 cell line appears to be a suitable surrogate source of cells for the study of brain metastases from the lung. Use of this cell line would be particularly appropriate for the study of sphere formation, proliferation, and tumour formation *in vivo*.

There are limitations surrounding the use of the NCI-H1915 cell line, such as potential enrichment of CSC populations as compared to clinical samples, potential resistance to differentiation, and the fact that is representative of a single patient, rather than all brain metastases from the lung. For these reasons, it would be advisable to only use NCI-H1915 cells for cell population-based studies upon confirmation of marker expression in a variety of clinical samples. For example, the sorting experiments in this work using CD15 were based upon the expression level and pattern of the maker in the cell being similar to that which was observed in clinical samples; whereas, other markers – CD133 and Aldefluor – were variably expressed between clinical samples and the cell line, and were deemed unsuitable for further investigation in NCI-H1915 cells. It is critical that any cell population or marker-based studies performed in cell lines be validated based on marker expression, and ideally, function, in clinical samples.

As functional validation of $CD15^+$ and $CD15^-$ populations in clinical samples was unsuccessful, it is difficult to apply the findings regarding CD15 in NCI-H1915 cells to brain metastases from the lung as a whole. However, the limitations surrounding the use of cell surface markers for CSC or TIC identification can be universally applied to cell lines and clinical samples. Cell surface markers used for CSC/TIC identification may be non-functional themselves, where a loss of marker expression may not result in a change in the population function. It is also possible, as seen in primary brain tumours, that multiple BTIC markers do not always select the same population. This suggests that there may be a hierarchy even among BTIC markers, or that not all BTIC markers can be universally applied, making it difficult to consistently identify the same CSC or TIC population across groups of brain tumours. Furthermore, the current evidence for stochastic equilibrium between stem and non-stem populations in solid tumours, suggests that identification of TIC populations for therapeutic purposes may not be ideal; tumour cells are dynamic, and it is very difficult to hit a moving target.

An alternative approach, particularly to the study of brain metastasis would be to use a method of gene analysis, as described in this Thesis, to identify genes of pathways that might be important in the metastatic process. Further use of the NCI-H1915 cell line to study the effects of gene knockdown or overexpression would be advantageous, due to increased post-transduction viability, and the ability to be flow-sorted prior to use in experiments assessing sphere formation, proliferation, or tumour-formation. Using

appropriate models to study metastasis from the lung to the brain, such as those proposed with the NCI-H1915 cell line, would enable for the testing of chemical compounds, or antibodies to pathways found to be important in this metastatic process. Such pathway interference may result in the prevention of metastasis to the brain. In addition, it is possible that this gene analysis approach would indirectly lead to the identification of a BMIC population, as perhaps only a subset of cells have the ability to metastasize, and rely almost exclusively on the identified pathways.

In addition to being therapeutic targets, genes identified as being necessary for metastasis to the brain could be useful prognostic markers in patients with primary lung cancer. The presence of some of these genes in the primary tumour may be indicative of future brain metastases, and would suggest the use of some form of proactive anti-metastasis therapy. Such prognostic benefits would be restricted to patients presenting with low grade lung cancer, and no metastases; alternative prognostic and therapeutic approaches would be needed for patients presenting with high grade lung cancer and initial metastases.

Furthermore, any genes or pathways identified as being essential to metastasis from the lung to the brain may also be relevant to brain metastasis from other primary tumours, or potentially to systemic metastasis in general. This could mean the development of therapies leading to the universal inhibition of the metastatic process, and substantial increase patient survival in a variety of cancers. As the deaths from many cancers are due

to metastasis, inhibition of the metastatic process would render a previously uniformly fatal and systemic disease, into a more locally controlled and treatable one.

CHAPTER 8: REFERENCES

1. Clarke, M.F., et al., *Cancer stem cells--perspectives on current status and future directions: AACR Workshop on cancer stem cells.* Cancer Res, 2006. **66**(19): p. 9339-44.
2. Dick, J.E., *Stem cell concepts renew cancer research.* Blood, 2008. **112**(13): p. 4793-807.
3. Reya, T., et al., *Stem cells, cancer, and cancer stem cells.* Nature, 2001. **414**(6859): p. 105-11.
4. Singh, S.K., et al., *Identification of a cancer stem cell in human brain tumors.* Cancer Res, 2003. **63**(18): p. 5821-8.
5. Singh, S.K., et al., *Identification of human brain tumour initiating cells.* Nature, 2004. **432**(7015): p. 396-401.
6. Mao, X.G., et al., *Brain Tumor Stem-Like Cells Identified by Neural Stem Cell Marker CD15.* Transl Oncol, 2009. **2**(4): p. 247-57.
7. Al-Hajj, M., et al., *Prospective identification of tumorigenic breast cancer cells.* Proc Natl Acad Sci U S A, 2003. **100**(7): p. 3983-8.
8. Ginestier, C., et al., *ALDH1 is a marker of normal and malignant human mammary stem cells and a predictor of poor clinical outcome.* Cell Stem Cell, 2007. **1**(5): p. 555-67.
9. O'Brien, C.A., et al., *A human colon cancer cell capable of initiating tumour growth in immunodeficient mice.* Nature, 2007. **445**(7123): p. 106-10.
10. Ricci-Vitiani, L., et al., *Identification and expansion of human colon-cancer-initiating cells.* Nature, 2007. **445**(7123): p. 111-5.

11. Eramo, A., et al., *Identification and expansion of the tumorigenic lung cancer stem cell population.* Cell Death Differ, 2008. **15**(3): p. 504-14.
12. Ishizawa, K., et al., *Tumor-initiating cells are rare in many human tumors.* Cell Stem Cell. **7**(3): p. 279-82.
13. Quintana, E., et al., *Efficient tumour formation by single human melanoma cells.* Nature, 2008. **456**(7222): p. 593-8.
14. Huang, E.H., et al., *Aldehyde dehydrogenase 1 is a marker for normal and malignant human colonic stem cells (SC) and tracks SC overpopulation during colon tumorigenesis.* Cancer Res, 2009. **69**(8): p. 3382-9.
15. Schatton, T., et al., *Identification of cells initiating human melanomas.* Nature, 2008. **451**(7176): p. 345-9.
16. Chen, Y.C., et al., *Aldehyde dehydrogenase 1 is a putative marker for cancer stem cells in head and neck squamous cancer.* Biochem Biophys Res Commun, 2009. **385**(3): p. 307-13.
17. Li, C., et al., *Identification of pancreatic cancer stem cells.* Cancer Res, 2007. **67**(3): p. 1030-7.
18. Dean, M., T. Fojo, and S. Bates, *Tumour stem cells and drug resistance.* Nat Rev Cancer, 2005. **5**(4): p. 275-84.
19. Shervington, A. and C. Lu, *Expression of multidrug resistance genes in normal and cancer stem cells.* Cancer Invest, 2008. **26**(5): p. 535-42.
20. Pallini, R., et al., *Cancer stem cell analysis and clinical outcome in patients with glioblastoma multiforme.* Clin Cancer Res, 2008. **14**(24): p. 8205-12.

21. Zeppernick, F., et al., *Stem cell marker CD133 affects clinical outcome in glioma patients.* Clin Cancer Res, 2008. **14**(1): p. 123-9.

22. Horst, D., et al., *CD133 expression is an independent prognostic marker for low survival in colorectal cancer.* Br J Cancer, 2008. **99**(8): p. 1285-9.

23. Zhou, L., et al., *The prognostic role of cancer stem cells in breast cancer: a meta-analysis of published literatures.* Breast Cancer Res Treat, 2010. **122**(3): p. 795-801.

24. Jiang, F., et al., *Aldehyde dehydrogenase 1 is a tumor stem cell-associated marker in lung cancer.* Mol Cancer Res, 2009. **7**(3): p. 330-8.

25. Bertolini, G., et al., *Highly tumorigenic lung cancer CD133+ cells display stem-like features and are spared by cisplatin treatment.* Proc Natl Acad Sci U S A, 2009. **106**(38): p. 16281-6.

26. Korur, S., et al., *GSK3beta regulates differentiation and growth arrest in glioblastoma.* PLoS One, 2009. **4**(10): p. e7443.

27. Li, Y., et al., *Sulforaphane, a dietary component of broccoli/broccoli sprouts, inhibits breast cancer stem cells.* Clin Cancer Res, 2010. **16**(9): p. 2580-90.

28. Srivastava, R.K., et al., *Sulforaphane synergizes with quercetin to inhibit self-renewal capacity of pancreatic cancer stem cells.* Front Biosci (Elite Ed), 2011. **3**: p. 515-28.

29. Mimeault, M. and S.K. Batra, *New promising drug targets in cancer- and metastasis-initiating cells.* Drug Discov Today, 2010. **15**(9-10): p. 354-64.

30. Yin, A.H., et al., *AC133, a novel marker for human hematopoietic stem and progenitor cells.* Blood, 1997. **90**(12): p. 5002-12.

31. Uchida, N., et al., *Direct isolation of human central nervous system stem cells.* Proc Natl Acad Sci U S A, 2000. **97**(26): p. 14720-5.

32. Capela, A. and S. Temple, *LeX/ssea-1 is expressed by adult mouse CNS stem cells, identifying them as nonependymal.* Neuron, 2002. **35**(5): p. 865-75.

33. Read, T.A., et al., *Identification of CD15 as a marker for tumor-propagating cells in a mouse model of medulloblastoma.* Cancer Cell, 2009. **15**(2): p. 135-47.

34. Son, M.J., et al., *SSEA-1 is an enrichment marker for tumor-initiating cells in human glioblastoma.* Cell Stem Cell, 2009. **4**(5): p. 440-52.

35. Fox, N., et al., *Immunohistochemical localization of the early embryonic antigen (SSEA-1) in postimplantation mouse embryos and fetal and adult tissues.* Dev Biol, 1981. **83**(2): p. 391-8.

36. Storms, R.W., et al., *Isolation of primitive human hematopoietic progenitors on the basis of aldehyde dehydrogenase activity.* Proc Natl Acad Sci U S A, 1999. **96**(16): p. 9118-23.

37. Deng, S., et al., *Distinct expression levels and patterns of stem cell marker, aldehyde dehydrogenase isoform 1 (ALDH1), in human epithelial cancers.* PLoS One. **5**(4): p. e10277.

38. Croker, A.K., et al., *High aldehyde dehydrogenase and expression of cancer stem cell markers selects for breast cancer cells with enhanced malignant and metastatic ability.* J Cell Mol Med, 2009. **13**(8B): p. 2236-52.

39. Liang, D. and Y. Shi, *Aldehyde dehydrogenase-1 is a specific marker for stem cells in human lung adenocarcinoma.* Med Oncol, 2011.

40. Corti, S., et al., *Identification of a primitive brain-derived neural stem cell population based on aldehyde dehydrogenase activity.* Stem Cells, 2006. **24**(4): p. 975-85.

41. Rasper, M., et al., *Aldehyde dehydrogenase 1 positive glioblastoma cells show brain tumor stem cell capacity.* Neuro Oncol, 2010. **12**(10): p. 1024-33.

42. Bar, E.E., et al., *Cyclopamine-mediated hedgehog pathway inhibition depletes stem-like cancer cells in glioblastoma.* Stem Cells, 2007. **25**(10): p. 2524-33.

43. Fidler, I.J., *Seed and soil revisited: contribution of the organ microenvironment to cancer metastasis.* Surg Oncol Clin N Am, 2001. **10**(2): p. 257-69, vii-viiii.

44. Croker, A.K. and A.L. Allan, *Cancer stem cells: implications for the progression and treatment of metastatic disease.* J Cell Mol Med, 2008. **12**(2): p. 374-90.

45. Luzzi, K.J., et al., *Multistep nature of metastatic inefficiency: dormancy of solitary cells after successful extravasation and limited survival of early micrometastases.* Am J Pathol, 1998. **153**(3): p. 865-73.

46. Charafe-Jauffret, E., et al., *Aldehyde dehydrogenase 1-positive cancer stem cells mediate metastasis and poor clinical outcome in inflammatory breast cancer.* Clin Cancer Res. **16**(1): p. 45-55.

47. Marcato, P., et al., *Aldehyde Dehydrogenase Activity of Breast Cancer Stem Cells Is Primarily Due To Isoform ALDH1A3 and Its Expression Is Predictive of Metastasis.* Stem Cells. **29**(1): p. 32-45.

48. Sheridan, C., et al., *CD44+/CD24- breast cancer cells exhibit enhanced invasive properties: an early step necessary for metastasis.* Breast Cancer Res, 2006. **8**(5): p. R59.

49. Liu, H., et al., *Cancer stem cells from human breast tumors are involved in spontaneous metastases in orthotopic mouse models.* Proc Natl Acad Sci U S A. **107**(42): p. 18115-20.

50. Davis, S.J., et al., *Metastatic potential of cancer stem cells in head and neck squamous cell carcinoma.* Arch Otolaryngol Head Neck Surg. **136**(12): p. 1260-6.

51. Abraham, B.K., et al., *Prevalence of CD44+/CD24-/low cells in breast cancer may not be associated with clinical outcome but may favor distant metastasis.* Clin Cancer Res, 2005. **11**(3): p. 1154-9.

52. Minn, A.J., et al., *Genes that mediate breast cancer metastasis to lung.* Nature, 2005. **436**(7050): p. 518-24.

53. Minn, A.J., et al., *Distinct organ-specific metastatic potential of individual breast cancer cells and primary tumors.* J Clin Invest, 2005. **115**(1): p. 44-55.

54. Kang, Y., et al., *A multigenic program mediating breast cancer metastasis to bone.* Cancer Cell, 2003. **3**(6): p. 537-49.

55. van 't Veer, L.J., et al., *Gene expression profiling predicts clinical outcome of breast cancer.* Nature, 2002. **415**(6871): p. 530-6.

56. Bos, P.D., et al., *Genes that mediate breast cancer metastasis to the brain.* Nature, 2009. **459**(7249): p. 1005-9.

57. Minn, A.J., et al., *Lung metastasis genes couple breast tumor size and metastatic spread.* Proc Natl Acad Sci U S A, 2007. **104**(16): p. 6740-5.

58. Nguyen, D.X., et al., *WNT/TCF signaling through LEF1 and HOXB9 mediates lung adenocarcinoma metastasis.* Cell, 2009. **138**(1): p. 51-62.

59. Polyak, K. and R.A. Weinberg, *Transitions between epithelial and mesenchymal states: acquisition of malignant and stem cell traits.* Nat Rev Cancer, 2009. **9**(4): p. 265-73.

60. Kalluri, R. and R.A. Weinberg, *The basics of epithelial-mesenchymal transition.* J Clin Invest, 2009. **119**(6): p. 1420-8.

61. Baum, B., J. Settleman, and M.P. Quinlan, *Transitions between epithelial and mesenchymal states in development and disease.* Semin Cell Dev Biol, 2008. **19**(3): p. 294-308.

62. Kang, Y. and J. Massague, *Epithelial-mesenchymal transitions: twist in development and metastasis.* Cell, 2004. **118**(3): p. 277-9.

63. Yang, J. and R.A. Weinberg, *Epithelial-mesenchymal transition: at the crossroads of development and tumor metastasis.* Dev Cell, 2008. **14**(6): p. 818-29.

64. Thiery, J.P., *Epithelial-mesenchymal transitions in tumour progression.* Nat Rev Cancer, 2002. **2**(6): p. 442-54.

65. Turley, E.A., et al., *Mechanisms of disease: epithelial-mesenchymal transition--does cellular plasticity fuel neoplastic progression?* Nat Clin Pract Oncol, 2008. **5**(5): p. 280-90.

66. Xu, J., S. Lamouille, and R. Derynck, *TGF-beta-induced epithelial to mesenchymal transition.* Cell Res, 2009. **19**(2): p. 156-72.

67. Roussos, E.T., et al., *AACR special conference on epithelial-mesenchymal transition and cancer progression and treatment.* Cancer Res. **70**(19): p. 7360-4.

68. Cano, A., et al., *The transcription factor snail controls epithelial-mesenchymal transitions by repressing E-cadherin expression.* Nat Cell Biol, 2000. **2**(2): p. 76-83.

69. Casas, E., et al., *Snail2 is an essential mediator of Twist1-induced epithelial mesenchymal transition and metastasis.* Cancer Res. **71**(1): p. 245-54.

70. Chen, C., et al., *Evidence for epithelial-mesenchymal transition in cancer stem cells of head and neck squamous cell carcinoma.* PLoS One. **6**(1): p. e16466.

71. Mani, S.A., et al., *The epithelial-mesenchymal transition generates cells with properties of stem cells.* Cell, 2008. **133**(4): p. 704-15.

72. Yu, C.C., et al., *Bmi-1 Regulates Snail Expression and Promotes Metastasis Ability in Head and Neck Squamous Cancer-Derived ALDH1 Positive Cells.* J Oncol. **2011**.

73. Lo, W.L., et al., *MicroRNA-200c attenuates tumour growth and metastasis of presumptive head and neck squamous cell carcinoma stem cells.* J Pathol. **223**(4): p. 482-95.

74. Bao, B., et al., *Notch-1 induces epithelial-mesenchymal transition consistent with cancer stem cell phenotype in pancreatic cancer cells.* Cancer Lett, 2011. **307**(1): p. 26-36.

75. Biddle, A., et al., *Cancer stem cells in squamous cell carcinoma switch between two distinct phenotypes that are preferentially migratory or proliferative.* Cancer Res, 2011.

76. Jiang, L., J. Li, and L. Song, *Bmi-1, stem cells and cancer.* Acta Biochim Biophys Sin (Shanghai), 2009. **41**(7): p. 527-34.

77. Park, I.K., S.J. Morrison, and M.F. Clarke, *Bmi1, stem cells, and senescence regulation.* J Clin Invest, 2004. **113**(2): p. 175-9.

78. Shimono, Y., et al., *Downregulation of miRNA-200c links breast cancer stem cells with normal stem cells.* Cell, 2009. **138**(3): p. 592-603.

79. Burk, U., et al., *A reciprocal repression between ZEB1 and members of the miR-200 family promotes EMT and invasion in cancer cells.* EMBO Rep, 2008. **9**(6): p. 582-9.

80. Song, L.B., et al., *The polycomb group protein Bmi-1 represses the tumor suppressor PTEN and induces epithelial-mesenchymal transition in human nasopharyngeal epithelial cells.* J Clin Invest, 2009. **119**(12): p. 3626-36.

81. Mihic-Probst, D., et al., *Consistent expression of the stem cell renewal factor BMI-1 in primary and metastatic melanoma.* Int J Cancer, 2007. **121**(8): p. 1764-70.

82. Yang, M.H., et al., *Bmi1 is essential in Twist1-induced epithelial-mesenchymal transition.* Nat Cell Biol. **12**(10): p. 982-92.

83. Nichols, J., et al., *Formation of pluripotent stem cells in the mammalian embryo depends on the POU transcription factor Oct4.* Cell, 1998. **95**(3): p. 379-91.

84. Park, I.H., et al., *Reprogramming of human somatic cells to pluripotency with defined factors.* Nature, 2008. **451**(7175): p. 141-6.

85. Chambers, I., et al., *Functional expression cloning of Nanog, a pluripotency sustaining factor in embryonic stem cells.* Cell, 2003. **113**(5): p. 643-55.

86. Chiou, S.H., et al., *Coexpression of Oct4 and Nanog enhances malignancy in lung adenocarcinoma by inducing cancer stem cell-like properties and epithelial-mesenchymal transdifferentiation.* Cancer Res. **70**(24): p. 10433-44.

87. Ying, M., et al., *Regulation of glioblastoma stem cells by retinoic acid: role for Notch pathway inhibition.* Oncogene, 2011.

88. Sullivan, J.P., et al., *Aldehyde dehydrogenase activity selects for lung adenocarcinoma stem cells dependent on notch signaling.* Cancer Res, 2010. **70**(23): p. 9937-48.

89. Korpal, M., et al., *The miR-200 family inhibits epithelial-mesenchymal transition and cancer cell migration by direct targeting of E-cadherin transcriptional repressors ZEB1 and ZEB2.* J Biol Chem, 2008. **283**(22): p. 14910-4.

90. Park, S.M., et al., *The miR-200 family determines the epithelial phenotype of cancer cells by targeting the E-cadherin repressors ZEB1 and ZEB2.* Genes Dev, 2008. **22**(7): p. 894-907.

91. Hwang, W.L., et al., *SNAIL Regulates Interleukin-8 Expression, Stem Cell-Like Activity, and Tumorigenicity of Human Colorectal Carcinoma Cells.* Gastroenterology, 2011.

92. Vesuna, F., et al., *Twist modulates breast cancer stem cells by transcriptional regulation of CD24 expression.* Neoplasia, 2009. **11**(12): p. 1318-28.

93. Fang, X., et al., *Twist2 contributes to breast cancer progression by promoting an epithelial-mesenchymal transition and cancer stem-like cell self-renewal.* Oncogene, 2011.

94. *Facts & Statistics 2009*. 2009 [cited 2010 February 20]; Available from: http://www.abta.org/Tumor_And_Treatment_Info/12.

95. Schouten, L.J., et al., *Incidence of brain metastases in a cohort of patients with carcinoma of the breast, colon, kidney, and lung and melanoma.* Cancer, 2002. **94**(10): p. 2698-705.

96. Maher, E.A., et al., *Brain metastasis: opportunities in basic and translational research.* Cancer Res, 2009. **69**(15): p. 6015-20.

97. Gavrilovic, I.T. and J.B. Posner, *Brain metastases: epidemiology and pathophysiology.* J Neurooncol, 2005. **75**(1): p. 5-14.

98. Molina, J.R., et al., *Non-small cell lung cancer: epidemiology, risk factors, treatment, and survivorship.* Mayo Clin Proc, 2008. **83**(5): p. 584-94.

99. Hong, K.U., et al., *Basal cells are a multipotent progenitor capable of renewing the bronchial epithelium.* Am J Pathol, 2004. **164**(2): p. 577-88.

100. Kim, C.F., et al., *Identification of bronchioalveolar stem cells in normal lung and lung cancer.* Cell, 2005. **121**(6): p. 823-35.

101. Sutherland, K.D. and A. Berns, *Cell of origin of lung cancer.* Mol Oncol, 2010. **4**(5): p. 397-403.

102. Rawlins, E.L., et al., *The role of Scgb1a1+ Clara cells in the long-term maintenance and repair of lung airway, but not alveolar, epithelium.* Cell Stem Cell, 2009. **4**(6): p. 525-34.

103. Reynolds, S.D., et al., *Neuroepithelial bodies of pulmonary airways serve as a reservoir of progenitor cells capable of epithelial regeneration.* Am J Pathol, 2000. **156**(1): p. 269-78.

104. Sorensen, J.B., et al., *Brain metastases in adenocarcinoma of the lung: frequency, risk groups, and prognosis.* J Clin Oncol, 1988. **6**(9): p. 1474-80.

105. Quint, L.E., et al., *Distribution of distant metastases from newly diagnosed non-small cell lung cancer.* Ann Thorac Surg, 1996. **62**(1): p. 246-50.

106. Cox, J.D. and R.A. Yesner, *Adenocarcinoma of the lung: recent results from the Veterans Administration Lung Group.* Am Rev Respir Dis, 1979. **120**(5): p. 1025-9.

107. Komaki, R., J.D. Cox, and R. Stark, *Frequency of brain metastasis in adenocarcinoma and large cell carcinoma of the lung: correlation with survival.* Int J Radiat Oncol Biol Phys, 1983. **9**(10): p. 1467-70.

108. Beasley, M.B., *Immunohistochemistry of pulmonary and pleural neoplasia.* Arch Pathol Lab Med, 2008. **132**(7): p. 1062-72.

109. Jagirdar, J., *Application of immunohistochemistry to the diagnosis of primary and metastatic carcinoma to the lung.* Arch Pathol Lab Med, 2008. **132**(3): p. 384-96.

110. Sen, M., et al., *Prognostic factors in lung cancer with brain metastasis.* Radiother Oncol, 1998. **46**(1): p. 33-8.

111. Onn, A., et al., *Development of an orthotopic model to study the biology and therapy of primary human lung cancer in nude mice.* Clin Cancer Res, 2003. **9**(15): p. 5532-9.

112. Morozova, O., et al., *System-level analysis of neuroblastoma tumor-initiating cells implicates AURKB as a novel drug target for neuroblastoma.* Clin Cancer Res, 2010. **16**(18): p. 4572-82.

113. Li, H. and R. Durbin, *Fast and accurate short read alignment with Burrows-Wheeler transform.* Bioinformatics, 2009. **25**(14): p. 1754-60.

114. Smyth, G.K., *Linear models and empirical bayes methods for assessing differential expression in microarray experiments.* Stat Appl Genet Mol Biol, 2004. **3**: p. Article3.

115. Mortazavi, A., et al., *Mapping and quantifying mammalian transcriptomes by RNA-Seq.* Nat Methods, 2008. **5**(7): p. 621-8.

116. Okayama, H., et al., *Identification of genes upregulated in ALK-positive and EGFR/KRAS/ALK-negative lung adenocarcinomas.* Cancer Res, 2012. **72**(1): p. 100-11.

117. Zou, K.H., A.J. O'Malley, and L. Mauri, *Receiver-operating characteristic analysis for evaluating diagnostic tests and predictive models.* Circulation, 2007. **115**(5): p. 654-7.

118. Irizarry, R.A., et al., *Exploration, normalization, and summaries of high density oligonucleotide array probe level data.* Biostatistics, 2003. **4**(2): p. 249-64.

119. Hallett, R.M., et al., *A Gene Signature for Predicting Outcome in Patients with Basal-like Breast Cancer.* Sci Rep, 2012. **2**: p. 227.

120. Yau, C., et al., *A multigene predictor of metastatic outcome in early stage hormone receptor-negative and triple-negative breast cancer.* Breast Cancer Res, 2010. **12**(5): p. R85.

121. Kienast, Y., et al., *Real-time imaging reveals the single steps of brain metastasis formation.* Nat Med. **16**(1): p. 116-22.

122. Inagaki, A., et al., *Long-term maintenance of brain tumor stem cell properties under at non-adherent and adherent culture conditions.* Biochem Biophys Res Commun, 2007. **361**(3): p. 586-92.

123. Wu, W., et al., *Long-term cultured human neural stem cells undergo spontaneous transformation to tumor-initiating cells.* Int J Biol Sci, 2011. **7**(6): p. 892-901.

124. Seike, T., et al., *Interaction between lung cancer cells and astrocytes via specific inflammatory cytokines in the microenvironment of brain metastasis.* Clin Exp Metastasis. **28**(1): p. 13-25.

125. Arshad, F., et al., *Blood-brain barrier integrity and breast cancer metastasis to the brain.* Patholog Res Int. **2011**: p. 920509.

126. Wang, R., et al., *Glioblastoma stem-like cells give rise to tumour endothelium.* Nature, 2010. **468**(7325): p. 829-33.

127. Ricci-Vitiani, L., et al., *Tumour vascularization via endothelial differentiation of glioblastoma stem-like cells.* Nature, 2010. **468**(7325): p. 824-8.

128. Morshead, C.M., et al., *Hematopoietic competence is a rare property of neural stem cells that may depend on genetic and epigenetic alterations.* Nat Med, 2002. **8**(3): p. 268-73.

129. Reynolds, B.A. and R.L. Rietze, *Neural stem cells and neurospheres--re-evaluating the relationship.* Nat Methods, 2005. **2**(5): p. 333-6.

130. Tropepe, V., et al., *Distinct neural stem cells proliferate in response to EGF and FGF in the developing mouse telencephalon.* Dev Biol, 1999. **208**(1): p. 166-88.

131. Barrett, L.E., et al., *Self-renewal does not predict tumor growth potential in mouse models of high-grade glioma.* Cancer Cell, 2012. **21**(1): p. 11-24.

132. Elkabets, M., et al., *Human tumors instigate granulin-expressing hematopoietic cells that promote malignancy by activating stromal fibroblasts in mice.* J Clin Invest. **121**(2): p. 784-99.

133. McAllister, S.S., et al., *Systemic endocrine instigation of indolent tumor growth requires osteopontin.* Cell, 2008. **133**(6): p. 994-1005.

134. Wang, X., et al., *Sonic hedgehog regulates Bmi1 in human medulloblastoma brain tumor-initiating cells.* Oncogene, 2012. **31**(2): p. 187-99.

135. Gupta, P.B., et al., *Stochastic state transitions give rise to phenotypic equilibrium in populations of cancer cells.* Cell, 2011. **146**(4): p. 633-44.

136. Scaffidi, P. and T. Misteli, *In vitro generation of human cells with cancer stem cell properties.* Nat Cell Biol, 2011. **13**(9): p. 1051-61.

137. Chaffer, C.L., et al., *Normal and neoplastic nonstem cells can spontaneously convert to a stem-like state.* Proc Natl Acad Sci U S A, 2011. **108**(19): p. 7950-5.

138. Kemper, K., et al., *The AC133 epitope, but not the CD133 protein, is lost upon cancer stem cell differentiation.* Cancer Res, 2010. **70**(2): p. 719-29.

139. Osmond, T.L., K.W. Broadley, and M.J. McConnell, *Glioblastoma cells negative for the anti-CD133 antibody AC133 express a truncated variant of the CD133 protein.* Int J Mol Med, 2010. **25**(6): p. 883-8.

140. Chen, R., et al., *A hierarchy of self-renewing tumor-initiating cell types in glioblastoma.* Cancer Cell. **17**(4): p. 362-75.

141. Wu, X., et al., *Clonal selection drives genetic divergence of metastatic medulloblastoma.* Nature, 2012. **482**(7386): p. 529-33.

142. Gupta, G.P., et al., *Mediators of vascular remodelling co-opted for sequential steps in lung metastasis.* Nature, 2007. **446**(7137): p. 765-70.

143. Okajima, T., et al., *Molecular cloning of brain-specific GD1alpha synthase (ST6GalNAc V) containing CAG/Glutamine repeats.* J Biol Chem, 1999. **274**(43): p. 30557-62.

144. Hayashida, T., et al., *HOXB9, a gene overexpressed in breast cancer, promotes tumorigenicity and lung metastasis.* Proc Natl Acad Sci U S A. **107**(3): p. 1100-5.

145. Fingar, D.C. and J. Blenis, *Target of rapamycin (TOR): an integrator of nutrient and growth factor signals and coordinator of cell growth and cell cycle progression.* Oncogene, 2004. **23**(18): p. 3151-71.

146. Rojo, F., et al., *4E-binding protein 1, a cell signaling hallmark in breast cancer that correlates with pathologic grade and prognosis.* Clin Cancer Res, 2007. **13**(1): p. 81-9.

147. Pons, B., et al., *The effect of p-4E-BP1 and p-eIF4E on cell proliferation in a breast cancer model.* Int J Oncol, 2011. **39**(5): p. 1337-45.

148. Castellvi, J., et al., *Phosphorylated 4E binding protein 1: a hallmark of cell signaling that correlates with survival in ovarian cancer.* Cancer, 2006. **107**(8): p. 1801-11.

149. Takata, M., et al., *Double-layered collagen gel hemisphere for cell invasion assay: successful visualization and quantification of cell invasion activity.* Cell Commun Adhes, 2007. **14**(4): p. 157-67.

150. Doki, Y., et al., *Mediastinal lymph node metastasis model by orthotopic intrapulmonary implantation of Lewis lung carcinoma cells in mice.* Br J Cancer, 1999. **79**(7-8): p. 1121-6.

SUPPLEMENTAL MATERIALS

Supplemental Table 1: Antibody staining information. Ex., excitation wavelength; Em., emission wavelength; App., application; FC, flow cytometry; IF, immunofluorescence.

Antibody or Dye	**Company**	**Dil.**	**Control**	**Ex. (nm)**	**Em. (nm)**	**App.**
7-AAD Viability Dye	Beckman Coulter	1:10	N/A	546	647	FC
Aldefluor Kit	Stem Cell Technologies	1:50	N/A	488	512	FC
MAP2B Alexa Fluor 647	BD Biosciences	1:5	IgG1 Alexa647	652	668	FC
GFAP PE	BD Biosciences	1:20	IgG2a PE	499	519	FC
Human CD133/2 APC	Miltenyi Biotec	1:10	IgG2b APC	650	660	FC
Human CD15 PE	Beckman Coulter	1:10	IgG2a PE	480	578	FC
Anti-human EpCAM-FITC	Miltenyi Biotec	1:50	Unstained	495	519	FC
Rabbit monoclonal antibody to human TTF-1	Abcam	1:30	Alexa700 alone	N/A	N/A	FC
IOTest IgG2a PE (mouse)	Beckman Coulter	1:10	N/A	480	578	FC
Mouse IgG2b APC	Miltenyi Biotec	1:10	N/A	650	660	FC
Mouse IgG1 Alexa-Fluor 647	BD Biosciences	1:10	N/A	652	668	FC
Alexa Fluor 700 (goat anti-rabbit IgG H+L)	Invitrogen	1:2000	N/A	696	719	FC
GFAP Mouse mAb (Alexa Fluor 488)	Cell Signaling Technology	1:100	Alexa488 alone	499	519	IF
Rabbit polyclonal antibody to human EpCAM	Abcam	2µg/mL	Alexa647 alone	N/A	N/A	IF
Rabbit monoclonal antibody to human TTF-1	Abcam	1:200	Alexa647 alone	N/A	N/A	IF
Monoclonal anti-MAP2	Sigma	1:200	Alexa488 alone	N/A	N/A	IF
Alexa Fluor 488 (goat anti-mouse IgG H+L)	Invitrogen	1:200	N/A	499	519	IF
Alexa Fluor 647 (goat anti-rabbit IgG H+L)	Invitrogen	1:200	N/A	652	668	IF

Supplemental Table 2: List of primers for qRT-PCR. Dir., direction; F, forward; R, reverse.

Gene Symbol	Accession #	Dir.	Primer Sequence (5'→3')	Anneal Temp (°C)
GAPDH	NM_002046.3	F	TGCACCACCAACTGCTTAGC	60
		R	GGCATGGACTGTGGTCATGAG	60
EpCAM	NM_002354	F	CTGTCATTTGCTCAAAGCTGG	60
		R	TCGCAGTCAGGATCATAAAGC	60
SPC	NM_003018	F	CGGACACATATAAGACCCTGG	60
		R	CAGGGAATGCCAAATCGG	60
MAP2	NM_002374.3	F	TTCTGTGAGTGCAGATGCTGAGGT	60
		R	AGGTGATGGCAATGGGACTGTGTA	60
GFAP	NM_002055.3	F	AGATTCGAGAAACCAGCCTGGACA	60
		R	TCCTGCCTCACATCACATCCTTGT	60
TTF1	NM_001079668	F	GCCAAACTGCTGGACGTCTTTCTT	60
		R	CCTTGAGATTGGATGCGCTTGGTT	60

Supplemental Table 3: Patient sample information. M, male; F, female; yrs, years.

Sample ID	Diagnosis	Age (yrs)	Gender	History
BT16	Poorly differentiated metastatic carcinoma	49	F	Poorly differentiated lung carcinoma
BT41	Glioblastoma multiforme	59	M	---
BT47	Glioblastoma multiforme	59	M	---
BT69	Metastatic carcinoma	79	M	Lung carcinoma
BT82	Glioblastoma multiforme	49	M	---
BT199	Anaplastic small cell carcinoma	58	M	Small cell lung carcinoma
BT219	Metastatic carcinoma	50	M	Lung carcinoma
BT222	Metastatic adenocarcinoma	55	M	Lung adenocarcinoma
BT250	Metastatic adenocarcinoma	78	M	Lung adenocarcinoma
BT256	Poorly differentiated squamous carcinoma	64	F	Poorly differentiated squamous lung carcinoma
BT291	Metastatic adenocarcinoma	52	M	Lung adenocarcinoma
BT296	Metastatic adenocarcinoma	81	F	Lung adenocarcinoma
BT298	Metastatic carcinoma	56	M	Lung carcinoma
BT312	Metastatic carcinoma	55	M	Lung carcinoma
BT324	Metastatic carcinoma	66	M	Lung carcinoma
BT364	Metastatic adenocarcinoma	69	M	Lung adenocarcinoma
BT367	Poorly differentiated metastatic carcinoma	61	M	Poorly differentiated lung carcinoma
BT370	Metastatic adenocarcinoma	63	M	Lung adenocarcinoma

BT381	Metastatic carcinoma	62	M	Lung carcinoma
BT382	Metastatic adenocarcinoma	54	F	Lung adenocarcinoma
BT390	Metastatic papillary adenocarcinoma	64	F	Papillary adenocarcinoma (lung)
BT391	Metastatic adenocarcinoma	66	M	Lung adenocarcinoma
BT397	Metastastic adenocarcinoma	73	F	Lung adenocarcinoma

Supplemental Table 4: Quantification of clinical sample differentiation using immunofluorescence. IF results are the percentage positive in a single experiment; ---, combination not done; *, percent of total population; †, percent of TTF1 or EpCAM positive cells.

Sample: BT222				
	EpCAM	**TTF1**	**GFAP**	**MAP2**
EpCAM	25.03*	---	0.00†	0.00†
TTF1	---	2.72*	1.09†	1.54†
GFAP	0.00†	1.09†	0.023*	---
MAP2	0.00†	1.54†	---	0.092*
Sample: BT312				
	EpCAM	**TTF1**	**GFAP**	**MAP2**
EpCAM	60.23*	---	0.20†	0.00†
TTF1	---	0.37*	0.00†	0.00†
GFAP	0.00†	0.00†	0.031*	---
MAP2	0.00†	0.00†	---	0.00*
Sample: BT324				
	EpCAM	**TTF1**	**GFAP**	**MAP2**
EpCAM	47.27*	---	0.00†	0.89†
TTF1	---	0.22*	0.00†	0.00†
GFAP	0.00†	0.00†	0.00*	---
MAP2	0.89†	0.00†	---	0.34*
Sample: BT364				
	EpCAM	**TTF1**	**GFAP**	**MAP2**
EpCAM	0.00*	---	0.00†	0.00†
TTF1	---	2.34*	0.00†	0.00†
GFAP	0.00†	0.00†	0.00*	---
MAP2	0.00†	0.00†	---	0.00*

Supplemental Table 5: Quantification of NCI-H1915 differentiation using immunofluorescence (IF) and flow cytometry (FC). IF results are the percentage positive in a single experiment; ---, combination not done; *, percent of total population; †, percent of TTF1 or EpCAM positive cells. FC results are the percent positive of the total population of a single a representative flow cytometry analysis.

Immunofluorescence (% positive)				
	EpCAM	**TTF1**	**GFAP**	**MAP2**
EpCAM	50.84*	---	81.94†	97.71†
TTF1	---	52.93*	11.65†	95.99†
GFAP	81.94†	11.65†	25.77*	---
MAP2	97.71†	95.99†	---	51.83*
Flow Cytometry (% positive)				
	EpCAM	**TTF1**	**GFAP**	**MAP2**
EpCAM	97.54	88.23	3.80	4.17
TTF1	88.23	90.13	3.76	2.76
GFAP	3.80	3.76	3.80	0.89
MAP2	4.17	2.76	0.89	3.46

Supplemental Table 6: CD15-sort information for NCI-H1915 cells. *$CD15^+$ cells were sorted from $CD15^+$ -derived tumours; $CD15^-$ cells were sorted from $CD15^-$ -derived tumours.

Sort No.	Initial %		Purity		Assay(s)
	CD15 Pos	CD15 Neg	CD15 Pos	CD15 Neg	
1	6.73	92.76	90.99	99.31	Sphere formation, CD15 analysis
2	13.04	85.98	98.60	99.74	Sphere formation, CD15 analysis
3	13.86	84.61	85.01	95.61	Sphere formation, CD15 analysis, Differentiation
4	10.32	87.74	88.46	97.19	Differentiation
5	7.05	90.33	92.53	98.82	Differentiation
6	14.5	84.24	91.61	96.55	Differentiation
7	7.59	90.39	86.16	99.04	Alamar blue, CD15 clonal analysis
8	5.07	93.95	88.02	98.97	Alamar blue, CD15 clonal analysis
9	4.97	95.16	87.48	99.28	Alamar blue
10	18.72	80.17	---	---	CD15 clonal analysis
11	7.23	91.05	85.85	99.4	*in vivo* (P1)
12	9.42	89.49	89.01	98.37	*in vivo* (P1)
13	5.38	93.72	95.44	98.27	*in vivo* (F1)*
14	17.44	97.11	84.08	97.33	*in vivo* (F2)*

Supplemental Table 7: Candidate gene-list relative expression and *p*-values. . ODG, oligodedroglioma; Met, brain metastasis from the lung; GBM, glioblastoma; Lung, lung carcinoma/adenocarcinoma.

Gene	Full Gene Name	ODG1	ODG2	Met1	Met2	GBM	Lung1	Lung2
PROM1	prominin 1; CD133	1.32	2.09	60.57	57.22	0.10	7.71	1.65
PLEKHG6	pleckstrin homology domain containing, family G (with RhoGef domain) member 6	0.090	0.16	11.96	15.26	0.20	0.94	1.04
CAPN1	calpain 1	24.48	32.96	88.39	82.37	41.61	19.78	18.72
DSG2	desmoglein 2	0.0044	0.0069	65.40	70.67	0.51	5.90	23.43
LAMC2	laminin gamma 2	0.034	0.064	51.92	38.33	0.43	11.46	18.22
SLC9A3R2	solute carrier family 9 (sodium/hydrogen exchanger), member 3 regulator 2	11.94	9.73	38.38	39.66	10.41	5.56	15.28
DSP	desmoplakin	0.62	0.50	98.60	72.38	1.07	24.27	32.50
CTSZ	cathepsin Z (or X, P)	8.22	13.09	120.97	96.67	0.30	48.13	36.46
MYH14	myosin, heavy chain 14	12.22	12.52	62.12	47.43	1.17	10.77	7.97
RASAL1	RAS protein activator like 1	1.10	0.28	19.41	14.60	0.28	1.00	2.55
MRPL3	mitochondrial ribosomal protein L3	48.30	57.76	96.87	93.00	19.87	54.30	61.77
IRF6	interferon regulatory factor 6	0.37	0.066	36.72	27.75	0.059	7.57	9.81
TCP1	t-complex 1	73.86	79.83	137.28	147.44	47.80	87.00	77.84
NAT15	N(alpha)-acetyltransferase 60, NatF catalytic subunit	24.28	29.72	56.77	50.57	16.17	12.64	15.95
LPGAT1	lysophosphatidylglycerol acyltransferase 1	6.72	8.39	29.74	32.33	8.35	7.25	11.28
NARS	asparaginyl-tRNA synthetase	73.36	45.80	135.27	121.65	63.33	85.09	88.20
KRT7	Keratin 7	0.020	0.00	302.90	363.02	0.67	134.26	197.40
GYLTL1B	Glycosyltransferase - like 1B	0.031	0.042	18.97	16.60	1.58	3.83	0.90

ZNF768	zinc finger protein 768	17.42	18.48	44.79	47.42	17.09	12.25	7.21
KRT8P9	keratin 8 pseudogene 9	0.034	0.00	578.81	723.15	9.12	66.43	117.94
RPS7	ribosomal protein S7	9.56	39.02	121.00	120.46	69.47	52.38	55.04
CYC1	cytochrome c-1	53.49	91.13	266.76	285.19	157.52	109.41	133.13
FAM83H	family with sequence similarity 83, member H	0.24	0.15	54.53	50.86	1.54	16.38	14.24
NOC4L	nucleolar complex associated 4 homolog	9.15	14.48	31.54	34.42	12.07	4.66	5.82
MCRS1	microspherule protein 1	17.34	22.81	48.22	54.24	23.42	8.29	10.79
EIF4EBP1	eukaryotic translation initiation factor 4E binding protein 1	16.28	43.25	137.21	139.84	53.88	12.48	19.15
SRC	v-src sarcoma (Schmidt-Ruppin A-2) viral oncogene homolog (avian)	12.02	15.85	39.56	30.82	3.21	5.72	12.38
CTNND1	catenin (cadherin-associated protein), delta 1	38.50	49.87	84.13	82.88	30.96	34.69	30.44
BAT3	BCL2-associated athanogene 6	64.01	76.71	144.35	136.87	80.00	27.94	19.06
AC079031.39		2.58	6.51	21.79	24.16	4.71	0.56	0.62

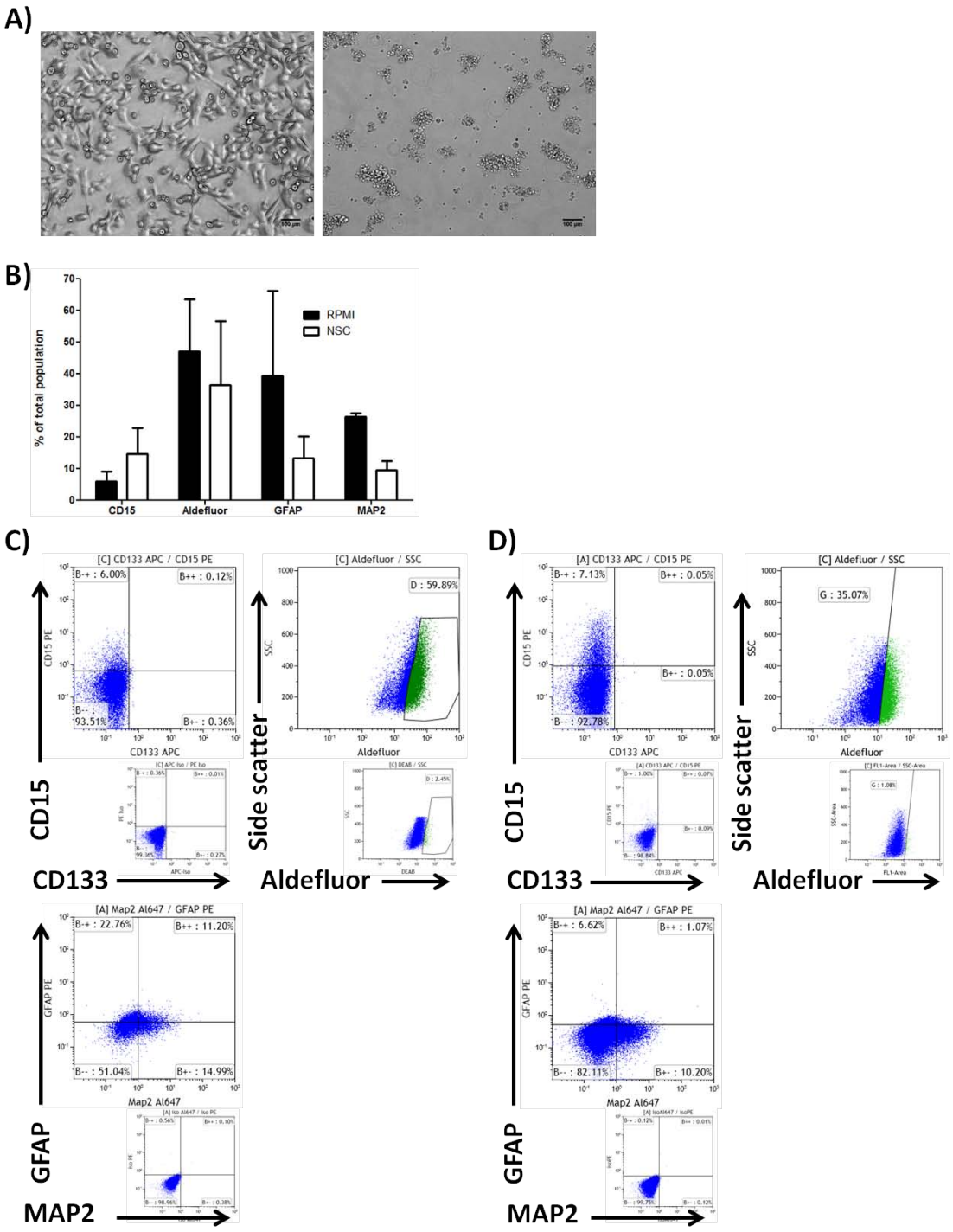
A)
B)
% of total population
RPMI
NSC
CD15
Aldefluor
GFAP
MAP2
C)
[C] CD133 APC / CD15 PE
B+- : 6.00%
B++ : 0.12%
B-- : 93.51%
B+- : 0.36%
CD15 PE
CD133 APC
[C] Aldefluor / SSC
D : 59.89%
SSC
Aldefluor
Side scatter
CD15
CD133
[A] Map2 Al647 / GFAP PE
B+- : 22.76%
B++ : 11.20%
B-- : 51.04%
B+- : 14.99%
GFAP PE
Map2 Al647
GFAP
MAP2
D)
[A] CD133 APC / CD15 PE
B+- : 7.13%
B++ : 0.05%
B+- : 0.05%
B-- : 92.78%
[C] Aldefluor / SSC
G : 35.07%
[A] Map2 Al647 / GFAP PE
B+- : 6.62%
B++ : 1.07%
B-- : 82.11%
B+- : 10.20%

Supplemental Figure 1: Comparison of NCI-H1915 cells cultured in RPMI+10% FBS and complete NSC conditions. NCI-N1915 cells were originally isolated and cultured in RPMI+10% FBS, prior to being cultured in complete NSC conditions. **(A)** NCI-H1915 cells grow adherently in RPMI+10% FBS conditions (left), and as spheres in suspension when cultured in NSC conditions (right). Scale bars are 100µm. **(B)** Cells in each culture condition were analyzed by flow cytometry for CD133 (not shown), CD15, GFAP, and MAP2 expression, and Aldefluor activity. Data are presented as mean ± SD of three independent experiments. Culture in NSC conditions appears to increase the expression of BTIC marker CD15, and decreases the expression of mature neural lineage markers GFAP and MAP2, suggesting NSC conditions select for a more stem-like state. CD133 was minimally expressed in both cultures (<1% of the population; data not shown). **(C&D)** Representative flow plots of RPMI **(C)** and **(D)** NSC conditions. Plots are, from left to right, top to bottom: CD15-PE/CD133-APC, side-scatter/Aldefluor, and GFAP-PE/MAP2-Alexa647. Isotype and control plots are shown below their respective flow plots. Epcam, epithelial cell adhesion molecule; TTF1, thyroid transcription factor 1; GFAP, glial fibrillary acidic protein; MAP2, microtubule-associated protein 2; NSC, neural stem cell.

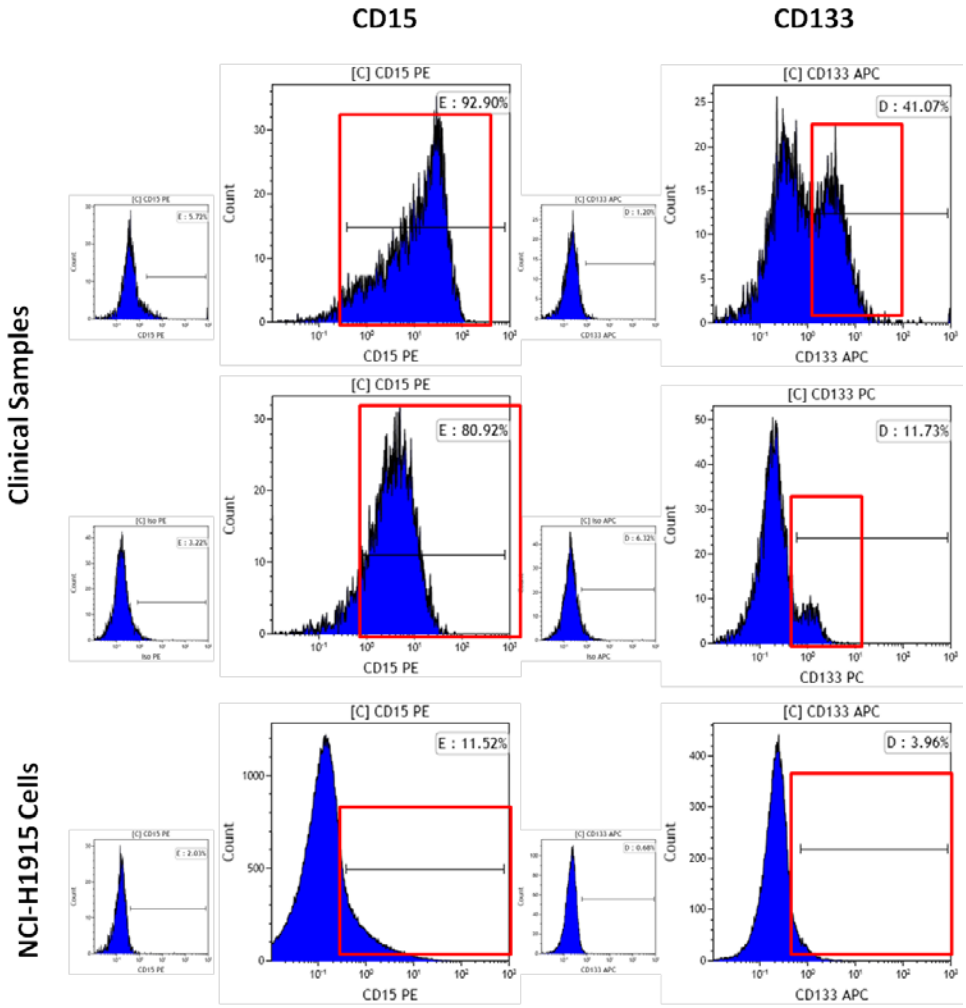

Supplemental Figure 2: CD15 identifies a semi-distinct (shoulder) population in clinical brain metastases and the NCI-H1915 cell line. Samples were analyzed by flow cytometry for CD15 and CD133 expression; single-parameter histogram plots of clinical samples BT219 (top) and BT381 (middle) and the NCI-H1915 cell line (bottom) for CD15-PE and CD133-APC are shown. CD15 consistently identified a distinct ("shoulder") population in clinical samples and the cell line (red box); whereas, CD133 expression was extremely variable, and often undetectable. Isotype or unstained controls are shown to the left of their respective histogram.

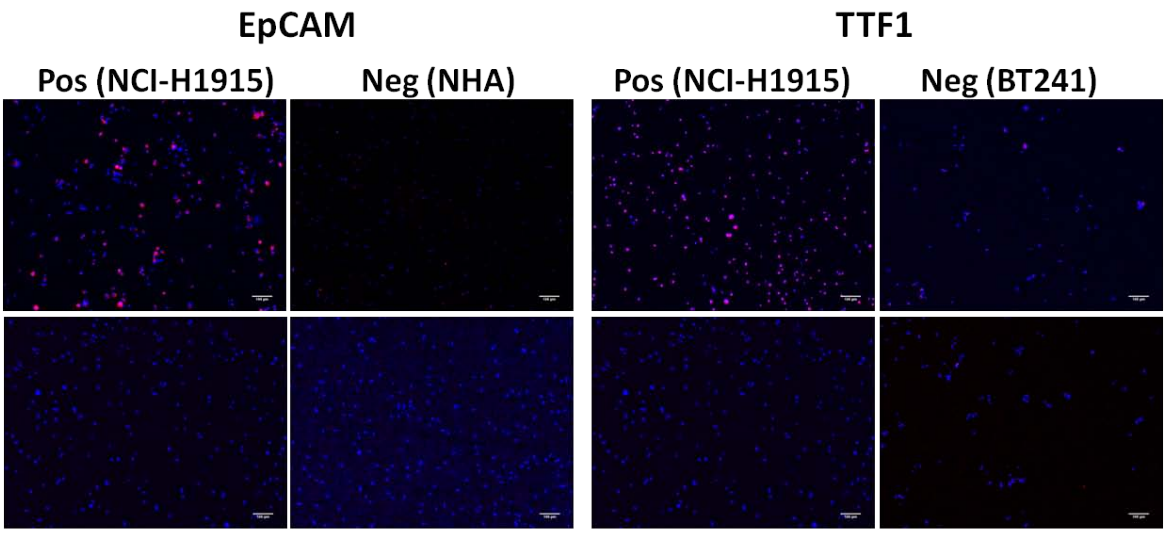

224.22 ± 8.53	229.71 ± 9.16
217.16 ± 35.93	226.50 ± 1.97

Stain 2° only

272.16 ± 21.70	246.35 ± 8.55
230.46 ± 3.40	233.07 ± 4.22

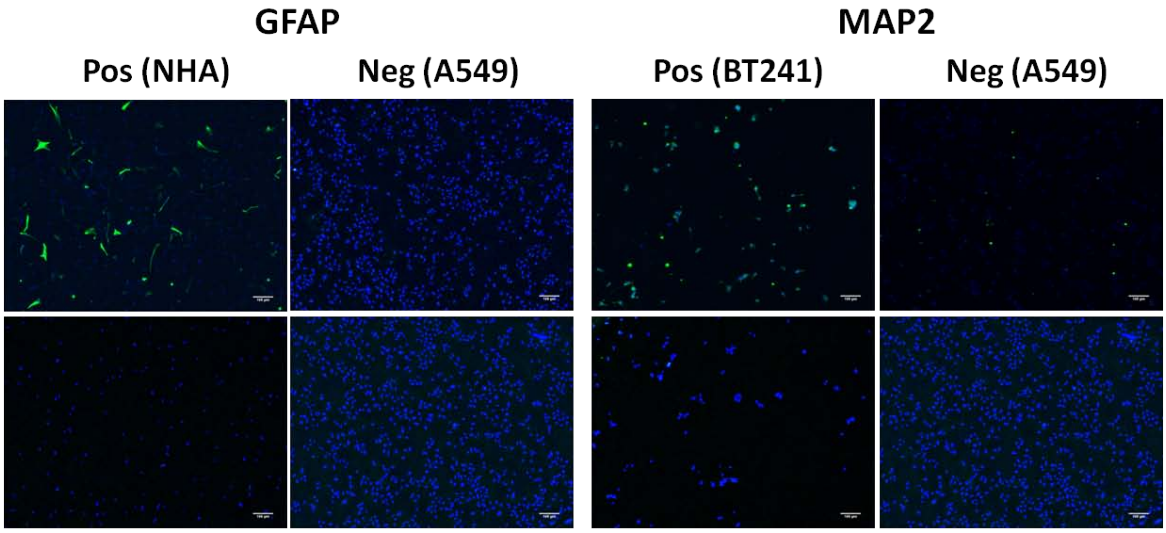

979.98 ± 363.23	369.84 ± 6.11
386.90 ± 6.86	372.68 ± 4.51

Stain 2° only

574.01 ± 122.29	409.88 ± 40.15
407.75 ± 21.64	402.37 ± 16.54

Supplemental Figure 3: Immunofluorescence positive and negative controls used for setting minimum fluorescence quantification thresholds. Cells lines positive or negative for the expression of EpCAM, TTF1, GFAP, or MAP2 were stained with appropriate primary antibodies, followed by staining with fluorescently-labeled secondary antibodies. The following minimum fluorescence thresholds were used for subsequent analyses: EpCAM, 225; TTF1, 250; GFAP, 450; MAP2, 450. Images are shown as stained (top panel) versus secondary only (bottom panel). Scale bars are 100μm. Tables are presenting the mean fluorescence intensity value ± SD. Cell lines used were NCI-H1915 (brain metastasis from the lung), NHA (normal human astrocytes), BT241 (glioblastoma), and A549 (primary lung adenocarcinoma) cells. Epcam, epithelial cell adhesion molecule; TTF1, thyroid transcription factor 1; GFAP, glial fibrillary acidic protein; MAP2, microtubule-associated protein 2.

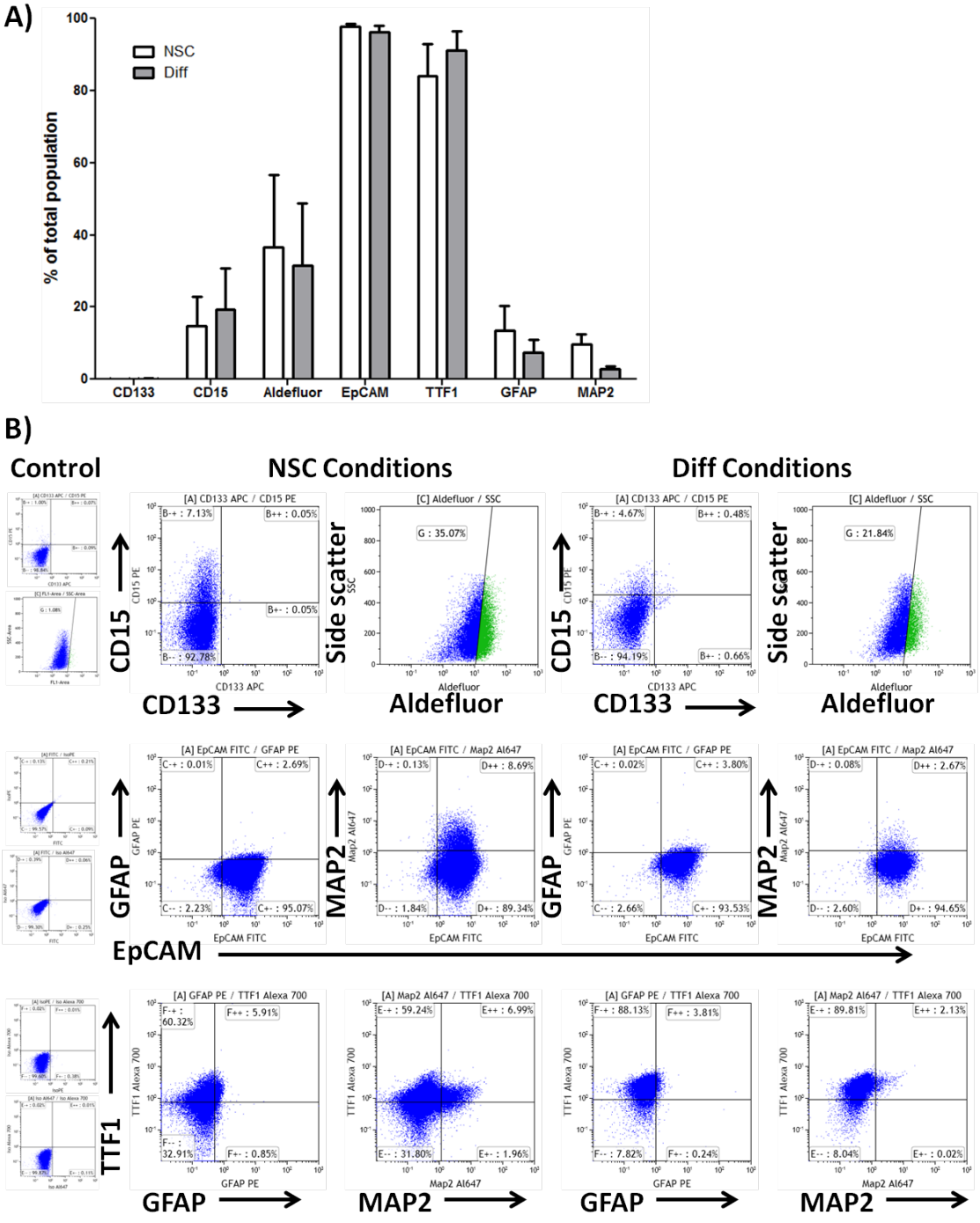
A)
NSC
Diff
% of total population
CD133
CD15
Aldefluor
EpCAM
TTF1
GFAP
MAP2
B)
Control
NSC Conditions
Diff Conditions
CD15
CD133
Side scatter
Aldefluor
GFAP
MAP2
EpCAM
TTF1

Supplemental Figure 4: NCI-H1915 cells may be refractory to differentiation. NCI-H1915 cells were grown in either differentiation or NSC conditions, and assessed for CD133, CD15, EpCAM, TTF1, GFAP, and MAP2 expression, as well as Aldefluor activity by flow cytometry. **(A)** There was no significant difference in BTIC marker (CD133, CD15, Aldefluor) expression/activity between the two culture conditions. There was also no significant difference in the expression of mature neural lineage markers, or in EpCAM or TTF1 expression. Representative flow plots are shown in **(B)**. Plots for each culture condition are, from left to right, top to bottom: CD15-PE/CD133-APC, side-scatter/Aldefluor, GFAP-PE/EpCAM-FITC, MAP2-Alexa647/EpCAM-FITC, TTF1-Alexa700/GFAP-PE, and TTF1-Alexa700/MAP2-Alexa647. Isotype and control plots are shown vertically and in line with their respective flow plots. Epcam, epithelial cell adhesion molecule; TTF1, thyroid transcription factor 1; GFAP, glial fibrillary acidic protein; MAP2, microtubule-associated protein 2; NSC, neural stem cell.

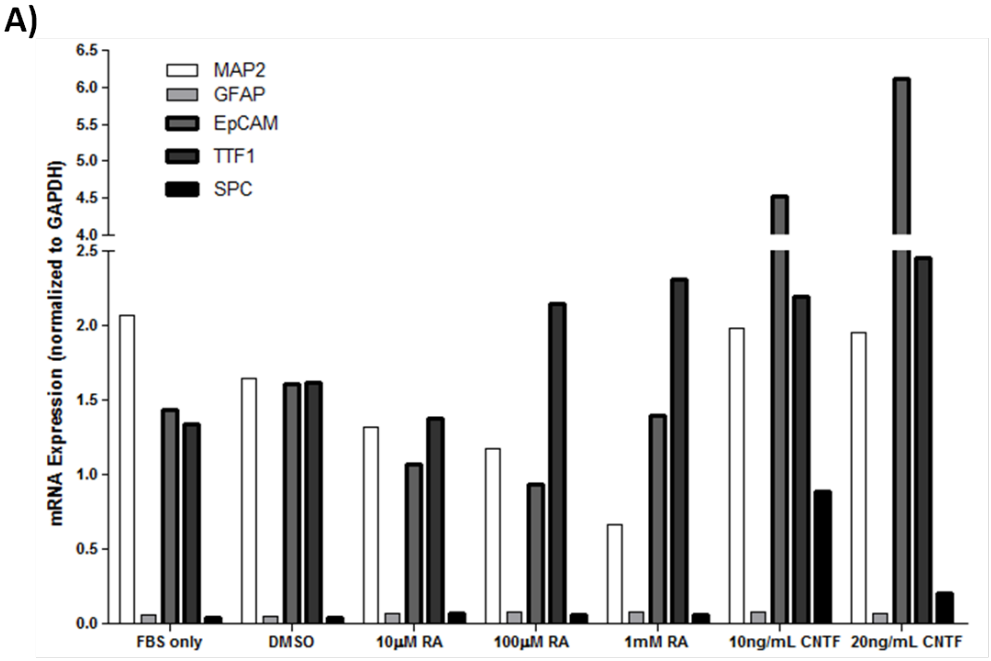
A)
MAP2
GFAP
EpCAM
TTF1
SPC
mRNA Expression (normalized to GAPDH)
FBS only
DMSO
10µM RA
100µM RA
1mM RA
10ng/mL CNTF
20ng/mL CNTF

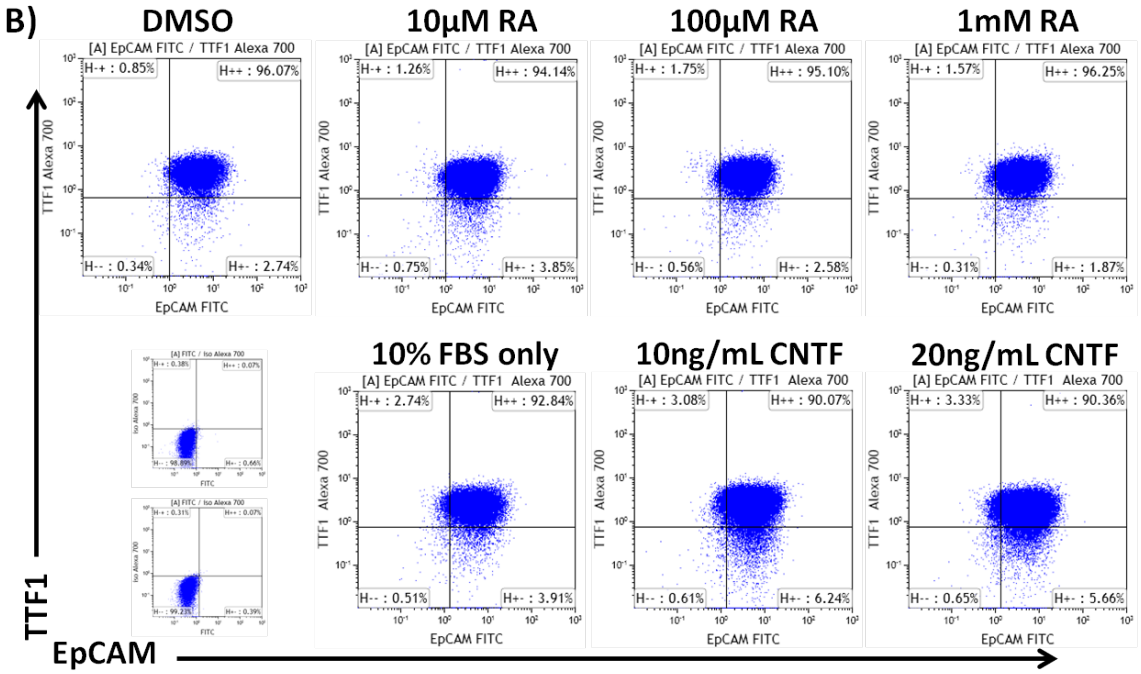
B)
DMSO
10µM RA
100µM RA
1mM RA
10% FBS only
10ng/mL CNTF
20ng/mL CNTF
[A] EpCAM FITC / TTF1 Alexa 700
TTF1 Alexa 700
EpCAM FITC
TTF1
EpCAM

Supplemental Figure 5: NCI-H1915 cells are unresponsive to directed differentiation cues. NCI-H1915 were subjected to directed differentiation using increasing concentrations of retinoic acid (RA; diluted in DMSO), or ciliary neurotrophic factor (CNTF; diluted in PBS) added to basal NSC media +10% FBS. DMSO, and 10% FBS only conditions served as controls. **(A)** Cells were collected for transcript level analysis of lineage markers using qRT-PCR. Results are shown as the mean of duplicates in a single experiment. **(B)** Analysis by flow cytometry showed no change in EpCAM or TTF1 levels during the experiment. Plots are TTF1-Alexa700/EpCAM-FITC. Inset, isotypes: top, DMSO and RA treatments; bottom, FBS only and CTNF treatments. RA, retinoic acid; CTNF, ciliary neurotrophic factor; MAP2, microtubule-associated protein 2; GFAP, glial fibrillary astrocytic protein; EpCAM, epithelial cell adhesion molecule; TTF1, thyroid transcription factor 1; SPC, surfactant protein C.

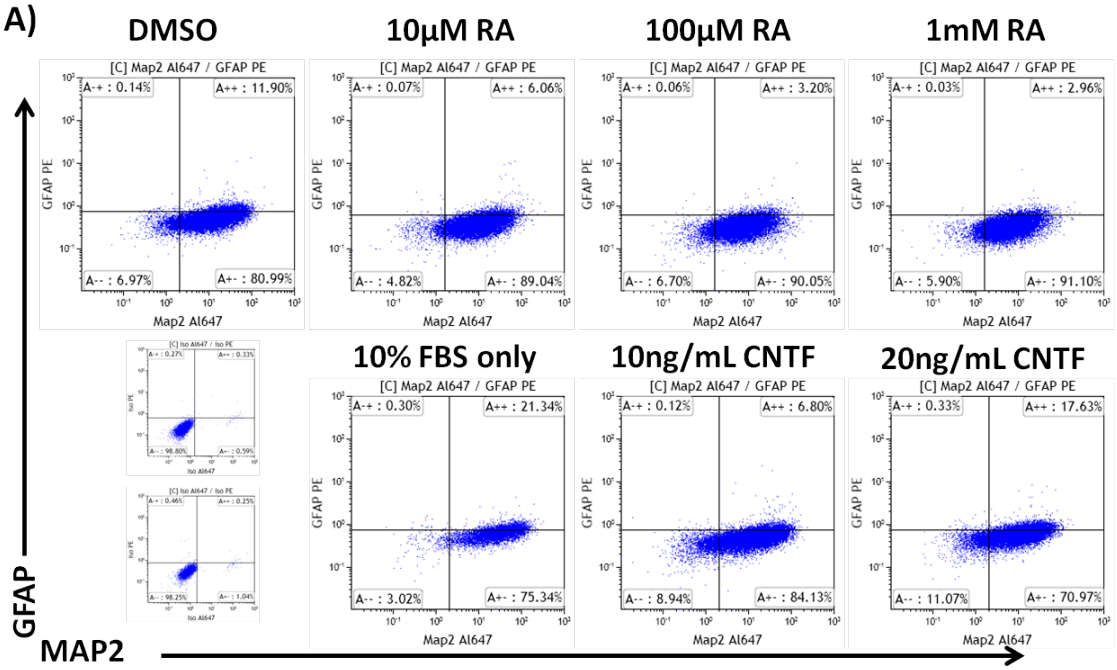
A)
DMSO
10µM RA
100µM RA
1mM RA
10% FBS only
10ng/mL CNTF
20ng/mL CNTF
GFAP
MAP2
[C] Map2 Al647 / GFAP PE
Map2 Al647
GFAP PE
A-+ : 0.14%
A++ : 11.90%
A-- : 6.97%
A+- : 80.99%
A-+ : 0.07%
A++ : 6.06%
A-- : 4.82%
A+- : 89.04%
A-+ : 0.06%
A++ : 3.20%
A-- : 6.70%
A+- : 90.05%
A-+ : 0.03%
A++ : 2.96%
A-- : 5.90%
A+- : 91.10%
A-+ : 0.30%
A++ : 21.34%
A-- : 3.02%
A+- : 75.34%
A-+ : 0.12%
A++ : 6.80%
A-- : 8.94%
A+- : 84.13%
A-+ : 0.33%
A++ : 17.63%
A-- : 11.07%
A+- : 70.97%

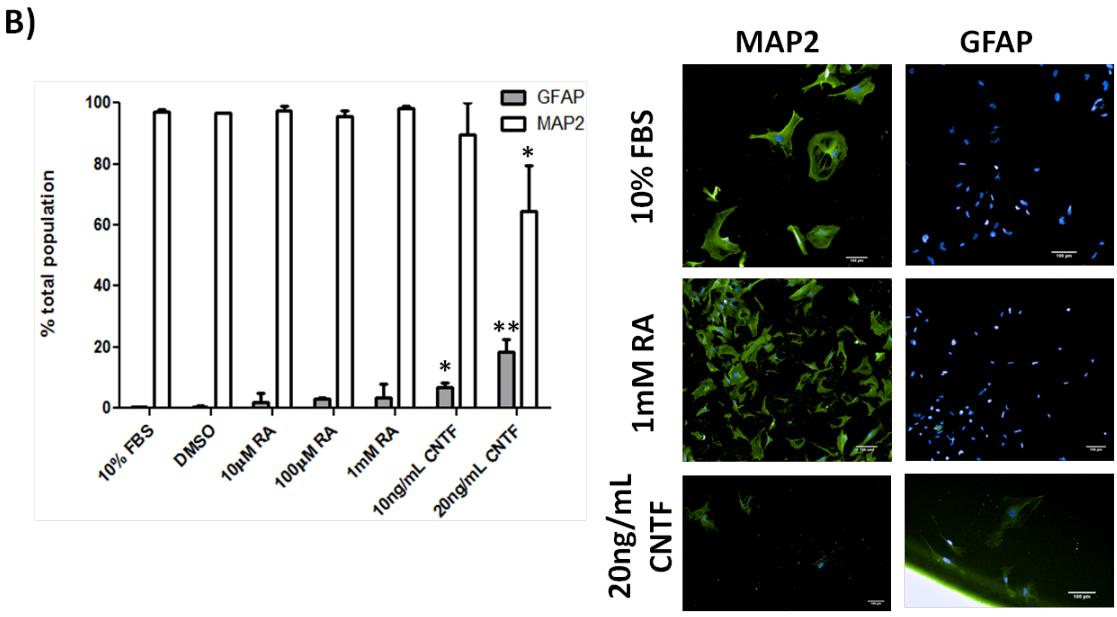
B)
GFAP
MAP2
% total population
100
80
60
40
20
0
*
**
10% FBS
DMSO
10µM RA
100µM RA
1mM RA
10ng/mL CNTF
20ng/mL CNTF
MAP2
GFAP
10% FBS
1mM RA
20ng/mL CNTF

Supplemental Figure 6: The normal H9-derived NSC cell line demonstrates neuronal and astrocytic differentiation when subjected to directed differentiation cues. H9-NSC cells were subjected to directed differentiation using increasing concentrations of retinoic acid (RA; diluted in DMSO), or ciliary neurotrophic factor (CNTF; diluted in PBS) added to basal NSC media +10% FBS. DMSO, and 10% FBS only conditions served as controls. After 7 days, cells were collected, and assessed for their expression of GFAP and MAP2. **(A)** Analysis by flow cytometry showed almost complete differentiation to the neuronal lineage (MAP2) in controls and RA-treated cells. Addition of CNTF; however, led to a loss of MAP2 expression, and an increase in that of GFAP (astrocytes). Flow plots are GFAP-PE/MAP2-Alexa647. Inset, isotype controls for DMSO and RA treatments (top), 10% FBS and CNTF treatments (bottom). **(B)** Cells were also examined by IF, which demonstrated responses consistent with that seen using flow cytometry. Significant increases in GFAP expression were seen upon addition of CNTF, while H9-NSC cells remained largely neuronal in the other conditions. *, $p<0.05$; **, $p<0.01$; scale bar, 100μm. These results confirm that this method of directing neuronal and astrocytic lineage differentiation is appropriate. GFAP, glial fibrillary acidic protein; MAP2, microtubule-associated protein 2.

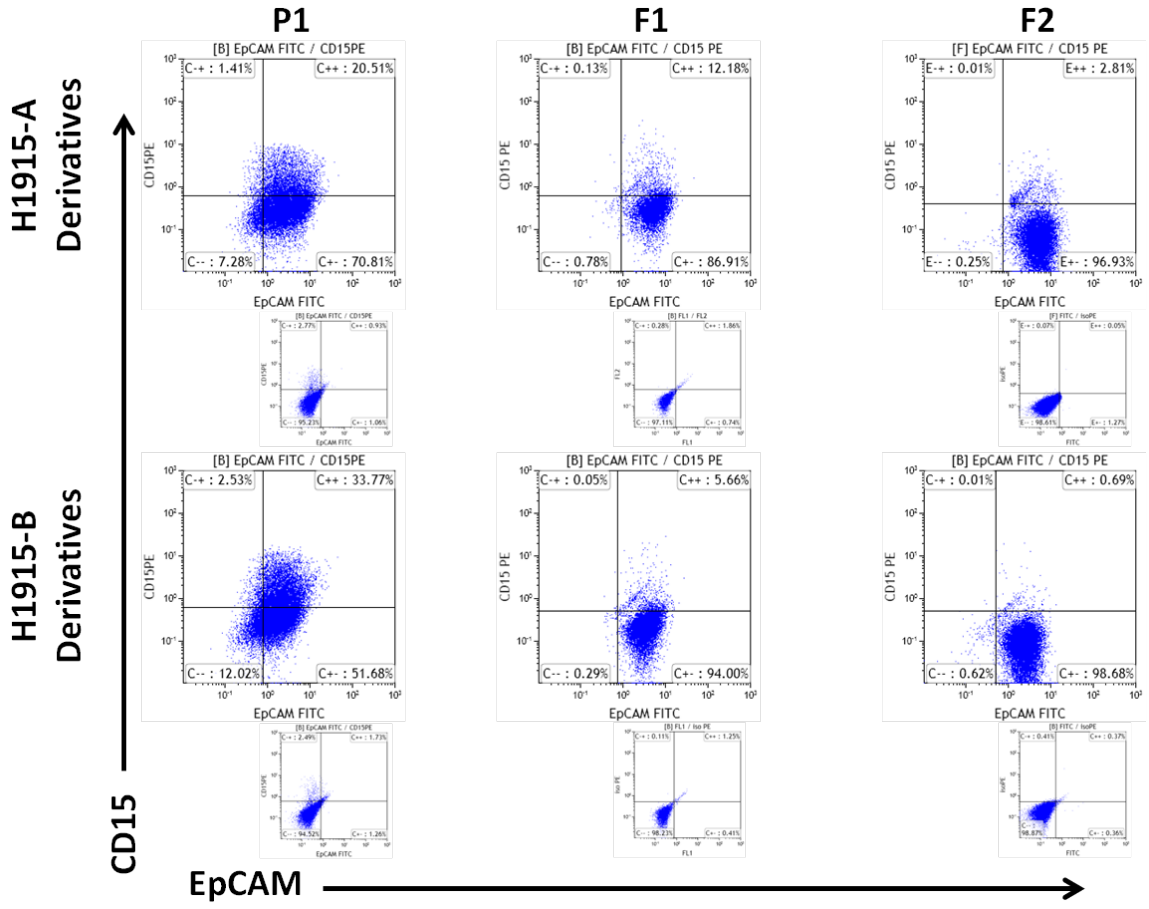

Supplemental Figure 7: Representative flow plots of serially-injected NCI-H1915 tumours. Tumour cells were grown in NSC conditions for seven days post-collection, and assessed for their expression of CD133 (not shown) and CD15 by flow cytometry. Plots are CD15-PE/EpCAM-FITC; $EpCAM^{+}$ cells are those of tumour origin, as opposed to mouse origin. Isotype plots are shown below their respective flow plots. Epcam, epithelial cell adhesion molecule; NSC, neural stem cell.

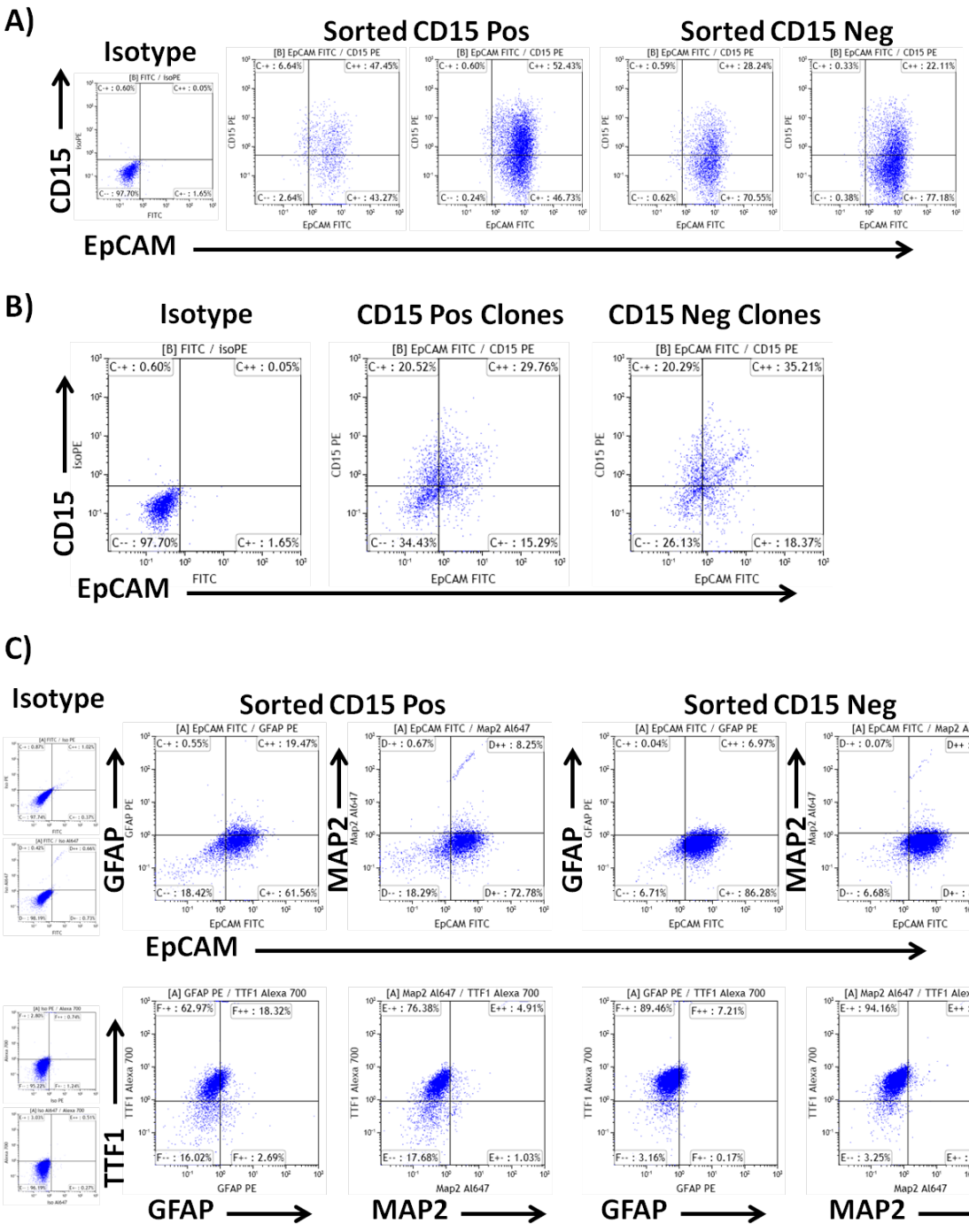
A)
Isotype
Sorted CD15 Pos
Sorted CD15 Neg
CD15
EpCAM
B)
Isotype
CD15 Pos Clones
CD15 Neg Clones
CD15
EpCAM
C)
Isotype
Sorted CD15 Pos
Sorted CD15 Neg
GFAP
MAP2
EpCAM
TTF1
GFAP
MAP2
GFAP
MAP2

Supplemental Figure 8: Representative flow plots of CD15-sort experiments. NCI-H1915 cells were sorted into $CD15^+$ and $CD15^-$ populations; sorted cells were used to reassess CD15 expression **(A)**, in clonal analysis **(B)**, or differentiation experiments **(C)**. **(A)** Sorted populations were analyzed for CD15 expression at secondary (left) and tertiary (right) sphere formation. Plots are CD15-PE/EpCAM-FITC. **(B)** Single cells were sorted into 96 well plates, and cultured in NSC conditions. After 14 days post-sort, clonal populations were pooled and assessed for CD15 expression. Plots are CD15-PE/EpCAM-FITC. **(C)** Sorted populations were grown in differentiation conditions for seven days post-sort, and analyzed for their expression of EpCAM, TTF1, GFAP, and MAP2. Plots are, from left to right, top to bottom: GFAP-PE/EpCAM-FITC, MAP2-Alexa647/EpCAM-FITC, TTF1-Alexa700/GFAP-PE, and TTF1-Alexa700/MAP2-Alexa647. Isotype controls are shown vertically, in line with their respective flow plots. Epcam, epithelial cell adhesion molecule; TTF1, thyroid transcription factor 1; GFAP, glial fibrillary acidic protein; MAP2, microtubule-associated protein 2; NSC, neural stem cell.

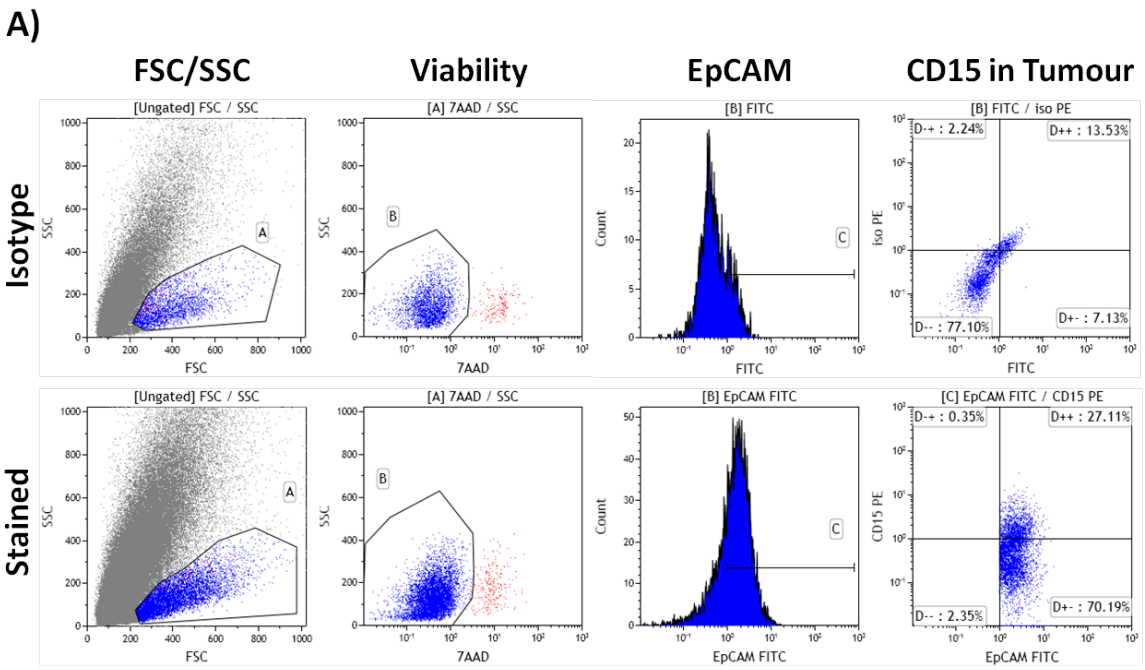
A)
FSC/SSC
Viability
EpCAM
CD15 in Tumour
Isotype
Stained
[Ungated] FSC / SSC
[A] 7AAD / SSC
[B] FITC
[B] FITC / iso PE
[B] EpCAM FITC
[C] EpCAM FITC / CD15 PE
FSC
SSC
7AAD
FITC
Count
iso PE
CD15 PE
EpCAM FITC
D-+ : 2.24%
D++ : 13.53%
D-- : 77.10%
D+- : 7.13%
D-+ : 0.35%
D++ : 27.11%
D-- : 2.35%
D+- : 70.19%

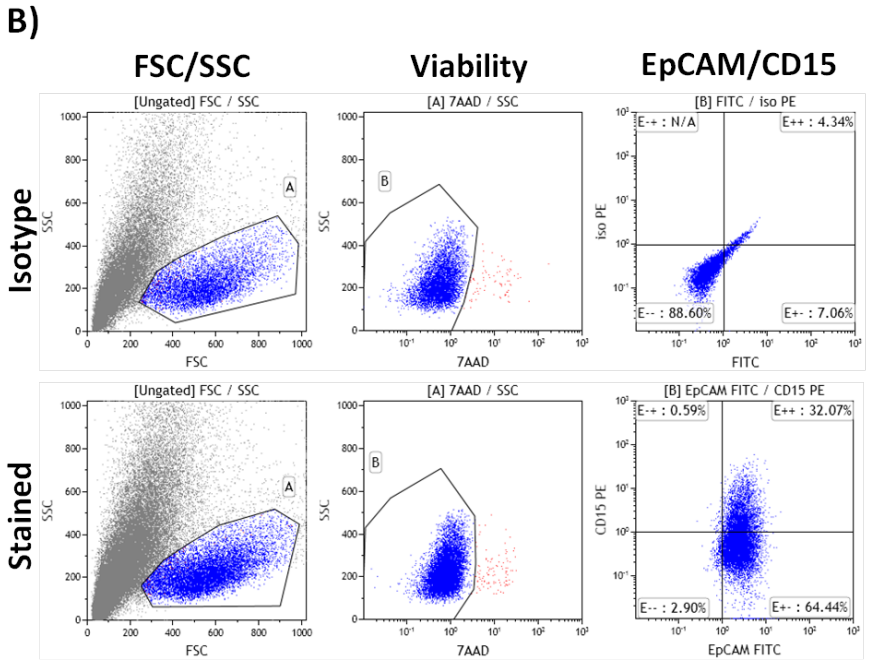
B)
FSC/SSC
Viability
EpCAM/CD15
Isotype
Stained
[Ungated] FSC / SSC
[A] 7AAD / SSC
[B] FITC / iso PE
[B] EpCAM FITC / CD15 PE
FSC
SSC
7AAD
FITC
iso PE
CD15 PE
EpCAM FITC
E-+ : N/A
E++ : 4.34%
E-- : 88.60%
E+- : 7.06%
E-+ : 0.59%
E++ : 32.07%
E-- : 2.90%
E+- : 64.44%

Supplemental Figure 9: Gating strategy for CD15 expression analysis of NCI-H1915 CD15-sorted tumours. Single cell suspensions of NCI-H1915 tumour cells were stained with CD15-PE and EpCAM-FITC, and assessed by flow cytometry for CD15 expression in the tumour cells. **(A)** For cells assessed immediately after tumour collection, a gating strategy to eliminate contaminating mouse brain cells was employed. NCI-H1915 cells were first selected based on their low side-scatter and high forward scatter pattern. Dead cells were excluded from this population using 7AAD. Histograms for EpCAM were created, where the threshold for positivity was set based on the isotype EpCAM expression. Any additional contaminating mouse cells are eliminated this way, before view on the CD15-PE/EpCAM-FITC scatter plot. **(B)** Tumour cells cultured in NSC conditions are much more easily segregated from any remaining mouse cells, and do not require gating based on EpCAM positivity. Epcam, epithelial cell adhesion molecule.

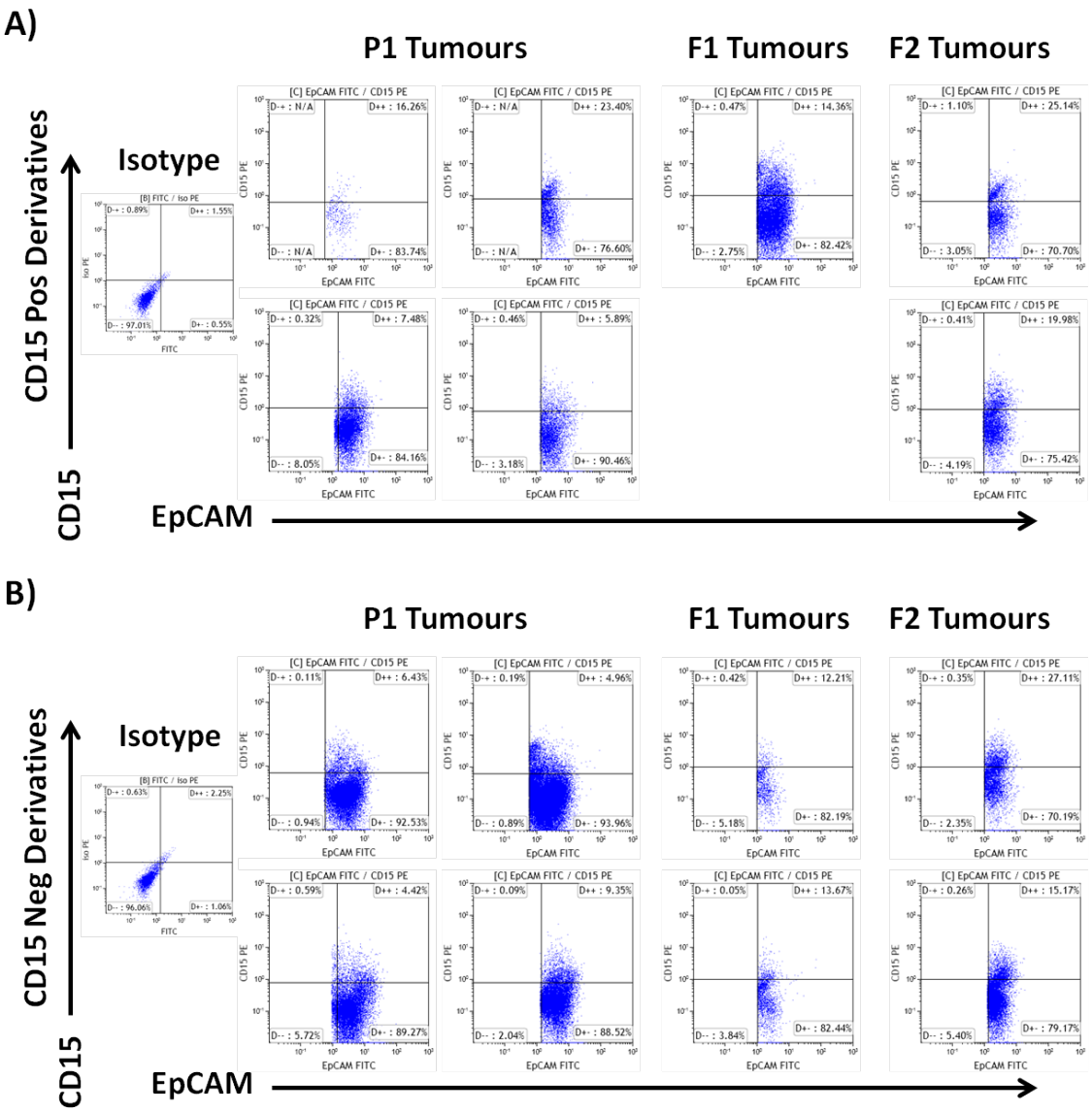

Supplemental Figure 10: Flow plots of serially-injected CD15-sorted NCI-H1915 tumours, initial CD15 percentage. Tumours were analyzed immediately after collection for CD15 expression by flow cytometry. Flow plots for all tumours assessed are shown. Plots are CD15-PE/EpCAM-FITC; **(A)** $CD15^{+}$ -derived tumours; **(B)** and $CD15^{-}$ -derived tumours. Isotype controls are shown in the left-most panels. Epcam, epithelial cell adhesion molecule.

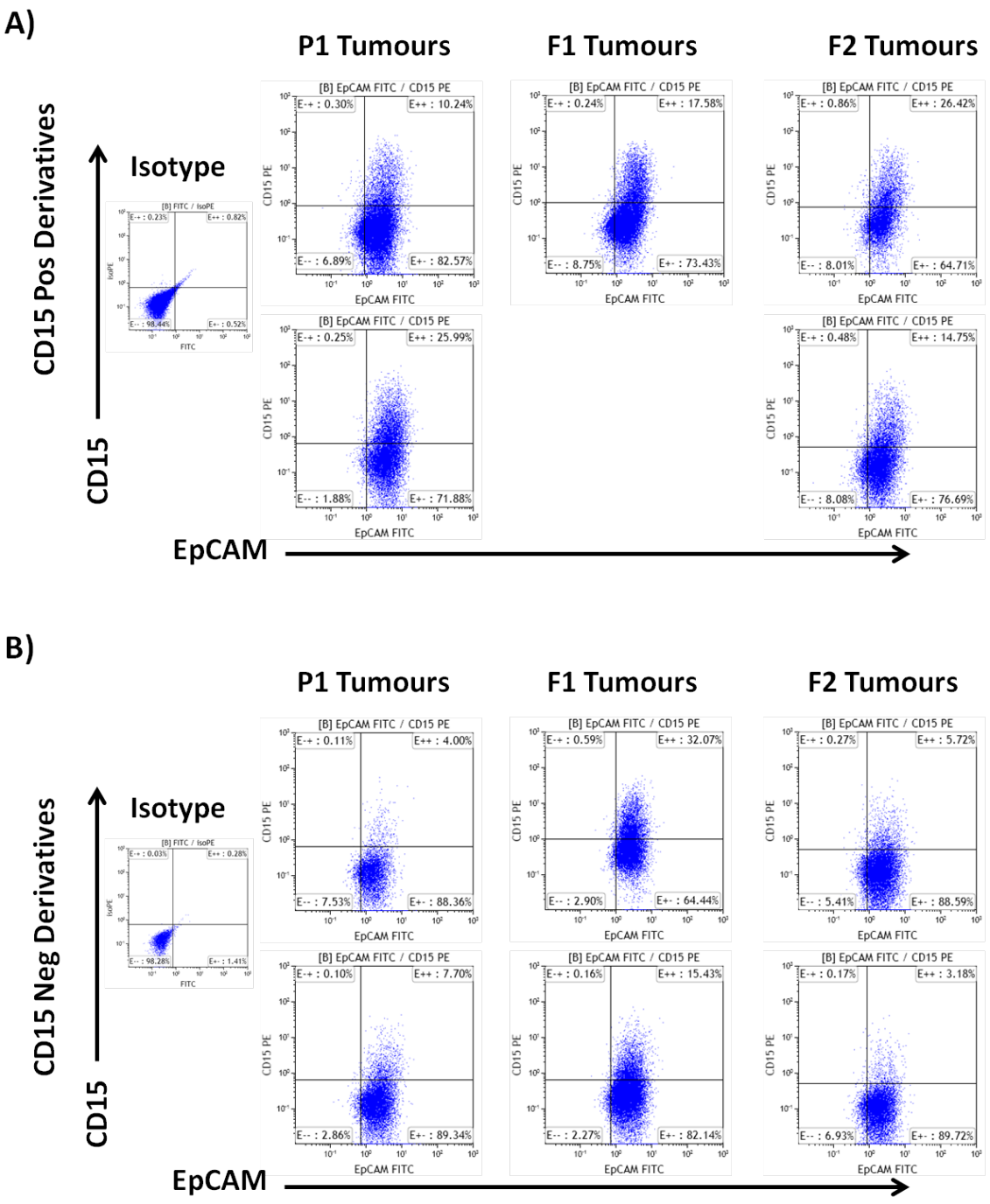
A)
P1 Tumours
F1 Tumours
F2 Tumours
CD15 Pos Derivatives
Isotype
CD15
EpCAM
[B] EpCAM FITC / CD15 PE
E-+ : 0.30%
E++ : 10.24%
E-- : 6.89%
E+- : 82.57%
[B] EpCAM FITC / CD15 PE
E-+ : 0.24%
E++ : 17.58%
E-- : 8.75%
E+- : 73.43%
[B] EpCAM FITC / CD15 PE
E-+ : 0.86%
E++ : 26.42%
E-- : 8.01%
E+- : 64.71%
[B] EpCAM FITC / CD15 PE
E-+ : 0.25%
E++ : 25.99%
E-- : 1.88%
E+- : 71.88%
[B] EpCAM FITC / CD15 PE
E-+ : 0.48%
E++ : 14.75%
E-- : 8.08%
E+- : 76.69%
[B] FITC / IsoPE
E-+ : 0.23%
E++ : 0.82%
E-- : 98.44%
E+- : 0.52%
B)
P1 Tumours
F1 Tumours
F2 Tumours
CD15 Neg Derivatives
Isotype
CD15
EpCAM
[B] EpCAM FITC / CD15 PE
E-+ : 0.11%
E++ : 4.00%
E-- : 7.53%
E+- : 88.36%
[B] EpCAM FITC / CD15 PE
E-+ : 0.59%
E++ : 32.07%
E-- : 2.90%
E+- : 64.44%
[B] EpCAM FITC / CD15 PE
E-+ : 0.27%
E++ : 5.72%
E-- : 5.41%
E+- : 88.59%
[B] EpCAM FITC / CD15 PE
E-+ : 0.10%
E++ : 7.70%
E-- : 2.86%
E+- : 89.34%
[B] EpCAM FITC / CD15 PE
E-+ : 0.16%
E++ : 15.43%
E-- : 2.27%
E+- : 82.14%
[B] EpCAM FITC / CD15 PE
E-+ : 0.17%
E++ : 3.18%
E-- : 6.93%
E+- : 89.72%
[B] FITC / IsoPE
E-+ : 0.03%
E++ : 0.28%
E-- : 98.28%
E+- : 1.41%

Supplemental Figure 11: Flow plots of serially-injected CD15-sorted NCI-H1915 tumours, 1 week-post collection. Tumour cells were grown in NSC conditions for seven days post-collection, and assessed for their expression CD15 by flow cytometry. Flow plots for all tumours assessed are shown. Plots are CD15-PE/EpCAM-FITC; **(A)** $CD15^{+}$ -derived tumours; **(B)** and $CD15^{-}$ -derived tumours. Isotype controls are shown in the left-most panels. Epcam, epithelial cell adhesion molecule; NSC, neural stem cell.

Appendix: Springer Sciences and Business Media copyright permission.

Dear Ms. Nolte,

With reference to your request (copy herewith) to reprint material on which Springer Science and Business Media controls the copyright, our permission is granted, free of charge, for the use indicated in your enquiry.

This permission

- allows you non-exclusive reproduction rights throughout the World.

- permission includes use in an electronic form, provided that content is

    * password protected

    * at intranet;

- excludes use in any other electronic form. Should you have a specific project in mind, please reapply for permission.

- requires a full credit (Springer/Kluwer Academic Publishers book/journal title, volume, year of publication, page, chapter/article title, name(s) of author(s), figure number(s), original copyright notice) to the publication in which the material was originally published, by adding: with kind permission of Springer Science and Business Media.

The material can only be used for the purpose of defending your dissertation, and with a maximum of 100 extra copies in paper.

Permission free of charge on this occasion does not prejudice any rights we might have to charge for reproduction of our copyrighted material in the future.

Kind regards,

Maaike Duine
Springer
Rights and Permissions

Van Godewijckstraat 30, 3311 GX
P.O. Box 17, 3300 AA
Dordrecht, The Netherlands
Tel +31 (0) 78 657 6537
Fax +31 (0) 78 657 6377
maaike.duine@springer.com

From: sara.m.nolte@gmail.com [mailto:sara.m.nolte@gmail.com] **On Behalf Of** Sara M. Nolte
Sent: Tuesday, April 03, 2012 3:44 PM
To: Permissions Europe/NL
Subject: Copyright permission

To whom it may concern,

I am writing to you to request permission to use copyrighted material from a book chapter I have previously prepared for one of your books in the preparation of my Master's (MSc) Thesis.

The chapter in question (Chapter 11: The origin of metastasis-initiating cells) is to be published in the book entitled Stem Cells and Human Diseases (#299763), edited by Dr. Srivastava. I would like to use the following figures and tables in my Thesis: Figures 11.1 (p.6) and 11.3 (p12); Table 11.1 (p7). I would also like to use parts of the main body of the text as part of my Introduction/Background and Discussion.

My Thesis will be available online through the McMaster University Digital Commons, and I will likely request a printed and bound copy for my personal use. The Thesis will NOT be published in any journal, or available on PubMed.

My contact information is listed below:

Sara M. Nolte
McMaster Stem Cell and Cancer Research Institute
1280 Main Street West, MDCL 5077B
McMaster University
Hamilton, ON, Canada
L8S 4K1
Fax: 1-905-522-7772

Please let me know if there is any additional information you require to assess my request.

Thank you, and I look forward to your reply.

Sara M. Nolte Hon. BHSc
MSc Candidate; Biochemistry & Biomedical Sciences